Dissertation zur Erlangung des Doktorgrades
der Fakultät für Chemie und Pharmazie
der Ludwig-Maximilians-Universität München

Influence of Size and Topology on the Efficiency of Sequence-defined Polycationic Carriers for Gene Delivery

Claudia Veronica Scholz
aus
Rüsselsheim, Deutschland
2014

Erklärung

Diese Dissertation wurde im Sinne von § 7 der Promotionsordnung vom 28. November 2011 von Herrn Prof. Dr. Ernst Wagner betreut.

Eidesstattliche Versicherung

Diese Dissertation wurde eigenständig und ohne unerlaubte Hilfe erarbeitet.

München, 07.01.2014

_____

(Claudia Scholz)

Dissertation eingereicht am 17.01.2014

1. Gutachter: Prof. Dr. Ernst Wagner
2. Gutachter: Prof. Dr. Wolfgang Frieß

Mündliche Prüfung am 27.03.2014

Meinen Eltern

1 TABLE OF CONTENTS

2 INTRODUCTION

2.1 Nucleic acid-based therapies

Gene therapy offers a wide spectrum of approaches including regulation, repair and replacement of genes which directly cure at the molecular genetic origin of the disease. For monogenetic diseases like cystic fibrosis [1], severe combined immunodeficiency (SCID) [2] and hyperlipidemia [3], the replacement of the defective gene is a successfully used approach. Furthermore, the interference on the genetic level is a promising option for cancer, which is usually promoted by complex genetic disregulations and still constitutes an often incurable disease and one of the main causes of death.

The first gene transfer in mammalian cells was already documented over 50 years ago [4]. Only some years later Rogers and Pfuderer provided evidence of the first viral gene transfer in plants [5]. Over the last decades the field of gene therapy expanded tremendously in regard to vector diversity as well as the applied type of nucleic acid.

In addition to the initial strategy of successfully substituting defective genes with the corresponding intact gene inserted into plasmid DNA (pDNA), the option of suppressing pathogenic genes has emerged as a widely-used tool. Such a blockade is based on specific complementary binding of an antisense nucleic acid strand to messenger RNA (mRNA) in the RNA-induced silencing complex (RISC), leading to enzymatic mRNA degradation or to steric hindrance preventing the translation into the encoded protein. Classical approaches for specific gene suppression include the application of single-stranded oligodesoxy-ribonucleotides (ODNs), whereas RNA interference (RNAi) was discovered as a novel strategy for the silencing of a specific gene in nematodes in 1998 by Fire et al. [6]. However, this technique was not as effective in mammalian cells, where the initially applied long double-stranded RNA (dsRNA) with over 30 base pairs (bp) induced immune reactions and cell death. It was only with the direct application of the shorter 21 bp small interfering RNA (siRNA) that effective gene silencing was achieved in mammalian cells at the same time circumventing immune responses [7]. This finding marks a milestone in the development of therapeutic nucleic acids for gene silencing. Another key discovery in the 1990s was the existence of genes which instead of encoding for proteins, resulted in the production of small RNA molecules, the so-called microRNAs (miRNAs) [8]. These widely found non-coding

miRNAs regulate the expression of specific genes by interference with the mRNA, allowing for phenotypic fine-tuning [9, 10]. As many miRNA targets were identified to be oncogenes, the application of exogenous miRNA provides a promising therapeutic option for cancer. Conversely, inhibition of endogenous miRNA by antagomirs [11] is an interesting approach for inactivation of miRNAs targeting tumor suppressors (oncomirs). Another exciting concept is the application of aptamers, 56-120 nucleotides long single-stranded RNAs, which due to their special 3D structure are able to bind to their targets with high specificity and affinity [12]. Although preferentially used for diagnostics or targeted delivery, such as for the previously described siRNAs [13], aptamers are also applied as therapeutic principle itself. The most encouraging example is given by Pegaptanib, an aptamer against the Vascular endothelial growth factor (VEGF), that received FDA approval as a therapeutic against age-related macular degeneration (AMD) in 2004 [14].

Besides the exploration of different mechanistic approaches for the application of nucleic acid-based therapies, a crucial step towards promising therapeutic options was the introduction of a variety of chemical modifications leading to a better performance of the nucleic acid itself. Accomplished optimizations include the decrease of susceptibility to degradation by nucleases present in biological fluids, the avoidance of side effects caused by immune reactions or off-target downregulation, as well as the increase of potency [15]. In this context the RNA modification of the 2´-OH groups such as the 2´-O-methyl or 2´-fluoro became a widely-used strategy. Connecting the 2´-O with the 4´-C via a methylene bridge results in the locked nucleic acids (LNAs) adopting a blocked A-conformation, which provides a great enhancement in thermostability [16, 17]. Other commonly used backbone modifications are phosphorothioate [18] or phosphorodiamidate morpholino oligomers (PMOs) [19].

Altogether the diversity of natural and chemically modified nucleic acids offers a wide spectrum of therapeutic approaches. Nevertheless, these can only lead to success in combination with appropriate carrier systems.

2.2 Synthetic carrier systems for the delivery of nucleic acids

2.2.1 Features of different therapeutic carrier types

Inherent properties of nucleic acids like their anionic character, sizes up to the micrometer scale and instability in biological fluids emphasize the need for appropriate carrier systems in

order to use them as therapeutic principle. Although in more than 40 years of experience remarkable progress was made in the field of gene therapy with many approaches entering into clinical trials [20], the need for an ideal delivery system in regard to efficiency and biocompatibility has yet to be fulfilled. Important prerequisites for effective therapeutic application are the successful delivery to the desired site of action and subsequent release inside the target cells. The first step in this process is the packaging of the nucleic acid cargo into stable nanoparticles to prevent enzymatic degradation in the bloodstream after intravenous administration. At the same time particle aggregation and interaction with serum components have to be avoided, which can be achieved by appropriate shielding components. In this context PEGylation has become a popular strategy [21]. Accumulation at the target site can be accomplished via the enhanced permeability and retention effect (EPR), which exploits the leaky tumor vasculature and the insufficient lymphatic drainage in the tumor tissue for the enrichment of nanoparticles [22]. Besides this passive targeting effect, active cell targeting can be achieved through the attachment of specific targeting ligands enabeling receptor-mediated endocytosis preferentially into receptor overexpressing cells [23]. The next critical step is given by the endosomal escape. The rupture of the endosomal membrane can be conducted by lytic carrier domains as they are present in lipidic carriers [24], or via the proton sponge effect for carriers with proton buffering capacities at the relevant pH range [25]. In some cases, depending on the type of nucleic acid (e. g. siRNA), the place of action is reached in the cytosol and therefore the efficient and early endosomal escape is an essential demand. For pDNA further transport to the nucleus is required representing a further crucial step. In order to overcome all these extra- and intracellular barriers, a great variety of carriers with differing chemical and physical properties have been used so far.

The first attempts of gene delivery were performed with viral vectors by exploiting their natural property of infecting cells and transferring their genetic information to the host. Due to their dynamic alignment to the conditions prevailing in the host, viruses turned out to be very efficient carrier systems [26]. However, despite these advantages and the first reported complete cure of SCID-X1 by viral gene therapy [2], many drawbacks are known connected to the use of viral vectors. These include a limited cargo loading, the elicitation of immune responses and most alarming the risk of promoting cancer by insertional mutagenesis [26].

In this context in recent times the field of synthetic carriers for gene delivery, which in most cases are cationic liposomes, peptides or polymers, has undergone enormous advances.

Direct complexation of nucleic acids with cationic lipids results in the self-assembly of so-called lipoplexes [27, 28]. Lipopolyplexes are formed by the addition of liposomes to pre-formed polyplexes [29], whereas liposomes are characterized by the encapsulation of the nucleic acid in uni- or multilamellar lipid bilayers [30]. Nowadays lipid-based carriers constitute one of the most advanced fields of nucleic acid delivery by synthetic vectors, with several formulations entering into clinical trials [31]. “Stabilized nucleic acid lipid particles” (SNALPS), a carrier system consisting of PEGylated liposomes, showed success as therapeutics for liver diseases exploiting the effect of liver accumulation. Ongoing clinical trials include for example treatment of hypercholesterolemia or liver cancer [32, 33].

Besides the lipid-mediated approaches, also polymer-based transfection agents like polyethylenimine (PEI) or polylysine (PLL) provided promising results entering into clinical trials [34-36]. The first clinical polyplex-mediated gene therapy trial in patients was based on an *ex vivo* approach using adenovirus-enhanced transferrinfection (AVET) [37, 38] for the transfection of the Interleukin 2 (IL-2) gene to autologous tumor cells of melanoma patients [39, 40]. The IL-2 expressing tumor cells were used as tumor vaccine, stimulating antitumoral effects due to immune response activation after intradermal injection [41]. Recently, a clinical trial was started to study the first targeted polymer-based siRNA carrier system in humans [42]. Based on cyclodextrin, Davis and coworkers designed a nanoparticle carrying PEGylation and transferrin ligands [43]. The transferrin receptor is overexpressed in many cancer types and therefore constitutes a well-known specific tumor target [44]. By detection of a specific mRNA cleavage product in tumor cells the authors provided the first evidence for RNAi in humans after systemic application [43].

2.2.2 Polydisperse versus precise carrier structures

Since it was first demonstrated that PLL is capable of condensing DNA into nanosized structures in 1975 [45], gene delivery with cationic polymers became an extensively explored field. Among the synthetic polymers, PEI has emerged as a gold standard for gene delivery due to its high transfection efficiency. However, cytotoxicity and its polydisperse character constitute main drawbacks hampering the clinical application. After the first use as a gene delivery agent by Jean-Paul Behr and colleagues in 1995 [25], many optimizations

have been performed on PEI to improve its physicochemical and biological properties. Surface modification of branched PEI (brPEI) with neutral or negative moieties resulted in reduction of cytotoxicity [46, 47]. To tackle the problem of polydispersity, the synthesis was optimized by the use of sequence-controlled polymerization techniques [48, 49] or by additional purification steps like size exclusion chromatography helping to define the MW range of polymer-based carriers. Nevertheless, the mentioned techniques still do not provide complete sequence control. Up to now many approaches were developed and exploited to synthesize precise carriers. For nucleic acid delivery especially two techniques, the use of solid-phase synthesis for the development of peptide-based carriers and the assembly of dendrimers have gained importance [36, 50, 51]. Dendrimers consist of a core molecule and a defined amount of branches, which multiply with increasing generation number. Polyamidoamine (PAMAM) and polypropylenimine (PPI) are prominent examples for dendrimer-based nucleic acid delivery systems, not only in the original form, but also with diverse surface modifications in order to improve their properties [52-54]. Among the peptide-based carriers, the cell-penetrating peptides (CPPs) represent a widely used platform for the design of nucleic acid delivery systems [55] with encouraging results for pDNA [56, 57] as well as for siRNA delivery [58-60]. In the Wagner lab artificial amino acids containing the diaminoethane motif were designed for their use in the synthesis of sequence-defined carriers for DNA and siRNA delivery [61]. Furthermore, derivatization with an amino and carboxylic acid linker of functional domains, like PEG or the targeting ligand folic acid, makes them applicable to solid-phase synthesis. Combination with natural amino acids allowed the synthesis of a huge library of efficient carriers for DNA and siRNA delivery providing multifunctionality and maintaining control of the sequence at each position [62-70].

In some cases the applied chemistry comes across limitations for the synthesis of carriers with multifunctional domains, e.g. when certain domains are incompatible with specific reaction conditions necessary for the assembly of another domain, as it can be the case for peptide-oligonucleotide conjugate assembly on solid-phase [71]. Furthermore, already existing carriers can turn out not to be optimal for a certain application leading to the need for subsequent modification. In this context other approaches for the design of precise carriers, in particular specific conjugation techniques allowing the production of covalent conjugates, come into use. A widely-utilized method is the conjugation of activated thiols

which result in biodegradable disulfide bonds. The activation of one reaction partner with a pyridylsulfenyl (Pys) or 3-nitropyridylsulfenyl (Npys) group allows the site-specific conjugation provided that only one free thiol group is present in the other reaction partner. A more stable bond can be obtained by thioether linkages between free thiols with halogen compounds or by Michael-type addition of thiols to maleimides [71]. Click chemistry, first defined by Sharpless in 2001 [72], is a further approach which amongst other features is characterized by high selectivity, high yields and simple reaction conditions making it a popular tool for the production of precise carriers. It involves different types of conjugation strategies, among which the 1,3-dipolar cycloadditon between alkines and azides forming a triazole is one of the most commonly used as it can even be performed in living organisms [73]. Click chemisty has, for example, been applied to covalently attach targeting ligands to siRNA [69, 74], demonstrating its suitability for the synthesis of precise nucleic acid carriers. A different attractive linking strategy is the native chemical ligation (NCL), which was primarily developed for the conjugation of peptide fragments in protein synthesis [75]. A modification of this approach made it applicable to ligate peptide fragments synthesized with 9-fluorenylmethoxycarbonyl solid-phase peptide synthesis (Fmoc-SPPS) [76]. This conjugation technique has been recently applied in the Wagner lab for the attachment of targeting ligands to already existing cysteine-containing sequence-defined carriers for DNA and siRNA delivery (Zhang *et al*, submitted).

A rather new approach in precise carrier synthesis is to exploit the unique property of nucleic acids to self-assemble into defined nanostructures, which can be used as delivery devices for nucleic acids [77]. In contrast to natural nucleic acids, artificial DNA structures of specific size and shape can be taken up by cells and show much higher stability to nucleases. The easy way of cargo loading by direct integration (e.g. the immunostimulatory CpG motif [78]) or hybridization of the therapeutic nucleic acid with the DNA nanostructure turn them to attractive tools for nucleic acid delivery. Promising results including prolonged blood circulation, tumor accumulation and silencing effect in a mouse model after systemic application have been achieved using a DNA tetrahedron loaded with siRNA as well as several folic acid ligands with controlled density and orientation [79]. These findings support the notion that sequence-control at every single position of the carrier and exact determination of modification sites play a key role in optimization of carrier design.

2.3 Solid-phase assisted synthesis: an approach to design sequence-defined carriers

Peptide synthesis follows the chemical principle of amide bond formation between the α-amino group of one amino acid with the α-carboxy group of another amino acid. After the first peptide bond formation between two amino acids by using acyl chlorides in 1903 [80], developments of protecting groups and coupling reagents led to the successful synthesis of the hormone oxytocin, consisting of nine amino acids, in 1954 [81]. Nevertheless, the peptide synthesis with repeated deprotection and coupling steps as well as intercalating purifications still constituted a time-consuming procedure of high effort, until Merrifield introduced the principle of solid-phase peptide synthesis (SPPS) in 1963 [82]. Here the step by step assembled peptide was attached to resin beads consisting of a chloromethylated copolymer of styrene and divinylbenzene, which is completely insoluble in the used solvents but allows penetration of the reagents. The main benefit of this method is the addition of protected amino acids in high excess that shortens reaction times and drives the coupling reaction nearly to completion. By filtration in appropriate reactors, unreacted amino acid and coupling reagents can be easily removed. After the complete assembly of the desired sequence the peptide can be cleaved from the resin in a final step. Even though during the first attempt to synthesize a tetrapeptide the great value of the principle became apparent, also the need for optimized protocols to avoid side reactions, hazardous reactants or solvents and to improve yields and purities of the obtained peptides was recognized. In 1972, Carpino et al. [83] presented the 9-fluorenylmethoxycarbonyl (Fmoc) as a base-labile protection group for the N-terminus of the peptide, which is stable under the reaction conditions during SPPS and constitutes orthogonality to acid-labile side chain protection groups. It did not gain much attention until the chemical industry became aware of the potential provided by this strategy and made the spectrum of easy producible Fmoc-protected amino acids commercially available. A further advantage is given by the high UV absorption of the fluorene derivatives, which enables monitoring of the reaction process and facilitates automation of peptide synthesis. Nowadays, the Fmoc strategy is established as the standard procedure for SPPS besides the classical *tert*-butyloxycarbonyl (Boc) strategy.

Hartmann *et al* first used the solid-phase synthesis technique for the assembly of defined polyaminoamides (PAAs) by alternating coupling steps of diacids, activated as cyclic anhydrides, and diamines [84]. For PAAs with five diamine blocks the monodisperse chemical structure could be demonstrated and attachment of functional domains resulted in

useful DNA complexation systems [85]. Nevertheless, synthesis of longer PAAs bears the potential of cross-linking reactions when adding the diamine to the activated carboxylic acid residues (Schaffert, PhD thesis, 2010). In this context, Schaffert *et al* optimized this strategy by combining the diacid (succinic acid) and the diamine (tetraethylene pentamine) in one building block [61]. Properly protected with the acid-labile Boc protecting group at the secondary amines and the base-labile Fmoc group at the primary terminal amine, the resulting artificial amino acid Stp(boc)$_3$-OH was used for the synthesis of a wide spectrum of sequence-defined carriers for nucleic acid delivery [63, 66-68, 86].

Taking advantage of the SPPS strategy, Mixson and coworkers synthesized highly-branched peptides consisting of lysine and histidine and demonstrated their potency for DNA [87] and siRNA delivery [88]. Also EHCO, an amphiphilic surfactant containing histidine, cysteine and oleoyl tails was synthesized by Lu and colleagues by combination of organic synthesis and classical peptide bond formation, both performed on solid-phase [89]. Based on this lipopeptide further modification by PEG shielding and attachment of the peptide bombesin as a targeting ligand resulted in an efficient siRNA delivery system [90].

Andaloussi *et al* exploited the strategy of SPPS for the assembly of PepFect6, which had proven to be an efficient siRNA carrier [58]. The synthesis of the CPP transportan-10 (TP-10) as well as the subsequent stearylation and attachment of a chloroquine analog were performed on solid-phase thereby ensuring the precise structure of this carrier system.

All mentioned examples emphasize the suitability of SPPS for the synthesis of synthetic vectors for nucleic acid delivery and especially the opportunity for rational design due to sequence control at every single position of the assembled molecule. In addition, the described studies also reveal that not only classic amino acids can be applied, but also a wide diversity of functional domains can be incorporated by the means of solid-phase synthesis.

2.4 Impact of size on gene carrier properties

Besides remarkable success in the use of lipidic carriers for nucleic acid delivery, cationic polymers have gained great attention among the synthetic vectors. Due to its remarkable DNA condensation efficiency PLL has been widely used in delivery systems for DNA [91] and for siRNA [92]. Normally synthesized by N-carboxy anhydride polymerization, it is commercially available in a wide MW range from 500 Da up to over 200 kDa. Testing PLL of

different polymerization degrees (4 – 224 kDa) for DNA binding and transfection efficiency, revealed a clear influence of the MW on its properties as a gene carrier [93]. Whereas the maximum DNA binding was found for PLL of intermediate MW (24 kDa), a clear increase of transfection efficiency was found with increasing MW up to the MW of 53.7 kDa. Also PEI became a commonly used DNA delivery agent due to its great efficiency for nucleic acid transfection, but cytotoxicity as well as polydispersity are inherent characteristics of the polymer that need to be addressed before its safe therapeutical application. By now, evidence has emerged indicating that the cytotoxicity of cationic polymers is often correlated with their molecular weight (MW), showing greater cytotoxicity with increasing MW [94-96]. Therefore several studies have been performed modifying the original PEI structure (22 kDa linear or 25 kDa brPEI) aimed at decreasing the cytotoxicity while simultaneously maintaining or even increasing the delivery efficiency. These include the conjugation of low molecular weight (LMW) PEI via biodegradable linkages [97-103], the attachment of LMW PEI to other polymer backbones [104, 105] or the functionalization of the amine groups of the native PEI for the purpose of changing its chemical and thus biological properties [46, 106-108]. In contrast to consistent data regarding the cytotoxicity dependency on MW, for the transfection efficiency contradictory findings were published. Whereas Godbey *et al* found a correlation of higher gene transfer with increasing MW from 1.8 to 70 kDa [109], Werth *et al* could isolate a low MW fraction around 4 – 10 kDa out of the 25 kDa brPEI with enhanced efficiency compared to the original polymer [96]. Comparing in vivo gene transfer to the brain of 25, 50 and 800 kDa PEI, Abdallah *et al* identified the 25 kDa sample as the most potent one [110]. These opposing findings point out the general importance of MW for gene transfer activity, but do not allow general conclusions. In order to set up precise correlations it must always be considered which specific MW range has been analyzed.

Based on the artificial amino acid succinyl-tetraethylene pentamine (Stp), PEI analogs have recently been designed in order to overcome the already mentioned main disadvantages of PEI [61]. Both carriers contain the diaminoethane motif responsible for nucleic acid complexation and endosomal buffering. Properly protected (Fmoc/tBoc) Stp is applicable to standard Fmoc-based SPPS, thus allowing the synthesis of precise, sequence-defined carriers [63, 111] and the controlled variation of size. A simple linear sequence of five Stp units was found inactive in gene transfer [111]. This was not surprising as the number of only 16

protonatable nitrogens was much smaller than the approximately 500 (±200) protonatable nitrogens of standard linear PEI (LPEI). Nevertheless, the general knowledge of the size-dependency of transfection efficiency and the initial finding that increasing the number of Stp units improved DNA binding and gene transfer provided the basis for further evaluations of the effect of MW on the properties of the described structures in the course of this thesis.

2.5 Influence of topology on gene carrier properties

Cationic polymers have gained more and more interest as synthetic carriers for nucleic acid delivery. The importance of carrier topology for the purpose of modulating their biophysical properties and biological performance has long been recognized. Differences in biophysical characteristics and in the transfection efficiency of brPEI and LPEI have been shown in several studies [112, 113]. Wightman *et al* found a much higher aggregation tendency of LPEI in salt-containing solution, but a 10- to 100-fold better transfection efficiency compared to brPEI under saltfree conditions [112]. Also Kwok *et al* found better performance of LPEI for DNA delivery [113]. However, LPEI was completely inactive for siRNA transfer, whereas brPEI displayed considerable knockdown. These findings are explained based on the different PEI structures, resulting in differing basicity of incorporated amines determining the nucleic acid condensation ability. A study using PAAs with different branched architectures reported an improved DNA compaction ability and buffer capacity, and therefore enhanced transfection efficiency with increasing degree of branching [114].

Further polymeric carriers that have been extensively investigated for DNA and siRNA delivery are the hyperbranched PAMAM dendrimers and their modifications [52, 53, 115, 116]. The change of topology by using a triethanolamine core instead of commonly used diamines provides the dendrimer with increased flexibility and high efficiency for siRNA delivery [116]. This modification is based on the finding that partially degraded PAMAM shows better flexibility and DNA complexation ability [117]. To gain deeper insight into the influence of polymer structure on DNA complexation and polyplex morphology, Tang *et al* compared the DNA interaction and polyplex formation of four polycations, namely PLL, intact PAMAM dendrimer, fractured PAMAM dendrimer and PEI [118]. According to the measured biophysical properties of the carrier and the corresponding particles formed with DNA, the authors concluded that the polymer structure and MW are only minor determinants of DNA binding ability, particle size and morphology, but the individual type of

polymer greatly influences the aggregation tendency. However, the polymer structure greatly impacts on the polymer flexibility and buffer capacity, constituting two parameters with distinct effect on the transfection efficiency.

Several studies have investigated the effect of varying the length of oligoamine moieties in polymeric carriers on biophysical properties, buffer capacity and especially nucleic acid transfection efficiency [68, 119-121]. Significant effects of the number and type of amines and total amine density have been demonstrated. Uchida *et al* reported an "odd-even effect", stating an enhanced buffer capacity and transfection efficiency for polymers containing even-numbered ethylenamine side chains [120], emphasizing the number of protonatable amines in row. The importance of the spacer length between the amino groups was revealed by Lin *et al* showing that the extension of the ethylene unit to propylene reduced the transfection efficiency and increased the toxicity [119], pointing out the importance of the spacer length between the amino groups.

More recently, in order to overcome the main disadvantage of cationic polymers, namely their polydispersity and significant toxicity as known for PEI [122-124], novel analogs containing defined smaller ethylenimine units were designed [98, 99, 101, 102, 125-127]. For example, the diaminoethane motif was introduced into the artificial amino acid Stp [61]. This motif was found to be effective for nucleic acid binding and endosomal buffering and thus provides the basis for the production of precise, sequence-defined carriers [54, 63, 64, 67, 68, 111, 128]. The importance of carrier topology was once more emphasized by the finding that 3-arm and 4-arm branched or differently shaped structures, which vary in the site of fatty acid modification, can differ greatly in terms of DNA binding and transfection efficiency [63]. Besides structural changes also the use of oligo(aminoethane) building blocks of different length was shown to have considerable influence on the DNA binding characteristics and the buffering profile [66]. These findings underline the importance of investigating structure-activity relationships by variation of structure as well as of total number and type of the amine for the optimization of carrier design.

2.6 Aim of the thesis

Gene delivery holds great promise for the treatment of several incurable diseases by directly addressing the cause of the dysfunction. Major drawbacks result from the fact that nucleic

acids, in contrast to many protein- or peptide-based therapies, have their place of action inside the cell and for this reason need an appropriate delivery system.

Based on the prevailing notion that polymer length is a major determinant of carrier efficacy, the first aim of this thesis was to investigate the effect of increasing MW on the properties of precise cationic carriers for DNA delivery. More specifically, it had to be explored if an exclusive enlargement of the carrier size could compensate for the lack of additional functional domains, thus eliminating the commonly recognized requirement for stabilization motifs or endosomal release helper domains. For this purpose a small library of linear oligo(ethanamino)amides of increasing chain length had to be synthesized in order to systemically examine the influence of different MWs on biophysical and biological carrier properties. The findings of this study should provide fundamental insights for the design of sequence-defined oligo(ethanamino)amide carriers.

With increasing carrier size, conventional methods for analytical characterization as NMR and mass spectrometry (MS) reach their threshold of applicability and can be applied adequately only with distinct expertise. This limitation determined a further focus of the thesis, namely finding suitable methods for the analytical characterization of precise, polycationic oligo(ethanamino)amide carriers. Capillary electrophoresis (CE) and Taylor dispersion analysis (TDA) were to be tested in a collaboration project for their application for the analysis of oligomers of increasing length, both representing methods of great potential for the characterization of charged species of a wide range of MW.

Besides the concept of size regulation, the modulation of functionality and topology constitutes a further promising approach to address the overriding objective of carrier optimization. In this context, as the second major aim of the thesis, a new comb-like topology was introduced and had to be optimized by subsequent application of different functionalities to this novel structural class. These functionalities included domains for DNA condensation and polyplex stabilization as well as components for modulating the endosomal buffering, all aimed at designing efficient carriers for DNA delivery. The final aim of the thesis was to work out the specific impact of carrier topology by directly comparing the most relevant carrier properties of these new comb-type structures with the corresponding linear ones. By this means the influence of changes in topology on relevant biophysical and biological features should be elucidated.

3 MATERIALS AND METHODS

3.1 Chemicals and reagents

Trityl OH-ChemMatrix resin was obtained from Biotage (Uppsala, Sweden). Allyl alcohol, N,N-dimethyl-barbituric acid (N,N-DMBA), 1-hydroxybenzotriazol (HOBt), tetrakis(triphenylphosphine)-palladium ($Pd(Ph_3P)_4$), triisopropylsilane (TIS), Triton X-100, hydrazine monohydrate, 2,2,2-trifluoroethanol (TFE), N-ethylmorpholine (NEM), 3-(4,5-dimethylthiazol-2-yl) - 2,5 - diphenyltetrazolium bromide (MTT), diethylene triamine (DETA), triethylene tetramine (TETA), tetraethylene pentamine (TEPA) and pentaethylene hexamine (PEHA) were purchased from Sigma-Aldrich (Munich, Germany); benzotriazol-1-yl-oxy-tris-pyrrolidino-phosphonium hexafluoro-phosphate (PyBOP), 2-(1H-benzotriazole-1-yl)-1,1,3,3-tetramethyluronium hexafluorophosphate (HBTU), and microreactors for manual and automatic synthesis from MultiSynTech (Witten, Germany). Linear PEI (LPEI, 22kDa average MW) was synthesized as described previously [129]. Fmoc-PEG_{24}-OH was obtained from Quanta biodesign (Powell, Ohio, USA) and trifluoroacetyl pteroic acid from Niels Clauson-Kaas A/S (Farum, Denmark). All other amino acids, peptide grade dimethylformamide (DMF), peptide grade N-methylpyrrolidone (NMP), diisopropyl-ethylamine (DIPEA) and trifluoroacetic acid (TFA) were purchased from Iris Biotech (Marktredwitz, Germany). Sephadex G-10 material for size exclusion chromatography was obtained from GE Healthcare (Freiburg, Germany). GelRed was purchased from Biotum Inc. (Hayward, USA). Cell culture media, antibiotics and fetal calf serum (FCS) were purchased from Invitrogen (Karlsruhe, Germany). Plasmid pCMVLuc was produced with the Qiagen Plasmid Giga Kit (Qiagen, Hilden, Germany) according to the manufacturer protocol. Cy5-labeling kit for pDNA labeling was obtained from Mirus Bio (Madison, WI, USA). Luciferase cell culture lysis buffer and D-luciferin sodium salt were obtained from Promega (Mannheim, Germany). CellTiter-Glo®Reagent was purchased from Promega (USA). Solvents and all small molecule reagents were bought in high quality from Sigma-Aldrich (Steinheim, Germany), Iris Biotech (Marktredwitz, Germany), AppliChem (Darmstadt, Germany) or Merck (Darmstadt, Germany), unless otherwise indicated. Water was used as purified, deionized water.

3.2 Solid-phase assisted peptide synthesis – general procedures

3.2.1 Automated peptide synthesis

The automated microwave peptide synthesis was performed on the Syrowave® system from Biotage AB (Uppsala, Sweden) applying the standard Fmoc/tBu protecting group strategy. Exact synthesis procedure is described in the sections 3.3 and 3.4. As solid support a 2-Chlorotrityl Chloride resin or Trityl-ChemMatrix resin was used. All structures were synthesized in a 7 to 15 µmol scale using a 2 mL or 5 mL syringe reactor. For automated synthesis the resin was pre-swollen for 20 min in NMP and for manual synthesis in DCM.

3.2.2 Resin loading

Loading of a Chlorotrityl Chloride resin with Dde-Lys-Fmoc-OH. 0.8 mmol of a chlorotrityl chloride resin (516 mg) were pre-swollen in DCM (1 mL/100 mg resin) for 15 min and Dde-Lys-Fmoc-OH (0.8 eq) and DIPEA (1.6 eq) dissolved in DCM (dried over $CaCl_2$) were added to the resin for 3 h. After draining the reaction solvent a mixture of DCM/MeOH/DIPEA (80/15/5) was added twice for 15 min. After the removal of the reaction mixture, the resin was washed 5 times with DCM (1 mL/100 mg resin). Some resin was separated for determination of the resin loading and the remaining resin was treated 3 times for 5, 10 and 20 min with 20 % piperidine in DMF for removal of the N^{α}-Fmoc protection group. Deprotection was checked by a positive Kaiser test. Afterwards, the resin was washed 3 times with DMF and DCM and dried in vacuum.

Loading of a Chlorotrityl Chloride resin with Fmoc-Cys-Trt-OH. 0.8 mmol of a chlorotrityl chloride resin (516 mg) were pre-swollen in DCM (1 mL/100 mg resin) for 15 min. Fmoc-Cys-Trt-OH (0.4 eq) and DIPEA (0.8 eq) were dissolved in DCM (dried over $CaCl_2$) and added to the resin for 45 min to obtain a low loaded resin of 0.1 to 0.3 mmol/g. Subsequent steps were performed as described above for the loading of a chlorotrityl chloride resin with Dde-Lys-Fmoc-OH.

Loading of ChemMatrix-Trityl resin. 0.5 g ChemMatrix-Trityl-OH resin (0.2 mmol) were swollen in 3.3 mL DCM (1 mL/100 mg resin, dried over $CaCl_2$). 67 µL $SOCl_2$ were added to get a final concentration of 2 % $SOCl_2$ in DCM. The vessel was shaken over night. Then the resin was drained and rinsed with DCM (5 x 3 ml) and 2 % N-ethyl morpholine (NEM) in DCM (3 x 3 ml). Afterwards Fmoc-Cys(Trt) (0.6 mmol, 3 eq) and NEM (4 eq) dissolved in DCM were

added and the vessel was shaken over night. After addition of 167 µL of a solution of 25 % NEM in methanol and shaking for 1 h the resin was drained and rinsed 3 times each with 3 mL DCM, DMF, methanol and diethyl ether. The resin was dried over night at room temperature. Some resin was separated for determination of the resin loading.

Loading of a Chlorotrityl Chloride resin with Fmoc-Stp-(boc)$_3$-OH. 0.8 mmol of a chlorotrityl chloride resin (516 mg) were pre-swollen in DCM (1 mL/100 mg resin) for 15 min and Fmoc-Stp-(boc)$_3$-OH (0.8 eq) and DIPEA (1.6 eq) dissolved in DCM (dried over $CaCl_2$) were added to the resin for 2.5 h. After draining the reaction solvent a mixture of DCM/MeOH/DIPEA (80/15/5) was added twice for 15 min. After the removal of the reaction mixture, the resin was washed 5 times with DCM (1 mL/100 mg resin). Some resin was separated for determination of the resin loading and the remaining resin was treated 3 times for 5, 10 and 20 min with 20 % piperidine in DMF to remove the N^{α}-Fmoc protection group. Deprotection was checked by a positive Kaiser test. Afterwards, the resin was washed 3 times with DMF and DCM and dried in vacuum.

Loading of a Chlorotrityl Chloride resin with Fmoc-β-Ala-OH. 0.8 mmol of a chlorotrityl chloride resin (516 mg) were pre-swollen in DCM (1 mL/100 mg resin) for 15 min. Fmoc-β-Ala-OH (0.4 eq) and DIPEA (0.8 eq) were dissolved in DCM (dried over $CaCl_2$) and added to the resin for 45 min. All subsequent steps were performed as described above for the loading of a chlorotrityl chloride resin with Fmoc-Stp-(boc)$_3$-OH.

3.2.3 Determination of the resin loading – Fmoc quantification

For determination of the resin loading about 10 mg of the resin were separated from the main batch and dried under vacuum. An exact amount of resin was then treated with 1 mL deprotection solution (20 % piperidine in DMF) for 1 h, diluted in DMF and UV absorption was measured at 301 nm. Finally, the resin loading in [mmol/ g] is obtained by the following equation:

resin load [mmol/g] = (A*1000) / (m [mg]*7800*d_f) with d_f as dilution factor.

3.2.4 Kaiser test

Kaiser test was used for qualitative detection of free amino groups on the resin. For this purpose a small amount of resin beads, previously washed 3 times with DMF and 3 times with DCM, were transferred to an Eppendorf tube. One drop of each 80 % (w/v) phenol in

EtOH, 5 % (w/v) ninhydrin in EtOH and a solution of 0.02 mM KCN in pyridine were added to the resin and the tube heated for 4 min at 99 °C. In the absence of free amino groups the beads remained colorless and the solution yellow (negative Kaiser Test). The presence of free amino groups was indicated by a blue coloration of the resin beads and the solution (positive Kaiser test).

3.2.5 Synthesis of diaminoethane motif-containing building blocks

The cationic building blocks Stp(boc)$_3$-Fmoc and Sph(boc)$_4$-Fmoc were synthesized as described in [61] and [68], respectively. Briefly, the synthesis is based on selective protection of the primary amines of TEPA (for Stp(boc)$_3$-Fmoc) or PEHA (for Sph(boc)$_4$-Fmoc) with ethyl trifluoroacetate and subsequent Boc-protection of the secondary amines with di-tert butyl dicarbonate. Deprotection of the primary amines is done with NaOH. Assymetrical functionalization of one amine group with Fmoc-Osu and the other one with succinic anhydride results in the desired products that are purified with dry column vaccum chromatography (DCVC).

Synthesis of Boc-protected building block Stp(boc)$_4$-OH **5**

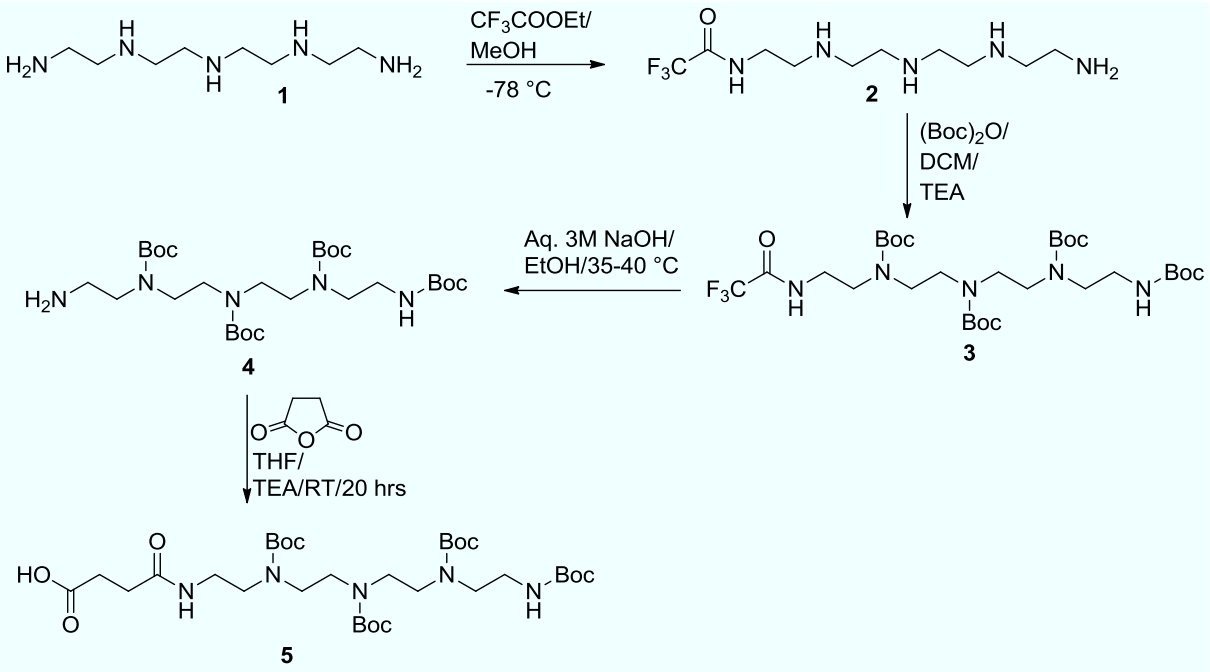

Synthesis of tfa-tetraboc-TEPA **3**

Tetraethylenepentamine hydrochloride (TEPA*HCl) (**1**) (22.58 g, 100 mmol, 1 eq, technical grade) was dissolved in 400 mL dry MeOH. Following addition of TEA (50.6 g, 5 eq) the mixture was stirred for 2 h and cooled down to -78 °C. Ethyl trifluoroacetate (14.2 g, 100 mmol, 1 eq) was diluted in 50 mL dry MeOH and added dropwise to the cooled mixture over 45 min. The temperature was then increased to 0 °C and the reaction mixture was stirred for 1 h. Without intermediate purification step, the remaining amines were protected by di-tert butyl dicarbonate. Therefore, first TEA (50.6 g, 500 mmol, 1.25 eq/amine) was added and stirred at 0 °C for 20 min. In the next step di-*tert*-butyl dicarbonate (109.07 g, 500 mmol, 1.25 eq/amine) was dissolved in 200 ml dry MeOH and added dropwise over 60 min at 0 °C. The mixture was stirred over night.

The organic phase was concentrated to remove MeOH and the residue was dissolved in DCM. It was washed 3 times with 100 mL of a saturated $NaHCO_3$ solution and then 3 times with H_2O. The organic phase was dried over Na_2SO_4 anhydrous and the solvent was evaporated to obtain a yellowish viscous liquid.

The yellow, oily residue was recrystallized from a minimum amount of about 30 mL boiling DCM under reflux. For this purpose precooled *n*-hexane was added slowly to the boiling DCM till clouding was observed at the drop-in site. The crystallization solution was stored over night at 4 °C. The microcrystalline residue was filtered, washed 3 times with cooled *n*-hexane and dried. Yield 37.4 g (54.5 mmol, 54.5 %). ^{1}H NMR (400 MHz, $CDCl_3$): δ 1.42 (s, 36H –CH_3 ter-But), 3.3-3.45 (m, 16H, -CH_2- Tepa) ppm.

Synthesis of tetraboc-TEPA **4**

To a suspension of compound **3** (34.25 g, 50 mmol) in EtOH (380 mL) a 3 M aqueous NaOH solution (175 mL) was slowly added under stirring and the reaction mixture was heated up to 40-50 °C until the solution was clear. The reaction mixture was stirred over night. The EtOH was evaporated and the aqueous phase was extracted 3 times with 150 mL DCM. The organic phase was dried over $NaSO_4$ and the solvent was evaporated, yielding an amorphous solid which was dried under high vacuum and stored at 4 °C. Purification was performed by DCVC (DCM/ MEOH; 10:0 to 7:3 v/v).

Yield: 11 g (18.7 mmol, 37, 3 %). ^{1}H NMR (400 MHz, $CDCl_3$): δ 1.42 (s, 36H –CH_3 ter-But), 3.3-3.45 (m, 16H, -CH_2- Tepa) ppm.

Synthesis of Stp(boc)$_4$-OH **5**

To a solution of compound **4** (11 g, 18.7 mmol, 1 eq) in THF (200 mL) TEA (2.81 g, 28.05 mmol, 1.5 eq) was added followed by dropwise addition of succinic anhydride (2.24 g, 22.44 mmol, 1.2 eq) in THF (50mL) at room temperature over 30 min and overnight stirring. H_2O (200 mL) was then added to the mixture and stirred for 1 h before THF was subsequently evaporated completely under vacuum. For purification H_2O (100 mL) and an aqueous solution of $NaHSO_4$ (5 % w/v, 200 mL) were added to the reaction mixture and extracted with pure DCM (4 x 80 mL). The organic phase was dried with Na_2SO_4, the solvent was concentrated and dried in high vacuum to get a white solid, which was directly used for solid-phase peptide synthesis.

Yield: 11 g (15.95 mmol, 85, 3 %). ^{1}H NMR (400 MHz, $CDCl_3$): δ 1.42 (s, 36H –CH_3 ter-But), 2.45-2.65 (m, 4H, -CH_2- succ), 3.3-3.45 (m, 16H, -CH_2- Tepa) ppm.

Synthesis of Boc-protected building blocks Sdt(boc)$_2$-OH and Stt(boc)$_3$-OH

The building blocks were synthesized in analogy to the protocol for Stp(boc)$_4$-OH, but using DETA (for Sdt(boc)$_2$-OH synthesis) and TETA (for Stt(boc)$_3$-OH synthesis) instead of TEPA.

(Sdt(boc)$_2$-OH and Stt(boc)$_3$-OH were synthesized by Dr. Naresh Badgujar (LMU, postdoctoral fellow).

Synthesis of Boc-protected building block Sph(boc)$_5$-OH

Sph(boc)$_5$-OH was synthesized in analogy to the protocol for Stp(boc)$_4$-OH with some modifications described in the following. For purification pentaethylene hexamine (PEHA, technical grade) was first converted into the hydrochloride salt. For this 40 mL PEHA were dissolved in 180 mL MeOH and cooled in an ice-bath. Concentrated HCl was added dropwise while stirring and a precipitate formed after the addition of about 60 mL. This was filtered, washed with acetone and ether and dried in vacuum. Tfa-pentaboc PEHA was synthesized in analogy to the protocol for tfa-tetraboc-TEPA. In the following step, to a suspension of tfa-pentaboc PEHA (24.87 g, 30 mmol) in EtOH (400 mL) and 50 mL DCM, a 3 M aqueous NaOH solution (175 mL) was slowly added under stirring and the reaction mixture was heated up to

50-60 °C until the solution was clear. The reaction mixture was further stirred over night, the solvent was evaporated and the aqueous phase was extracted 3 times with 200 mL DCM. The organic phase was dried over $NaSO_4$ and the solvent was evaporated, yielding an amorphous solid which was dried under high vacuum and stored at 4 °C. Purification was performed by DCVC (DCM/ MEOH; 10:0 to 7:3 v/v).

Yield: 11 g (18.7 mmol, 37, 3 %). ^{1}H NMR (400 MHz, $CDCl_3$): δ 1.42 (s, 45H –CH_3 ter-But), 3.3-3.45 (m, 20H, -CH_2- Peha) ppm.

3.3 Synthesis of linear (ethanamino)amide oligomers

Two different strategies were initially tested for the oligomer synthesis, namely the successive coupling of single Stp units or the stepwise attachment of blocks of 5 Stp units in a convergent manner. The convergent strategy was initially used with the aim of saving time during the assembly of long sequences, but at room temperature inefficient couplings were found to occur. The subsequent application of microwave irradiation during coupling and deprotection steps however demonstrated the suitability of both methods under these conditions. Using the later established automated synthesis strategy with successive couplings was less time-consuming and therefore preferentially used.

3.3.1 Oligomer assembly with successive couplings

The oligomers were assembled on a ChemMatrix-Trityl-Fmoc-Trp(boc) resin with a loading between 0.2 and 0.3 mmol/g pre-swollen in NMP for 20 min. Until cycle 10 N^{α}-Fmoc deprotection was performed 3 min at 50 °C with 40 % piperidine in DMF, followed by 3 min with 20 % piperidine in DMF at 60°C and 10 min at 50°C. Amino acids (4 eq, 0.2 – 0.5 M) were dissolved in HOBt (4 eq) in NMP, DIPEA (8 eq) was dissolved in NMP and HBTU (4 eq) was dissolved in DMF. Single couplings were performed from cycle 1 to 10 for 8 min at 75 °C. From cycle 11 on double couplings were performed for 6 minutes at 75 °C. Fmoc-deprotection was performed as described above for the previous cycles but with an additional deprotection step for 5 min at 50 °C with 20 % piperidine in DMF. After each deprotection as well as each coupling step the resin was washed 5 times with DMF.

Cleavage of oligomers from the resin

Cleavage from the resin was performed by treatment with a cleavage solution containing TFA/TIS/H_2O (95/2.5/2.5) for 1.5 h. After washing the resin twice with TFA and twice with

DCM all solutions were combined, concentrated and precipitated by dropwise addition into a mixture of n-hexane and MTBE (1:1) cooled to -20 °C. The pellet after centrifugation was dried under nitrogen and dissolved in the buffer for size exclusion containing 10 mM HCl and 30 % ACN. After purification by size exclusion on a G-10 column the appropriate fractions were combined, frozen in liquid nitrogen and lyophilized.

3.3.2 Oligomer assembly via convergent coupling strategy

Convergent synthesis of Fmoc-[Stp(boc)$_3$]$_5$-OH and Fmoc-[Stp(boc)$_3$]$_5$- β-Ala-OH

After swelling 500 mg of a Fmoc-Stp(boc)$_3$-OH chlorotrityl resin (loading 0.35 mmol/g) in DCM for 20 min, Fmoc-Stp(boc)$_3$-OH (3 eq) and DIPEA (6 eq) dissolved in DCM and PyBOP/HOBt (3 eq) dissolved in DMF were added for 2 h. The reaction solvent was drained and the resin was washed 3 times with DMF and DCM. If necessary, the coupling was repeated with 2 eq of Fmoc-Stp(boc)$_3$-OH until Kaiser test was negative. For removal of the Fmoc protecting group, the resin was treated with 20 % piperidine in DMF 3 times for 10 min and complete deprotection was monitored with a positive Kaiser test. After washing the resin with DMF and DCM the same procedure was repeated 3 times without Fmoc deprotection after the last coupling step. Indicating a negative Kaiser test, the resin was washed 5 times with DCM and dried in vacuum.

For the synthesis of *Fmoc-[Stp(boc)$_3$]$_5$-β-Ala-OH* a Fmoc-β-Ala-OH chlorotrityl resin (loading 0.35 mmol/g) was used and the coupling of Fmoc-Stp(boc)$_3$-OH was repeated 5 times as described above.

Cleavage of the convergent building blocks from the resin

A mixture of 30 % TFE in DCM (1 mL/80 mg resin) was added to the resin and replaced every 30 to 60 min. The reaction progress was monitored by TLC with a mobile phase of $CHCl_3$/MeOH (9/1) containing 1 % HOAc. Cleavage was finished when no absorption was detected on a thin layer chromatography plate anymore. All cleavage solutions were collected, the solvent evaporated and dried under vacuum.

Synthesis of [Stp5]$_8$-W with convergent building blocks

30 mg of the ChemMatrix resin loaded with Fmoc-Trp(boc)-OH (0.262 mmol/g) were pre-swollen in NMP. Subsequently, the convergent building block Fmoc-Stp(boc$_3$)$_5$-OH (4 eq) and DIPEA (8 eq) dissolved in a minimum amount of NMP, and HBTU/HOBt (4 eq) dissolved in a

minimum amount of DMF were added for 8 min for the first 4 couplings at 75 °C. For the last 4 couplings the coupling time was elongated to 10 min. Reaction progress was monitored by Kaiser test. For Fmoc deprotection the resin was treated twice with a solution of 20 % piperidine in DMF for 4 min at 60 °C and again monitored by Kaiser test. After the third coupling Fmoc deprotection was performed by several treatments of 5 min with a solution containing 20 % piperidine, 2 % DBU and 1 % Triton X-100 in DMF until the UV absorption at 301 nm of the deprotection solution was below 0.1.

Synthesis of [Stp5-βA]$_6$-W with convergent building blocks

To 25 mg of the pre-swollen ChemMatrix resin loaded with Fmoc-Trp(boc)-OH (0.22 mmol/g) the convergent building block *Fmoc-[Stp(boc)$_3$]$_5$*-β-*Ala-OH* (2 eq) and DIPEA (4 eq) dissolved in NMP and HBTU/HOBt (2 eq) dissolved in DMF were added for 45 min at 60 °C. For Fmoc deprotection the resin was treated twice (4 min and 20 min) with a solution of 20 % piperidine in DMF at 50 °C.

3.4 Synthesis of comb structure oligomers

Two different strategies, a convergent manual and an automated synthesis were established. Suitability of both methods was demonstrated (Figure 19), but the less time-consuming automated synthesis was preferentially used.

3.4.1 Comb structures synthesis with convergent coupling strategy

Convergent synthesis of Fmoc-Lys-Stp(boc)$_4$

After swelling 0.15-0.2 mmol of a Dde-Lys-OH chlorotrityl resin in DCM for 20 min, Stp(boc)$_4$-OH (4 eq) and DIPEA (8 eq) dissolved in DCM and PyBOP/HOBt (4 eq) dissolved in DMF were added for 90 min. The reaction solvent was drained and the resin was washed 3 times with DMF and DCM. If necessary, the coupling was repeated until Kaiser test was negative. For removal of the N$^{\varepsilon}$-Dde protection group, the resin was treated with 2 % hydrazine in DMF for 5 min and the procedure was repeated until the UV absorption of the deprotection solution measured at 290 nm was below 0.1. After washing the resin with DMF and DCM, Fmoc-Cl (6 eq) and DIPEA (12 eq) in DCM were added twice for 30 min. After a negative Kaiser test, the resin was washed 5 times with DCM and dried in vacuum.

Convergent synthesis of Fmoc-Ala-Lys-[Stp(boc)$_4$]-OH

After swelling 0.15-0.2 mmol of a Dde-Lys-OH chlorotrityl resin in DCM for 20 min, Stp(boc)$_4$-OH (4 eq) and DIPEA (8 eq) dissolved in DCM and PyBOP/HOBt (4 eq) dissolved in DMF were added for 90 min. The reaction solvent was drained and the resin was washed 3 times with DMF and DCM. If necessary, the coupling was repeated until Kaiser test was negative. For removal of the N$^{\varepsilon}$-Dde protection group, the resin was treated with 2 % hydrazine in DMF for 5 min and repeated until the UV absorption of the deprotection solution measured at 301 nm was below 0.1. After washing the resin with DMF and DCM, Fmoc-Ala-OH (4 eq) and DIPEA (8 eq) dissolved in DCM and PyBOP/HOBt (4 eq) dissolved in DMF were added for 90 min. After a negative Kaiser test, the resin was washed 5 times with DCM and dried in vacuum.

Convergent synthesis of Fmoc-His(boc)-Lys-[Stp(boc)$_4$]-OH

The synthesis was performed analogously to the synthesis of Fmoc-Ala-Lys-[Stp(boc)$_4$]-OH using Fmoc-His(boc)-OH instead of Fmoc-Ala-OH.

Cleavage of the convergent building blocks from the resin

A mixture of 30 % TFE in DCM (1 mL/80 mg resin) was added to the resin and replaced every 30 to 60 min. The reaction progress was monitored by TLC with a mobile phase of $CHCl_3$/MeOH (9/1) containing 1 % HOAc. Cleavage was finished when no UV absorption was detected on a thin layer chromatography plate anymore. All cleavage solutions were collected, the solvent evaporated and dried under vacuum.

Comb structure assembly with convergent building blocks

To the pre-swollen resin loaded with Cys-Trt-OH the convergent building block (4 eq) and DIPEA (8 eq) dissolved in a minimum amount of DCM and PyBOP/HOBt (4 eq) dissolved in a minimum amount of DMF were added for 90 min and the reaction progress was monitored by Kaiser test. The coupling was repeated with new reagents until the Kaiser test was negative. For N$^{\alpha}$-Fmoc deprotection the resin was treated with a solution containing 20 % piperidine, 2 % DBU and 1 % Triton X-100 in DMF for 5 to 30 min and repeated until the UV absorption at 301 nm of the deprotection solution was below 0.1. The coupling and deprotection procedure were repeated 8 times and in the final coupling step Boc-Cys-Trt was used instead of the convergent building block.

3.4.2 Comb structures via backbone assembly and subsequent “comb” attachment

The automated microwave peptide synthesis was performed on the Syrowave® system from Biotage AB (Uppsala, Sweden). The backbone was assembled on a ChemMatrix-Trityl-Fmoc-Cys-Trt resin with a loading of around 0.28 mmol/g pre-swollen in NMP for 20 min. N^{α}-Fmoc deprotection was performed at 50 °C, twice for 3 min with 40 % piperidine in DMF, followed by 5 and 10 min with 20 % piperidine in DMF. Amino acids (4 eq, 0.23 M) were dissolved in 0.23 M HOBt in NMP, DIPEA (8 eq) was dissolved in NMP and HBTU (4 eq) was dissolved in DMF. Double couplings were performed for 8 minutes at 75 °C. After each deprotection and coupling step the resin was washed 3 times with DMF. For backbone assembly Fmoc-Lys-Dde-OH was used as well as Boc-Cys-Trt in the last coupling step. For the backbones containing a spacer amino acid, Fmoc-Ala-OH or Fmoc-His-Trt-OH was coupled after every lysine. After the backbone assembly the Dde-protecting group was removed by washing the resin with 2 % hydrazine in DMF for 5 min and the UV absorbance of the cleavage solution was checked at 290 nm. The washing was repeated until the value of absorbance was below 0.1.

Cleavage of oligomers from the resin

To cleave the oligomers from the resin, the latter was treated with a cleavage solution containing TFA/TIS/H_2O (95/2.5/2.5) for 1.5 h. Afterwards the resin was washed twice with TFA and twice with DCM. All the solutions were combined, concentrated and precipitated by dropwise addition into a mixture of n-hexane and MTBE (1:1) cooled to -20 °C. The pellet after centrifugation was dried under nitrogen and dissolved in the buffer for size exclusion consisting of 10 mM HCl and 30 % acetonitrile. After purification by size exclusion on a G-10 column the product containing fractions were combined, frozen in liquid nitrogen and lyophilized.

3.4.3 Synthesis of a targeted comb structure by the use of the Dde-Alloc orthogonality

The synthesis of C-K(PEG_{24}-FolA)-[H-K(Stp)]$_8$-C was performed as described in section 3.4.2 with the following modifications. For the backbone assembly Fmoc-Lys-Alloc-OH was used before the last coupling of the terminal Boc-Cys-Trt-OH. The Dde cleavage was performed with 10 % hydrazine in DMF in the presence of 200 eq of allyl alcohol per Alloc protection group as described in [130]. The comb attachment was done as described in the previous section. In the next step the cleavage of the Alloc group was performed as described in

[131]. Briefly, $Pd(Ph_3P)_4$ (0.1 eq per Alloc group) and N,N-DMBA (5 eq per Alloc group) were flushed under argon, protected against light and dissolved together in DCM for 4 min. The mixture was transferred to the reaction vessel and stirred for 2 h under argon. The whole procedure was repeated up to 4 times until the positive Kaiser test indicated complete removal of the Alloc protection group. Finally, the resin was washed 3 times with DCM, 5 times with 0.2 M DIPEA in DMF and 6 times with DMF. Next, Fmoc-PEG_{24}-OH (4 eq) was double-coupled for 30 min at RT and 8 min at 70 °C. Fmoc deprotection was then performed 5 min at 50 °C and repeated several times until the UV absorption of the piperidine solution at 301 nm was below 0.1. Fmoc-Glu-OtBu was coupled according to the protocol of the backbone assembly (3.4.2). Trifluoroacetyl pteroic acid was attached as described for the PEG coupling. In the last step, before the cleavage of the peptide from the resin according to the standard procedure, the trifluoroacetyl group was removed by treating four times for 30 min with a 50 % (v/v) solution of 1 M aqueous NH_3 solution and DMF.

3.4.4 Synthesis of linear control sequences

The automated microwave peptide synthesis was performed on the Syrowave® system (Biotage AB). The sequences were assembled on a ChemMatrix-Trityl-Fmoc-Cys-Trt resin with a loading of around 0.28 mmol/g pre-swollen in NMP for 20 min. N^{α}-Fmoc deprotection was performed twice for 3 min at 50 °C with 40 % piperidine in DMF, followed by 5 and 10 min with 20 % piperidine in DMF. Amino acids (4 eq, 0.23 M) were dissolved in 0.23 M HOBt in NMP, DIPEA (8 eq) was dissolved in NMP and HBTU (4 eq) was dissolved in DMF. Double couplings were performed for 8 min at 75 °C. After each deprotection and after each coupling step the resin was washed 3 times with DMF. For backbone assembly Fmoc-Lys-Boc-OH was used alternating with the spacer amino acids Fmoc-Ala-OH or Fmoc-His(Trt)-OH as well as Boc-Cys-Trt in the last coupling step. Cleavage was performed as described above for the comb oligomers (3.4.2).

3.5 Oligomer purification and analytical characterization

3.5.1 Size exclusion chromatography

Size exclusion chromatography (SEC) was performed with an Äkta Basic HPLC system (GE Healthcare, Freiburg, Germany) using a Sephadex G-10 column (60 cm) and 10 mM HCl containing 30 % ACN as eluent at a flow rate of 2 mL/min. Olgiomers were detected by UV

absorbance at wavelengths of 214, 220 and 280 nm. All product-containing fractions were combined and lyophilized.

3.5.2 ^{1}H-NMR spectroscopy

^{1}H-NMR spectra were recorded using a Jeol JNMR-GX 400 (400 MHz) or JNMR-GX 500 (500 MHz) device. Chemical shifts are reported in ppm and refer to the solvent as internal standard. Data are reported as s= singulet, d= doublet, t= triplet, m= multiplet; integration was done manually. Spectra were analyzed using MestreNova by MestReLab Research.

3.5.3 Mass spectrometry

MALDI-TOF-MS was carried out on a Bruker Daltonics Autoflex II system using a saturated solution of 2,5-dihydroxy benzoic acid (2,5-DHB) in a 1:1 mixture of H_2O/ACN with 0.1% TFA as a matrix.

3.5.4 Analytical reversed phase HPLC

Analytical reversed phase HPLC (RP-HPLC) was performed using a Waters HPLC System containing a P-900 gradient pump system under the control of the Millenium software and a Waters SunFire C_{18} (4.6 x 150 mm) column. The gradient was run from 5 % to 100 % buffer B at a flow rate of 1mL/min in 20 min with buffer A containing H_2O with 0.1 % TFA and buffer B containing ACN with 0.1 % TFA. Absorption was monitored at λ = 214 nm with a 996 Photodiode array detector.

3.5.5 Buffer capacity – pH titrations

The oligomer sample, containing 15 µmol protonatable amines, was diluted in a total volume of 3.5 mL NaCl solution (50 mM) and the pH was adjusted to 2.1 by addition of 0.1 M HCl. Afterwards, a back titration with 0.05 M NaOH solution was performed with an automatic titration system (Titrando 905 from Metrohm, Germany) until pH of 11 was reached. Furthermore a titration with 50 mM NaCl was performed and the consumption of NaOH in this control titration was substracted from the consumption in the oligomer titrations at the corresponding pH values. Percentage of buffer capacity *C* in a certain pH range (x – y), where ΔV stands for the volume consumption of NaOH in the considered pH range, was calculated according to equation (1).

$$C_{pH\ x-y} = \frac{\Delta V_{pH\ x-y} \times 0.05\ M}{0.015\ mmol} \times 100 \qquad (1)$$

3.5.6 Capillary electrophoresis

Capillary electrophoresis (CE) was performed by our collaboration partners in the laboratory of Prof. Hervé Cottet in Montpellier, France. CE analysis was carried out on a P/ACE MDQ CE system (Beckman, Fullerton, CA, USA). Hydroxypropylcellulose (HPC) coated capillary of 40.6 cm total length (30.3 cm to the UV detector) × 50 µm in diameter was used for all samples. Prior injection, the capillary was rinsed with water for 10 min and then with the background electrolyte for 5 min. Temperature of the capillary cartridge was set at 25 °C. Samples were diluted in H_2O and injected hydrodynamically at the inlet end of the capillary (20 mbar, 4 s). A voltage of +30 kV was applied and data were collected using the Beckman System Gold software at 214 nm. As background electrolyte either 10 mM HEPES (pH 7.4), 250 mM HOAc (pH 2.68) or 400 mM α-aminocaproic acid (pH 5.7) were used. Electropherograms were plotted in electrophoretic mobility scale ($P(\mu_{ep})$ *vs.* μ_{ep} or *Abs(214nm) vs.* μ_{ep}) using the following equations:

$$\mu_{ep} = \frac{lL}{t_m V} \qquad (2)$$

$$P(\mu_{ep}) = C \times Abs(t_m) \times t_m \qquad (3)$$

where μ_{ep} is the effective mobility, l is the effective capillary length to the detection point, L is the total capillary length, V is the applied voltage, t_m is the migration time of the solute, $Abs(t_m)$ is the absorbance at 214 nm, C is a normalization constant (such as the total peak area equals one unit). HPC capillary coating: fused silica capillary (Composite Metal Services, Worcester, UK) was coated using a 5 % (w/w) HPC solution. The capillary (50 µm in diameter) was filled with the polymer solution using a syringe pump at 0.03 mL/h. A stream of N_2 gas at 3 bar was used to remove the excess of HPC solution and maintained during the immobilization process of the HPC performed by heating the capillary in a GC oven (GE-14A, Shimadzu, France). Temperature program was: 60 °C for 10 min followed by a temperature ramp from 60 to 140 °C at 5 °C/min and finally, 140 °C for 20 min.

3.5.7 Taylor dispersion analysis

Taylor dispersion analysis (TDA) was performed by our collaboration partners in the laboratory of Prof. Hervé Cottet in Montpellier, France. TDA was carried out on a P/ACE MDQ CE system (Beckman, Fullerton, CA, USA). UV detection was performed at 214 nm. R_h of all samples were determined in various eluents, namely HBG, HCl, NaCl, H_3PO_4, HOAc and

HEPES at different concentrations, as indicated in the results section. Temporal variance (σ^2) (equation 4) is obtained by integration of the elution profile. With this parameter the molecular diffusion coefficient (D) (equation 5) and the hydrodynamic radius (R_h) (equation 6) can be calculated as follows:

$$\sigma^2 = \frac{\int (h_i (t - t_d)^2 dt}{\int h_i dt} \quad (4)$$

$$D = \frac{R_c^2 t_d}{24\sigma^2} \quad (5)$$

$$R_h = \frac{k_B T}{6\pi\eta D} = \frac{4\sigma^2 k_B T}{\pi\eta R_c^2 t_d} \quad (6)$$

In this context, h_i is the detector response, t_d the average elution time at peak apex, R_c the capillary radius (in meter), k_B the Boltzmann constant, T the absolute temperature (in Kelvin) and η the viscosity of the eluent. Uncoated fused silica capillaries were purchased from Composite Metal Services (Worcester, UK) with dimensions of 40.6 cm total length (30.3 cm to the UV detector) × 50 µm in diameter.

For PDADMAC coated capillaries, coating was achieved by the following steps. The capillary was flushed with 1 M NaOH for 30 min, water for 15 min, 0.2 % PDADMAC solution in water for 30 min and finally with water for 15 min. Between the experimental runs, the capillaries were purged with water for 3 min followed by 5 min rinsing with the eluent. The coating of capillaries with HPC is described in the method section capillary electrophoresis (3.5.6).

All samples were diluted in the eluent and injected hydrodynamically (35 mbar, 4 s). Under these conditions, the ratio of the injected volume to the capillary volume up to the detector did not exceed 1 %. Mobilization pressure of 50 mbar was applied with eluent vials at both ends of the capillary. The temperature of the capillary cartridge was set at 25 °C. Data were collected using the Beckman System Gold software.

3.6 Biophysical analyses

3.6.1 Polyplex formation

Polyplexes were prepared by dissolving 200 ng of pDNA and oligomers at indicated nitrogen/ phosphate (N/P) ratios each in a total volume of 10 µL HBG buffer. The polycation solution was added to the nucleic acid, rapidly mixed and incubated for 30-40 min at RT.

3.6.2 Agarose gel shift assay – pDNA binding

For pDNA gel shift assay, a 1 % agarose gel was prepared by dissolving 1.2 g agarose in 120 g TBE buffer (trizma base 10.8 g, boric acid 5.5 g, disodium EDTA 0.75 g, in 1 L of water) and heating up to 100 °C. After addition of 120 µl GelRed (1000 x) for the detection of the nucleic acid, the agarose solution was poured into the electrophoresis chamber. Polyplexes were prepared as described in section 3.6.1. To each sample 4 µL of loading buffer (prepared from 6 mL of glycerine, 1.2 mL of 0.5 M EDTA, 2.8 mL of H_2O, 0.02 g of bromophenol blue) were added before loading into the gel sample pockets. Electrophoresis was performed at 120 V for 80 min.

3.6.3 Ethidium bromide assay – pDNA condensation

DNA condensation ability was tested using the ethidium bromide (EtBr) assay. The effect of stepwise addition of polymer solution to 10 µg pDNA in 1 mL HBG containing 0.4 µg EtBr was measured at increasing N/P ratios using a Cary Eclipse spectrophotometer (Varian, Germany) at exitation wavelength of 510 nm and emission at 590 nm. Maximal fluorescence intensity was set to 100 % for the EtBr solution containing free nucleic acid and fluorescence decrease was measured 0.5 min after each addition of polymer aliquot.

3.6.4 Dynamic light scattering – particle size and zeta potential

Particle size and zeta potential of polyplexes were measured by dynamic laser-light scattering (DLS) using a Zetasizer Nano ZS (Malvern Instruments, Worcestershire, U.K.). 5 µg of pDNA were used for polyplex formation in 500 µL HEPES pH 7.4. Before measurement 400 µL HEPES were added. Measurements were performed as triplicates.

3.7 Biological evaluation

3.7.1 Cell culture

Cell culture experiments were performed in our laboratory by Petra Kos (PhD student, LMU). Mouse neuroblastoma cells Neuro2A were grown in Dulbecco's modified Eagle's medium (DMEM), supplemented with 10 % FCS, 4 mM stable glutamine, 100 U/mL penicillin, and 100 μg/mL streptomycin, at 37 °C in humidified atmosphere containing 5 % CO_2 in air.

Human cervic carcinoma cells KB were grown in folate free RPMI-1640 medium, supplemented with 10 % FCS, 4 mM stable glutamine, 100 U/mL penicillin, and 100 μg/mL streptomycin, at 37 °C in humidified atmosphere containing 5 % CO_2 in air.

3.7.2 Flow cytometry – cellular association and internalization

Flow cytometry was performed by Petra Kos (PhD student, LMU). Neuro2A cells were seeded into 24-well plates coated with collagen at a density of 50,000 cells per well. After 24 h, culture medium was replaced with 400 µL fresh growth medium. Polyplexes prepared at N/P 12 in 100 µL HBG, containing 1 µg pDNA (20 % of the nucleic acid was Cy5-labeled) were added to each well and incubated either at 37 °C for internalization, or at 0 °C for association studies, both for 1 and 4 h. All experiments were performed in triplicates. Subsequently, only for measurement of internalization, polyplexes adhering on the cell surface were removed by washing the cells for 15 min with 500 µL PBS, containing 1000 I.U. of heparin. Cells were detached with trypsin/EDTA and taken up in PBS with 10 % FCS. Cellular uptake was assayed by excitation of Cy5 at 635 nm and detection of emission at 665 nm. Cells were appropriately gated by forward/sideward scatter and pulse width for exclusion of doublets. DAPI (4',6-diamidino-2-phenylindole) was used to discriminate between viable and dead cells. Data were recorded by Cyan™ ADP flow Cytometer (Dako, Hamburg, Germany) using Summit™ acquisition software (Summit, Jamesville, NY, USA) and analyzed by FlowJo® 7.6.5 flow cytometric analysis software.

3.7.3 Luciferase assay – gene transfer

Luciferase assays were performed by Petra Kos (PhD student, LMU). Neuro2A cells were seeded in 96-well plates 24 h prior to transfection using 10,000 cells per well. Polyplexes were formed in 20 µL HBG with 200 ng luciferase-encoding pCMVLuc plasmid per well and the calculated amount of polymer corresponding to the N/P ratio. All experiments were

performed in quintuplicates. Before transfection, medium was replaced with 80 µL fresh medium containing 10 % FCS. 24 h after transfection, cells were treated with 100 µL cell lysis buffer (25 mM Tris, pH 7.8, 2 mM EDTA, 2 mM DTT, 10 % glycerol, 1 % Triton X-100). Luciferase activity in the cell lysate was measured using a luciferase assay kit (100 µL Luciferase Assay buffer, Promega, Mannheim, Germany) and a Lumat LB9507 luminometer (Berthold, Bad Wildbad, Germany).

3.7.4 MTT assay – metabolic activity

MTT assays were performed by Petra Kos (PhD student, LMU). Neuro2A cells were seeded into 96-well plates at a density of 10,000 cells per well. After 24 h, culture medium was replaced with 80 µL fresh growth medium containing 10 % FCS and polyplexes (in 20 µL HBG) at different N/P ratios were added. All experiments were performed in quintuplicates. 24 h after transfection, 10 µL of MTT (5 mg/mL) were added to each well reaching a final concentration of 0.5 mg MTT/mL. After an incubation time of 2 h, unreacted dye and medium were removed. Optical absorbance was determined at 590 nm (reference wavelength 630 nm) using a micro plate reader (Spectrafluor Plus, Tecan Austria GmbH).

3.7.5 CellTiter-Glo® assay – metabolic activity

CellTiter-Glo®assays were performed by Petra Kos (PhD student, LMU). Neuro2A cells (5,000 per well) were seeded in 96-well plates. After 24h, medium was removed and replaced by fresh medium containing LPEI or the different Stp oligomers at increasing concentrations from 0.01 up to 1.0 mg/mL. All experiments were performed in triplicates. After 48h incubation, half of the medium was replaced by CellTiter-Glo®Reagent. The luminescent signal, which is proportional to the amount of ATP, was measured with a Lumat LB9507 luminometer (Berthold, Bad Wildbad, Germany). The luminescent signal of untreated cells was taken as the 100 % value to determine the relative metabolic activity of the oligomer treated cells.

3.8 Statistics

Results are presented as mean ± standard deviation (SD). The number of replicates is indicated in the corresponding methods section.

4 RESULTS

Among the synthetic carriers, PEI due to its high efficiency is regarded as the common standard reagent for pDNA transfection. The diaminoethane motif provides the polymer with positive charges at physiological pH and results in a strong binding ability of the negatively charged DNA. Furthermore this motif provides the polymer with a high buffer capacity in the pH range between 6 and 7.4, which results in the so-called “proton sponge effect” ensuring endosomal escape. The high molecular weight of 22 kDa is also responsible for the good binding and transfection properties, but due to the high amount of positive charges and lack of biodegradability also contributes to the cytotoxic effect. This toxicity as a main drawback together with its polydispersity impedes the clinical application and points out the need of carrier optimization. The demerit of polydispersity could successfully be overcome by the application of solid-phase synthesis for the assembly of gene carriers. In SPPS, which was first described by Merrifield in 1963 [82], a peptide is elongated step by step on a solid support offering the opportunity to produce sequence-defined structures (Scheme 1). Adding a high excess of the reagents, which can easily be removed in following washing steps, brings the advantage of fast and efficient coupling steps. The outlined principle of peptide synthesis on solid-phase was applied here using a variety of natural and artificial amino acids (Figure 1).

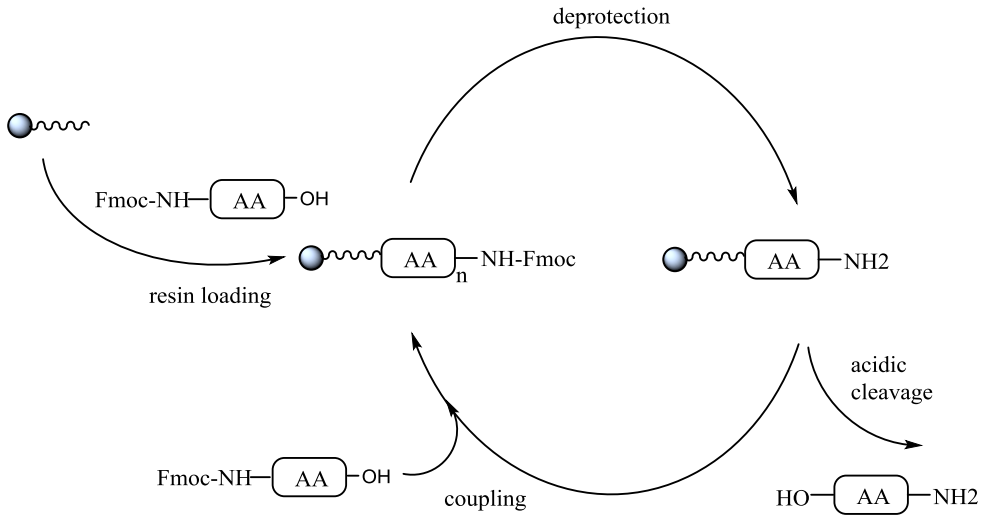

Scheme 1. Principle of solid-phase peptide synthesis showing resin loading, alternating deprotection and coupling steps and the final acidic cleavage from the resin. AA = amino acid

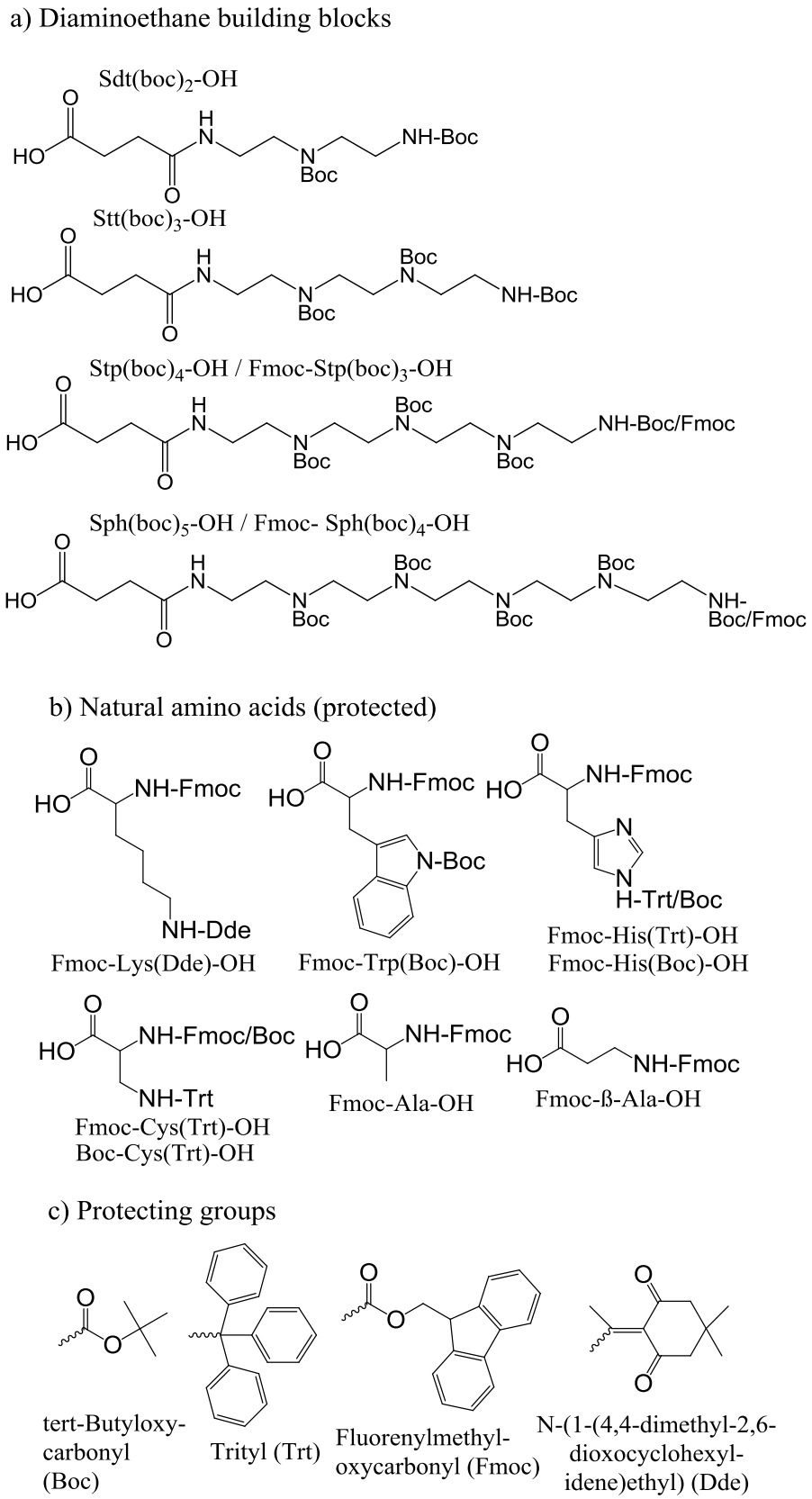

Figure 1. a) Structures of protected diaminoethane building blocks of which Stp(boc)$_3$-OH and Sph(boc)$_3$-OH were used in the MW study and the additional ones in the study of the comb topology. b) Structures of the used protected natural amino acids. c) Structures of the used protecting groups.

The artificial amino acid succinyl-tetraethylene pentamine (Fmoc-Stp(boc_3)-OH) was first developed by David Schaffert (PhD thesis LMU, 2010) with the aim of making the diaminoethane motif applicable to SPPS [61]. For this purpose the secondary amines of tetraethylene pentamine are protected with Boc, an acid-labile amine protecting group, and one terminal primary amine is protected with Fmoc, a base-labile amine protecting group, while to the other terminal amine a succinyl residue is attached. The latter provides the building block with a carboxylic linker enabling the coupling to free amino groups on the solid support. After incorporation in the peptide and cleavage of the side chain protecting groups, one Stp building block provides three protonatable amines enabling nucleic acid complexation and endosomal buffering. The Stp building block as well as the Sph building block, providing one additional ethylenamine unit, were used in the study of the length effect of linear oligo(ethanamino)amides carriers (section 4.1).

To assess the impact of variation of topology, a further focus of the conducted study (sections 4.3 and 4.4), branching points constitute an essential tool. Branching points can be introduced by the incorporation of lysine providing two primary amines. Using two orthogonal protecting groups, Fmoc for the α-*N* amino group and Dde for the ε-*N* amino group, allows performing the previously described backbone elongation in a defined sequential manner. By alternating amino acid coupling and Fmoc deprotection with subsequent attachment of “comb arms” to the ε-*N* amino groups after the Dde deprotection, branched peptides were synthesized for systematic evaluation of topological effects. In addition to lysine, other natural amino acids were used in order to obtain specific carrier properties (see section 4.3.2).

4.1 Evaluation of linear oligo(ethanamino)amide carriers of increasing molecular weight for pDNA delivery and comparison to linear PEI

4.1.1 Carrier design and synthesis

Previous studies have demonstrated the suitability of the artificial amino acid Stp to produce sequence-defined carriers for gene delivery via solid-phase assisted synthesis [63, 66, 67, 86]. Here a small library of linear oligo(ethanamino)amides without additional functional domains was generated in order to investigate specifically the length effect on gene carrier properties. Linear oligomers consisting of 5, 10, 15, 20, 30 and 40 Stp units were synthesized (Table 1). Furthermore a terminal tryptophane was attached at the C-terminus to facilitate

analytical characterization. A 30 Stp units long oligomer with terminal cysteine modification was synthesized to investigate if polyplex stabilization via disulfide formation, as observed in previous studies [63, 132], was beneficial also for these longer sequences. Furthermore, Stp was replaced with the Sph building block, which provides one ethylenamine unit more than Stp, in order to investigate whether a similar strong enhancement of DNA transfection efficiency could be obtained with Sph as observed in four-arm structures in a previous study [68]. The exact structures of all oligomers used in this study are displayed in Scheme 2.

Compound Id	Sequence	Molecular weight [Da]	Protonatable amines
681	Stp5-W	1561,02	16
643	Stp10-W	2917,82	31
644	Stp15-W	4274,61	46
645	Stp20-W	5650,56	61
554	Stp30-W	8345,0	91
555	Stp40-W	11058,59	121
556	$[Stp5\text{-}\beta A]_6$-W	8876,51	91
682	C-Stp30-W-C	8551,29	91
683	Sph20-W	6492,77	81
684	Sph30-W	9637,04	121

Table 1. Sequences of all oligomer structures written from N- to C-terminus and the corresponding MWs.

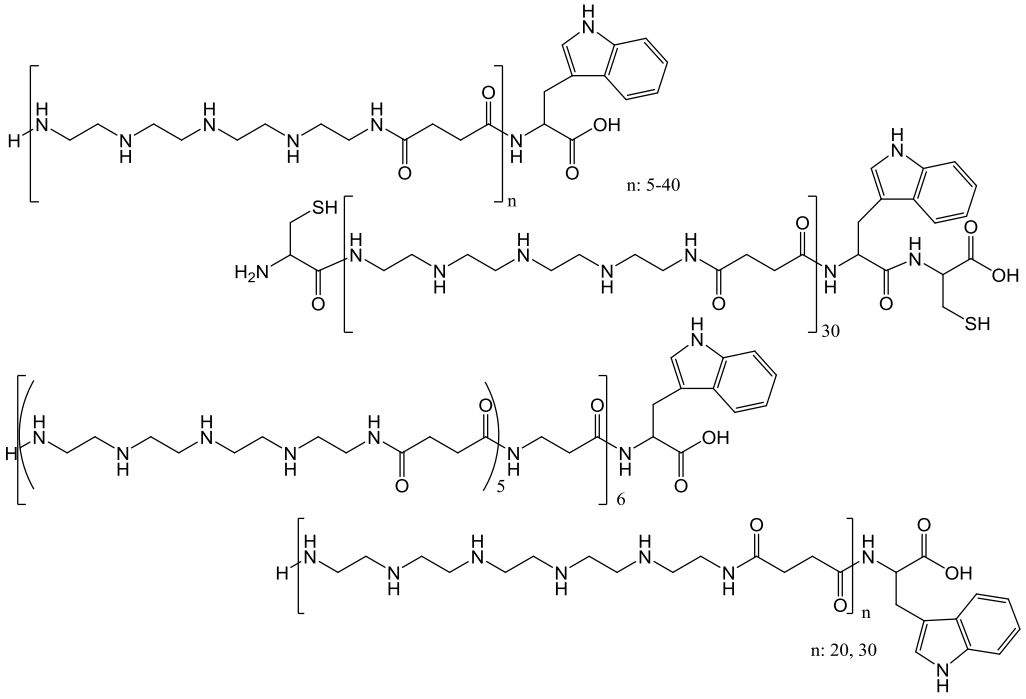

Scheme 2. Overview of all chemical structures used in this study. a) $(Stp)_{5\text{-}40}$-W, b) C-Stp_{30}-W-C, c) $[(Stp)5\text{-}\beta A]_6$-W, d) $(Sph)_{20,30}$-W

When standard SPPS at room temperature either on a Wang resin or a Tentagel trityl resin was used in initial experiments, oligomers of more than 20 Stp units were obtained only in low yield and showing deletion sequences (Figure 2 a). These unsatisfactory results were obtained using either a consecutive or convergent coupling strategy. For the convergent strategy protected blocks of five Stp units were applied in order to reduce the number of couplings and thus saving time. Optimizing the syntheses by using a ChemMatrix resin and microwave irradiation for coupling and deprotection led to purer products in a shorter period of time (Figure 2 b). Both, the convergent and consecutive coupling strategy were suitable with the optimized method. As the consecutive method was less time-consuming with the automated synthesis this procedure was maintained for the assembly of all structures in this study. Chromatograms of the analytical HPLC of LPEI and the two longest oligomers Stp30-W are shown in Figure 3.

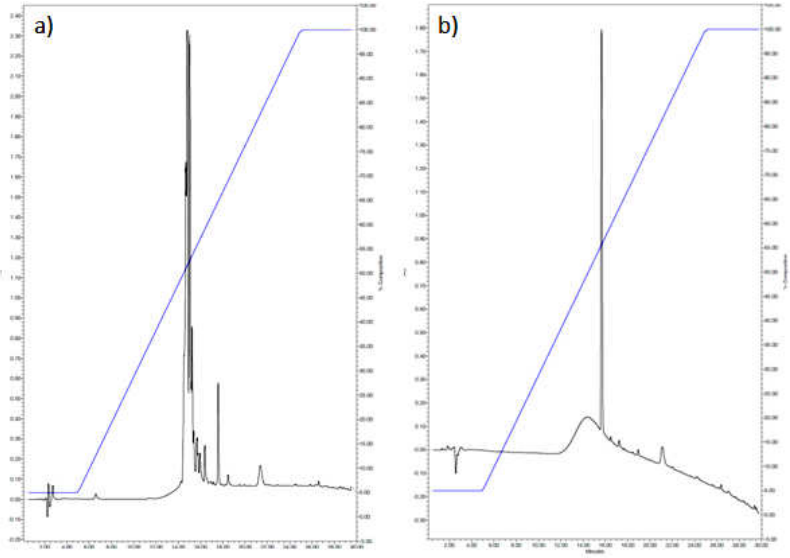

Figure 2. Analytical HPLC of the oligomer [Stp5-ßA]$_6$-W synthesized a) manually and b) with automated synthesis. HPLC was performed on a RP SunFire C 18 column using a gradient from 5 % to 100 % buffer B at a flow rate of 1mL/min in 20 min with buffer A containing H_2O with 0.1 % TFA and buffer B containing ACN with 0.1 % TFA. Absorption was monitored at λ = 214 nm.

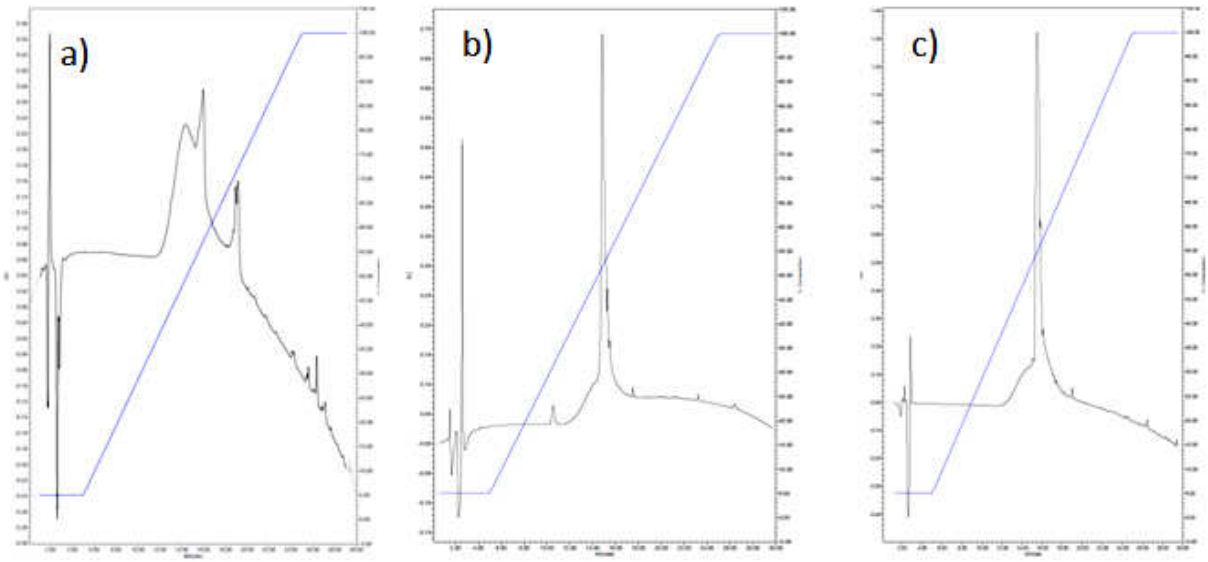

Figure 3. Chromatograms of analytical HPLC runs of a) LPEI, b) Stp30-W and c) Stp40-W. HPLC was performed on a RP SunFire C 18 column using a gradient from 5 % to 100 % buffer B at a flow rate of 1mL/min in 20 min with buffer A containing H_2O with 0.1 % TFA and buffer B containing ACN with 0.1 % TFA. Absorption was monitored at λ = 214 nm.

4.1.2 Biophysical characterization: DNA condensation, particle size and buffer capacity

Testing the pDNA binding characteristics revealed that an increasing number of Stp units improved the polyplex stability. Stp5-W was not able to form stable polyplexes even at N/P ratio of 24, Stp10-W showed partial DNA binding from N/P 12 to 24, Stp15-W showed complete binding at N/P 18 and higher, whereas all polymers with 20 or more Stp units exhibited complete DNA binding already at N/P 12 and partial binding at N/P 6 and 3 (Figure 4). A cysteine-containing oligomer C-Stp30-W-C showed similar good binding characteristics in the gel shift assay as the unmodified Stp30-W (Figure S4 a,b). Also a dissociation assay with the anionic polymer heparine resulted in polyplex disassembly at all tested heparine concentrations for both the unmodified and cysteine-modified oligomer (Figure 5 a,b). The improvement of DNA condensation ability through oligomer elongation becomes also clear in the EtBr exclusion assay were the decrease in fluorescence, resulting from higher EtBr exclusion by polyplex formation after oligomer addition, increases with increasing MW of the oligomers (Figure 6). LPEI still displays a higher DNA condensation ability compared to the best-performing Stp oligomer.

Substituting the Stp building block for Sph in the oligomers with 20 and 30 units provided one additional ethylenamine unit without significantly changing the binding characteristics (Figure 4). In order to investigate the effect of varied charge density on DNA complexation, β-alanine was incorporated into the Stp30-W oligomer after every fifth Stp unit. Decreased

DNA binding ability was observed (Figure 4). Continuous improvement was clearly seen with increasing N/P ratio, but even the highest tested N/P ratios of 18 and 24 did not display complete binding.

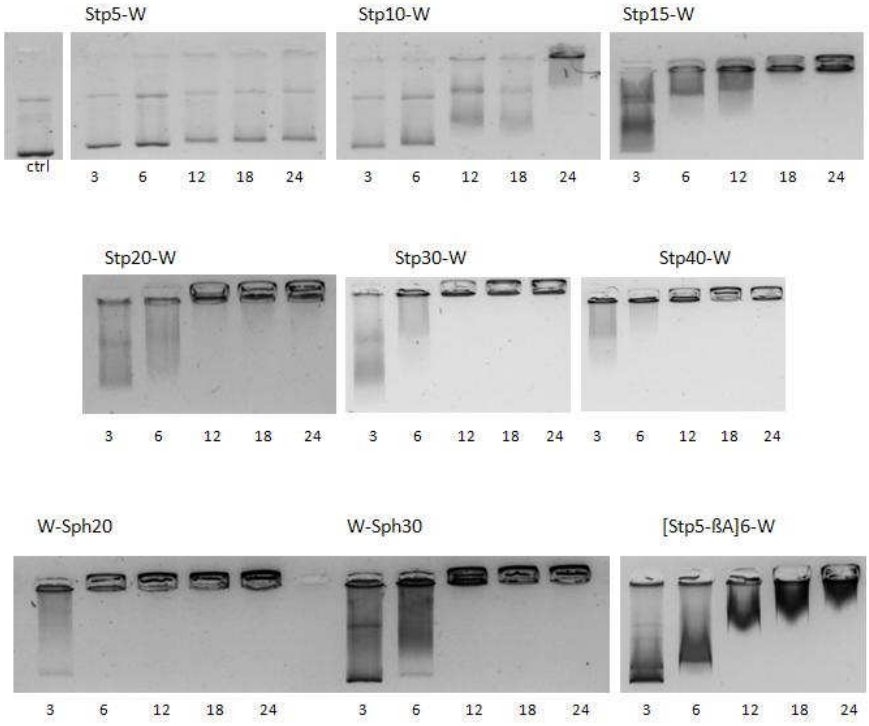

Figure 4. pDNA binding ability of linear Stp and Sph oligomers of increasing molecular weight determined by agarose gel shift assay at increasing N/P ratios as indicated. Last panel: effect of varied charge density by incorporation of β-alanine.

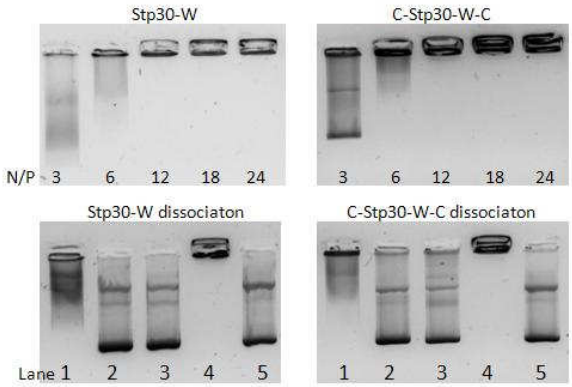

Figure 5 . Polyplex dissociaton analysis using the DNA agarose gel shift assay. Upper panels: Stp30-W and C-Stp30-W-C at different N/P ratios. Lower panels: Dissocation of polyplexes in the agarose gel shift assay at N/P 12 of Stp30-W and C-Stp30-W-C treated with 0.1 I.E. heparine (lane 1), 0.2 I.E. heparine (lane 2), 0.4 I.E. heparine (lane 3), TCEP (lane 4) and 0.2 I.E. heparine + TCEP (lane 5).

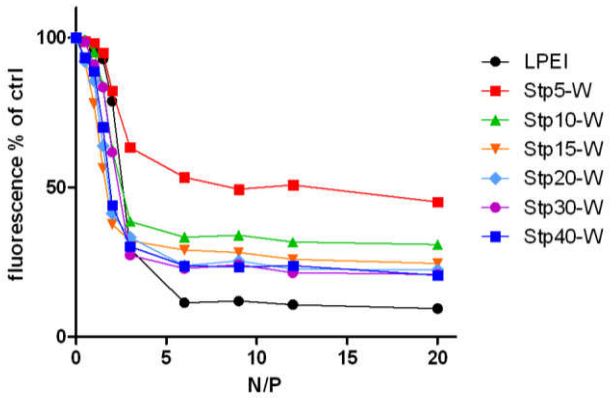

Figure 6. pDNA binding capacity of LPEI and linear Stp oligomers. EtBr exclusion assays with increasing N/P ratios obtained by stepwise addition of the oligomer to pDNA solution at pH 7.4. 100% value displays fluorescence intensity of DNA and EtBr before the addition of the polymer.

Determination of particle sizes measured by DLS indicated that with increasing number of Stp units the particle size decreased (Table 2). With a size over 1 µm, Stp5-W was the only polymer not able to form compact polyplexes with pDNA. For the oligomer with 10 Stp units a particle size of around 300 nm was observed, for 15 Stp units 140 nm and for 20 Stp units and more the measured particle sizes had values around 100 nm and were therefore similar to LPEI polyplexes with 130 nm. Also the cysteine-modified sequence C-Stp30-W-C and the Sph-containing sequences Sph20-W and Sph30-W formed DNA polyplexes around 100 nm, confirming the similar complexation characteristics observed in the gel shift assay. In comparison to Stp30-W, for polyplexes formed using the analog with incorporated β-alanine slightly larger complex sizes were detected. For all polyplexes a positive zeta potential around 20 mV was measured, except for Stp5-W in consequence of the absence of nanosized particles (Table 2).

Next, the buffer capacity of Stp and Sph oligomers was determined in the biological pH range of 5.0 to 7.4 in order to investigate the influence of increasing MW and building block type. This interest arose based on the odd-even rule established by Kataoka *et al* for N-substituted polyaspartamides, stating that diaminoethylene substituents containing an even number of protonatable amines provided higher buffer capacity and gene transfer activity than odd-numbered substituents [120]. Accordingly, in the Wagner lab Sph oligomers (4 protonatable amines in row) were found to show higher buffer capacities than Stp oligomers (3 protonatable amines in row) [66]. In the present work, Stp and Sph oligomers of increasing MW displayed similar buffer capacities between 15 and 20 % independent of type and

number of the used building block (Figure 7), also in the same range as LPEI. This observation suggests that the odd-even rule only applies to oligomers below a certain size-threshold.

	Z-average [nm]	PDI	Zeta potential [mV]
LPEI	129,0 ± 2,8	0, 310	26,0 ± 1,2
Stp5-W	1720,7 ± 62,9	0,549	3,2 ± 0,3
Stp10-W	331,1 ± 11,8	0,272	18,7 ± 0,3
Stp15-W	143,8 ± 5,5	0,294	20,2 ± 0,6
Stp20-W	103,5 ± 4,2	0,286	20,5 ± 0,8
Stp30-W	98,0 ± 8,6	0,31	19,4 ± 1,9
Stp40-W	118,4 ± 3,4	0,279	20,6 ± 1,0
C-Stp30-W-C	87,1 ± 0,9	0, 164	24,6 ± 0,5
[Stp5-βA]$_6$-W	127,7 ± 1,2	0, 251	20,4 ± 0,3
Sph20-W	86,4 ± 8,6	0,353	24,4 ± 4,1
Sph30-W	70,5 ± 0,6	0,278	26,9 ± 1,6

Table 2. Particle size (indicated as Z-average), polydispersity index (PDI) and zeta potential of all oligomer/pDNA complexes at N/P 12 measured by DLS.

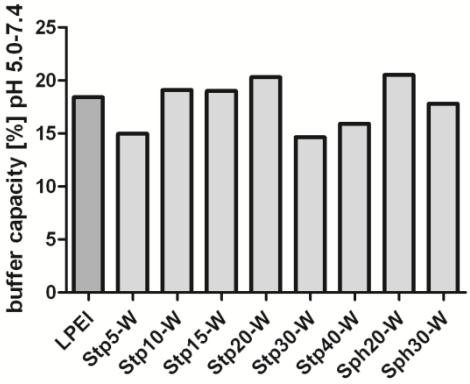

Figure 7. Buffer capacity of Stp and Sph oligomers and LPEI measured in the pH range of 5.0 and 7.4.

4.1.3 Biological evaluation: Cellular internalization, gene transfer and cytotoxicity

Cellular uptake studies performed to investigate the influence of the carrier length revealed that a certain minimum length of the oligomer is necessary for successful internalization of the polyplexes (Figure 8). Accordingly, particles formed with Stp5-W showed a rather weak uptake, which was already remarkably enhanced for the Stp10-W polyplexes and further improved for Stp15-W (Figure 8 a). Particles formed with oligomers containing more Stp units (20 to 40) all showed similar high internalization properties (Figure 8 b). Substituting the Stp building block for the Sph building block did not change the extent of internalization

(Figure 8 c). Also the cysteine modification did not alter the uptake compared to the unmodified Stp30-W (Figure 8).

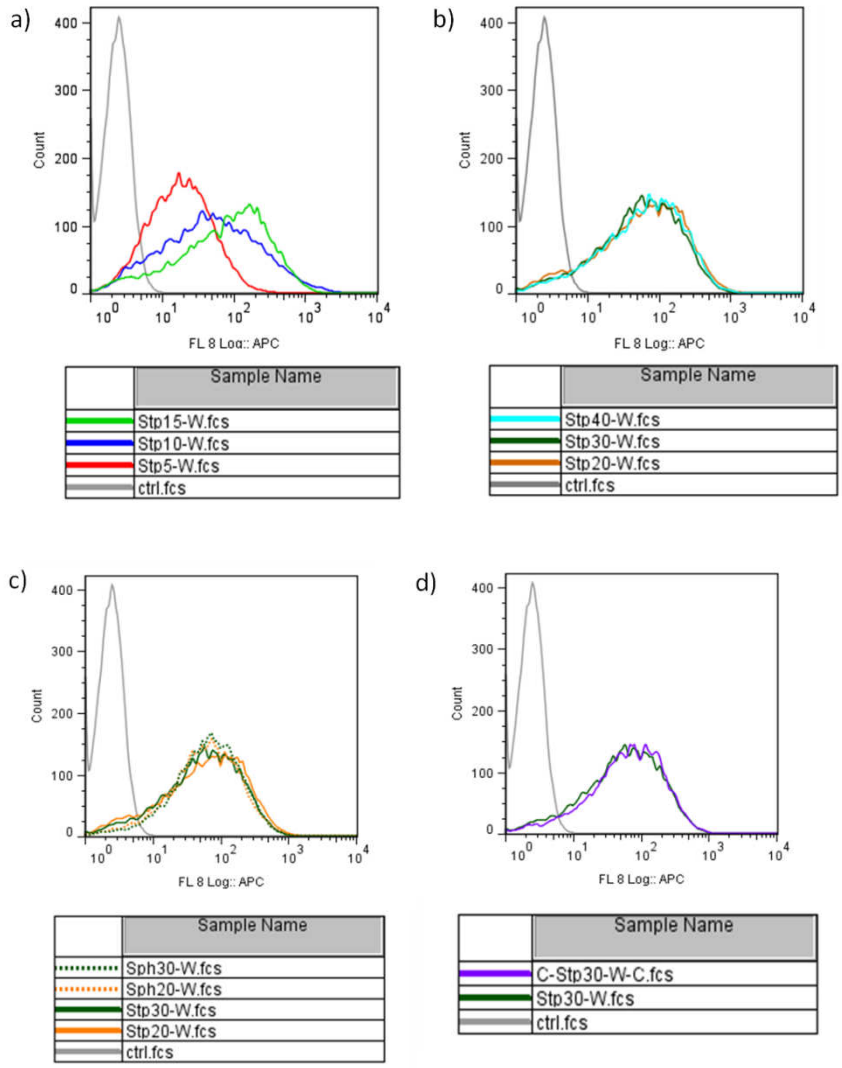

Figure 8. Cellular internalization of Cy5-labeled DNA/oligomer complexes at N/P 12 determined by flow cytometry in Neuro2A cells after 4 h at 37 °C. a) Stp5-W = red, Stp10-W = dark blue, Stp15-W = light green; b) Stp20-W = orange, Stp30-W = dark green, Stp40-W = light blue; c) Stp20-W = orange, Stp30-W = green, Sph20-W = orange dotted, Sph30-W = green dotted; d) Stp30-W = green, C-Stp30-W-C = purple. X-axis represents the intensity of the Cy5 signal and "Count" the number of cell counts with according fluorescence signal after appropriate gating. All incubations were performed in standard serum-supplemented culture medium. In the internalization studies, cells were washed for 15 min with heparin to remove polyplexes on the cell surface (see Materials and Methods). The experiments were performed by Petra Kos (PhD thesis LMU, 2014).

The influence of the oligomer MW on transfection efficiency was examined by luciferase pDNA gene transfer to Neuro2A neuroblastoma cells (Figure 9). Whereas the smallest Stp oligomer Stp5-W was completely inactive, increasing the number of Stp units led to a continuously improving gene transfer. Stp15-W at its highest N/P ratio 24 already exceeded

the activity of LPEI at its optimum, non-toxic concentration (N/P 6). Stp30-W displayed the highest transfection efficiency of all tested oligomers, outnumbering LPEI 6-fold. An additional elongation to 40 Stp units could not further improve pDNA delivery. Altogether the results nicely demonstrate a positive impact of increasing MW on transfection efficiency.

For the best-performing oligomer Stp30-W a cysteine-modified analog was synthesized, which led to comparable high luciferase expression levels (Figure 10). Also exchanging the Stp building block to Sph, which in previous studies significantly improved gene transfer activity of four-arm oligomers [68], could not further increase the transfection efficiency (Figure 10). However, a Stp30-W analog with β-alanine incorporation after every fifth Stp unit resulted in a clear decrease of gene transfer activity (Figure 10).

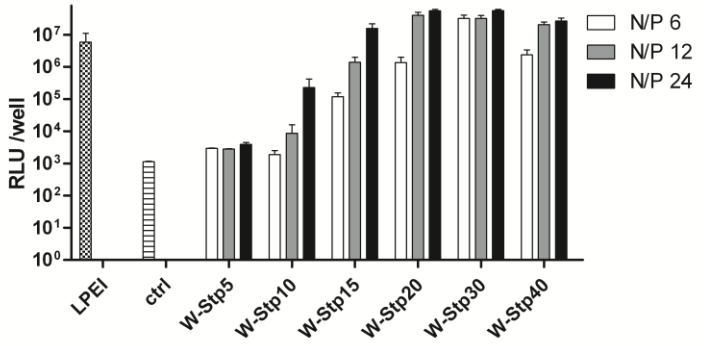

Figure 9. Luciferase gene transfer by LPEI and linear Stp oligomers tested with pCMVLuc pDNA in Neuro2A cells at N/P ratios 6, 12 and 24. The experiment was performed by Petra Kos (PhD thesis LMU, 2014).

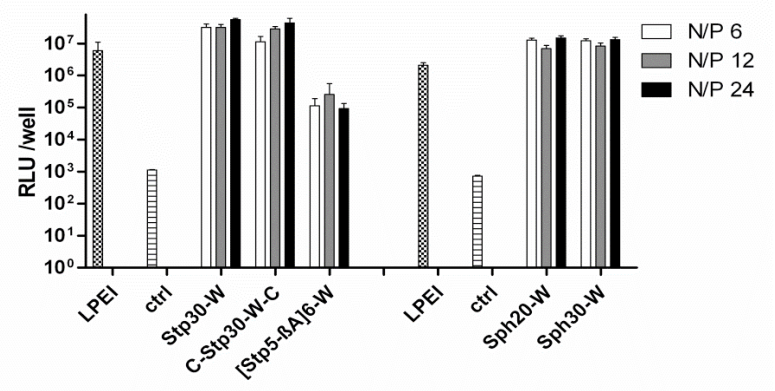

Figure 10. Luciferase gene transfer by LPEI and linear Stp and Sph oligomers tested with pCMVLuc pDNA in Neuro2A cells at N/P ratios 6, 12 and 24. The experiment was performed by Petra Kos (PhD thesis LMU, 2014).

As additional biological characteristic we next determined the cytotoxicity of the different oligomers by the MTT and CellTiter-Glo® assay. None of the polyplexes formed with oligomers or LPEI at optimum N/P ratios showed any significant cytotoxicity detectable by

the MTT assay which measures the mitochondrial redox state as a quantification of cell viability (Figure 11). When the oligomers were tested as free oligomers at increasing concentrations in the CellTiter-Glo® assay measuring intracellular ATP levels, considerable differences in cytotoxicity were observed (Figure 12). For cells treated with LPEI already at a concentration of 0.2 mg/mL metabolic activity was lost, whereas for Stp40-W, the most toxic of the linear Stp oligomers, still 90 % residual metabolic activity could be observed at a concentration of 0.4 mg/mL. For the Stp oligomers, toxicity levels were very low; nevertheless a clear increase of toxicity was detected with increasing MW. While Stp5-W did not show any toxicity at any examined concentration, all oligomers with 20 or more Stp units displayed a reduced metabolic activity (below 20 %) at the highest tested concentration of 1.0 mg/mL. It has to be emphasized that oligomer concentrations as used in optimum transfection experiments are around 10 µg/mL.

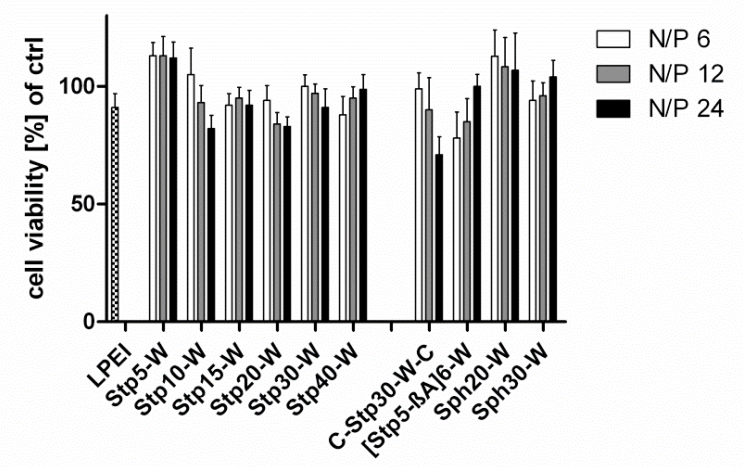

Figure 11. Metabolic activity determined with the MTT assay in Neuro2A cells of LPEI (N/P 6) and all linear Stp and Sph oligomers. The experiment was performed by Petra Kos (PhD thesis LMU, 2014).

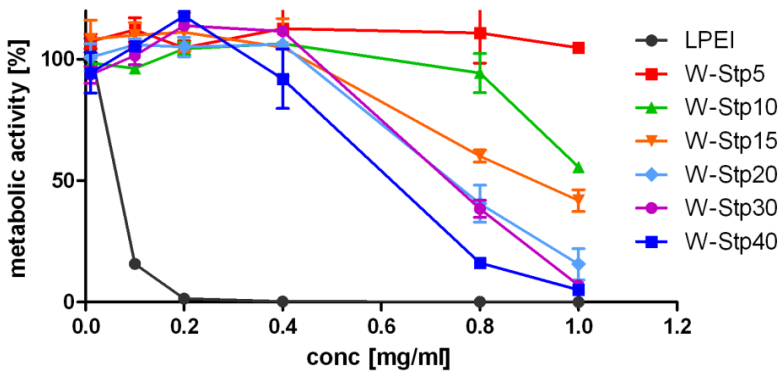

Figure 12. Metabolic activity of Neuro2A cells treated with increasing LPEI or oligomer concentrations determined by CellTiter-Glo® assay. For untreated cells 100 % metabolic acitivity was defined and all other values refer to this value. The experiment was performed by Petra Kos (PhD thesis LMU, 2014).

4.2 Analytical characterization of oligo(ethanamino)amides by capillary electrophoresis and Taylor dispersion analysis

4.2.1 Determination of the effective mobility of oligo(ethanamino)amides of different length by capillary electrophoresis

Determination of the electrophoretic mobility is of high interest in order to gain information about the charge, the size and the hydrodynamic behavior of charged species. Therefore we started a collaboration project with the lab of Dr. Laurent Leclercq and Prof. Dr. Hervé Cottet, U. Montpellier. Electrophoretic techniques, such as capillary electrophoresis (CE), constitute a useful tool for the determination of the effective mobility and for the separation of oligomers and polymers. CE is a separation procedure performed in a silica-filled capillary tube of a diameter around 50 µm. The instrumental arrangement is shown in Figure 17. Separation efficiency is generally controlled by longitudinal diffusion. This explains the extraordinary high resolution for macromolecules with low diffusion coefficient and its extensive application for analytical characterization of a large variety of small molecules, oligomers or polymers. The simplest separation principle using CE is the so-called capillary zone electrophoresis (CZE), where the sample is injected as a narrow band dissolved in the separation buffer. Each species migrates with its own velocity after application of an electric field resulting in separation of the sample components. The electrophoretic mobility μ_{ep} is proportional to the charge of the ion and inversely proportional to the friction coefficient. Consequently, in theory, a larger hydrodynamic radius results in a lower electrophoretic mobility for a given charge.

Here, CZE was applied to four representative oligomers of the library, namely Stp10-W, Stp20-W, Stp30-W and Stp40-W, to investigate the effect of increasing MW on the electrophoretic mobility. At low pH value of 2.7 (in 250 mM HOAc) all oligomers showed a high mobility, as it was expected due to the high degree of protonation at this pH (Figure 13).

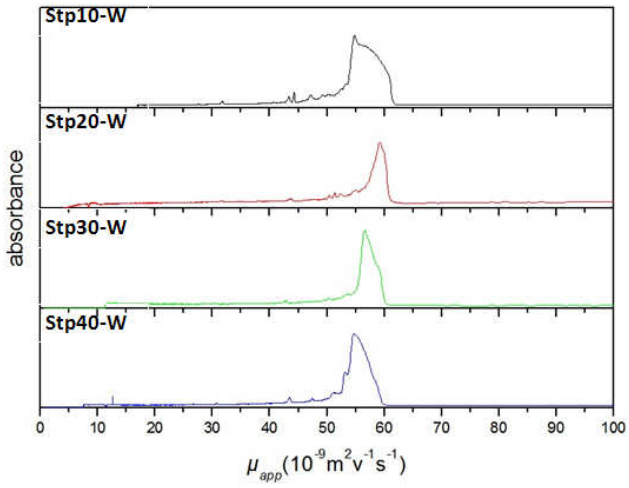

Figure 13. Electropherograms showing the electrophoretic mobility of the oligomers Stp10-W, Stp20-W, Stp30-W and Stp40-W recorded in 250 mM acetic acid at pH 2.70. Applied voltage was 30 kV. Y-axis displays UV absorbance at 214 nm. The experiment was performed by Xiaoyun Jin (PhD student) and Dr. Laurent Leclercq from the laboratory of H. Cottet, U. Montpellier.

Quite similar results were observed in a buffer containing 400 mM α-aminocaproic acid. As the pH value around 5.7 was much higher and therefore the cationic charge lower, decreased electrophoretic mobility was found (Figure 14). Stp10-W shows individual small peaks at lower mobilites, likely corresponding to the lower molar masses. For such small oligomers, the electrophoretic mobility increases with the molar mass. For larger oligomers (20, 30 and 40 Stp units), the mobility decreases with increasing number of Stp units. A further increase of the pH value to 7.4 using 10 mM HEPES as electrolyte results in conversion of the migration order compared to that obtained at lower pH values (Figure 15), likely due to specific effects of the buffer constituents.

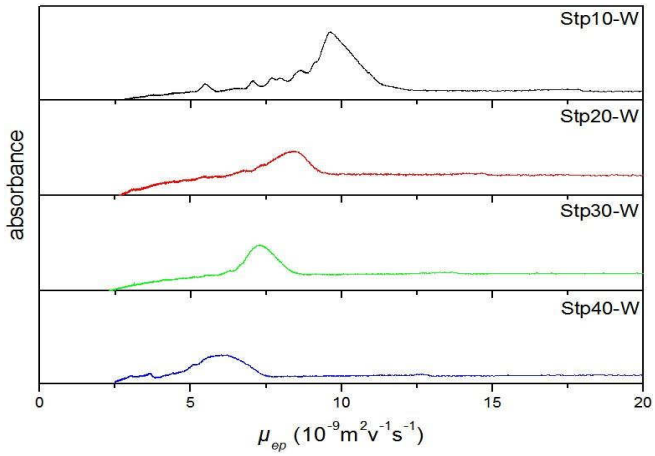

Figure 14. Electropherograms of the oligomers Stp10-W, Stp20-W, Stp30-W and Stp40-W recorded in 400 mM α-aminocaproic acid at pH 5.70. Applied voltage was 30 kV. Y-axis displays UV absorbance at 214 nm. The experiment was performed by Xiaoyun Jin (PhD student) and Dr. Laurent Leclercq from the laboratory of H. Cottet, U. Montpellier.

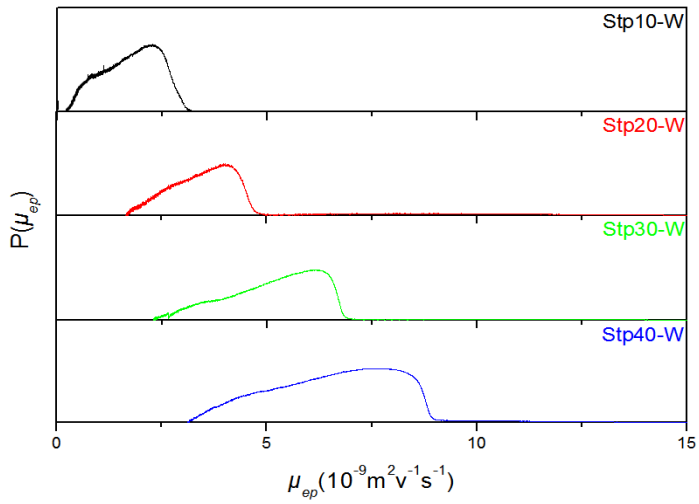

Figure 15. Electropherograms of the oligomers Stp10-W, Stp20-W, Stp30-W and Stp40-W recorded in 10mM HEPES at pH 7.4. Applied voltage was 30 kV. Diagram is plotted in the electrophoretic mobility scale ($P(\mu_{ep})$ vs. μ_{ep}). The experiment was performed by Xiaoyun Jin (PhD student) and Dr. Laurent Leclercq from the laboratory of H. Cottet, U. Montpellier.

In order to obtain size-dependent separation, capillary gel electrophoresis (CGE), which means performing CE in a gel network, was applied to the oligomers by addition of 5 % dextran solution (500 kDa) to the background electrolyte. In theory, the molecular sieve effect of the formed dextran gel should allow faster migration of small molecules and retardation of large molecules. The resulting electropherograms show a clear decrease in the electrophoretic mobility due to the gel network hindering migration (Figure 16). Furthermore, peak broadening can be observed as the migration through the gel provides a higher MW-dependent selectivity in the oligomer velocity. To improve the resolution of the separation a higher dextran concentration of 10 % was applied, but probable interactions of the dextran polymer with the oligomers did not lead to reliable results (data not shown).

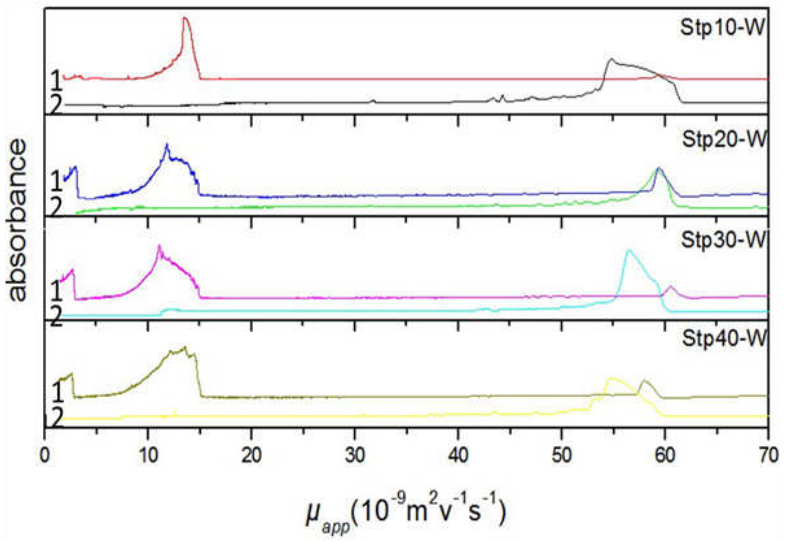

Figure 16. CGE electropherograms of the oligomers Stp10-W, Stp20-W, Stp30-W and Stp40-W recorded in 250 mM acetic acid at pH 2.7. Curve 1 shows the electropherogram in the presence of 5% dextran and curve 2 the electropherogram without dextran. Applied voltage was 10 kV. Y-axis displays UV absorbance at 214 nm. The experiment was performed by Xiaoyun Jin (PhD student) and Dr. Laurent Leclercq from the laboratory of H. Cottet, U. Montpellier.

4.2.2 Determination of the hydrodynamic radius R_h of oligo(ethanamino)amides of different length by Taylor dispersion analysis

The instrument used for CE can also be used to perform Taylor dispersion analysis (TDA) (Figure 17). TDA is an absolute method for the determination of the hydrodynamic radius R_h based on the dispersion of a sample plug in a laminar flow. The dispersion (over the tube cross section) results from the overlay of two phenomena: the dispersive velocity profile as a consequence of the laminar flow generated by a small pressure drop between the two capillary ends, and the molecular diffusion that redistributes the molecules in the capillary. The Taylor dispersion can be quantified with the temporal variance (σ^2) obtained by integration of the elution profile. This is recorded via measurement of the UV absorption of an UV active solute [133]. With the help of the temporal variance the molecular diffusion coefficient (D) and hydrodynamic radius (R_h) can be calculated without any calibration (absolute determination, see equations in the methods section 3.5.7).

In comparison to the commonly used size determination by DLS or SEC, TDA provides several advantages. The fact that it constitutes an absolute method for the size determination overcomes the need for complex calibration procedures. It can measure molecular sizes from angstrom to hundreds of nm, which is a great advantage for the characterization of nanomaterials. Moreover, it is considered more meaningful than the Z-average that is

derived from DLS measurements since it leads to a weight-averaged particle diameter when using weight sensitive detectors (which is the case for the UV absorbing oligomers of this work). In the case of bimodal samples, deconvolution of the recorded taylorgram allows the determination and quantification of each single population of the sample [134]. As an experimental procedure consuming sample volumes of only a few nanoliters, it is applicable to a wide spectrum of molecules, which might be available only in small quantities due to cost intensive, time-consuming or sophisticated production. TDA has already been used for the characterization of small molecules and polymers [133], but also for peptides, proteins and liposomes [135, 136].

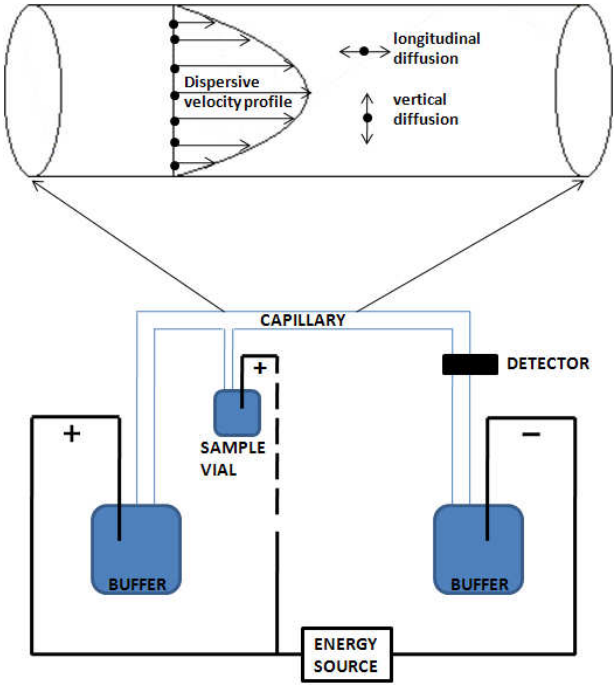

Figure 17. Capillary electrophoresis instrument and principle of Taylor dispersion analysis. For the Taylor dispersion analysis only pressure (no voltage) is applied.

Correlation of molecular weight and hydrodynamic radius

Here, TDA was applied to investigate the correlation of the hydrodynamic radius R_h and the oligomer length by analyzing four representative sequences containing 10, 20, 30 or 40 Stp units. Figure 18 illustrates a typical example of a taylorgram, displaying the time-dependent elution profile of the oligomer, detected by UV absorption. Table 3 displays the average R_h values obtained by TDA of the four tested oligomers in two different electrolytes. As expected, an increase of the hydrodynamic radius from 0.96 nm up to 1.94 nm with increasing oligomer length can be observed for the oligomers ranging from 10 to 30 Stp

units. However, a decreased R_h value was detected for the longest oligomer, Stp40-W. A further interesting observation was the appearance of two populations of different R_h for Stp20-W in both elution buffers and for all other oligomers only in HEPES buffer. Except for Stp-10-W, where the large population made up a ratio of 35 % and the smaller population 65%, for all other oligomers the percentages of species with higher and lower R_h value are approximately similar.

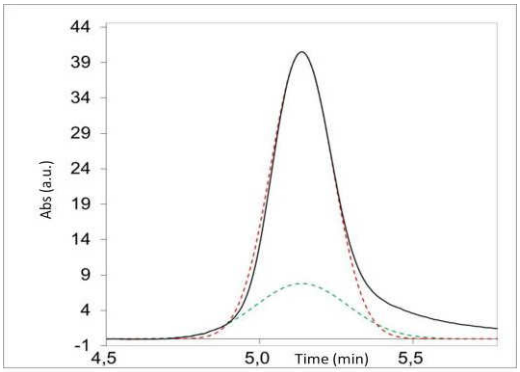

Figure 18. Exemplary Taylorgram of Stp30-W recorded in a PDADMAC coated capillary with HBG pH 7.4 as eluent. Deconvolution allows the detection of two populations with different R_h (R_{h1} = 0.55 nm (w % = 75), R_{h2} = 1.48 nm (w % = 25), R_{hav} = 0.78 nm). The experiment was performed by Xiaoyun Jin (PhD student) and Dr. Laurent Leclercq from the laboratory of H. Cottet, U. Montpellier.

	R_h average [nm] in 10 mM HEPES pH 7,30	**R_h of 2 populations**	**R_h [nm] average in 250 mM HOAc pH 2,68**	**R_h of 2 populations**
Stp10-W	0.96	1.65 (35 %) 0.61 (65 %)	0.87	-
Stp20-W	1.31	2.19 (45 %) 0.54 (55 %)	1.31	1.90 (50 %) 0.68 (50 %)
Stp30-W	1.94	2.64 (60 %) 0.91 (40%)	1.93	-
Stp40-W	1.24	2.19 (45 %) 0.51 (55 %)	1.18	-

Table 3. Hydrodynamic radius R_h of the oligomers Stp10-W, Stp20-W, Stp30-W and Sp40-W determined in 10 mM HEPES (pH 7.30) or 250 mM HOAc (pH 2.68) by Taylor dispersion analysis. The experiment was performed by Xiaoyun Jin (PhD student) and Dr. Laurent Leclercq from the laboratory of H. Cottet, U. Montpellier.

Effect of pH value and buffer on hydrodynamic radius R_h

The detected R_h of 0.78 nm of the oligomer Stp30-W (MW 8345.0) in HBG buffer appears quite small in comparison to the value of 0.25 nm determined for the small molecule

caffeine (MW 194.2). Based on the assumption that a high amount of glucose might disturb the measurement, the TDA experiment performed in pure HEPES buffer resulted in a R_h of 1.94 nm and was therefore more than two-fold higher than in glucose-containing buffer (Table 4). TDA experiments with the same oligomer, Stp30-W, in different buffer systems of decreasing pH, revealed a simultaneous increase of the hydrodynamic radius up to 3.06 nm in 50 mM HCl.

	HEPES (20mM) Glucose (280 mM)	**HEPES (10 mM)**	**HOAc (250 mM)**	**HCl (10 mM)**	**HCl (50 mM)**
pH	7.4	7.3	2.68	2.04	1.38
R_h average [nm]	0.78	1.94	1.93	2.61	3.06
R_h of 2 populations	1.48 (25 %) 0.55 (75 %)	2.64 (60 %) 0.91 (40 %)	-	3.45 (60 %) 1.40 (40 %)	-

Table 4. R_h values of the oligomer Stp30-W determined in different buffer solutions and pH values by TDA. The experiment was performed by Xiaoyun Jin (PhD student) and Dr. Laurent Leclercq from the laboratory of H. Cottet, U. Montpellier.

4.3 Optimization of comb-like oligomers for pDNA delivery

4.3.1 Design and synthetic strategy

The solid-phase assisted synthesis of cationic oligomers using the artificial oligoamino acids Stp or Sph has been used to establish polymer libraries including effective carriers for gene delivery [63, 68, 111]. In these previous studies the artificial amino acids were incorporated into the oligomer backbone, resulting in linear structures or structures with up to five arms when branching points were introduced. Here the cationic building blocks were attached to the ε-N of an oligolysine backbone producing eight comb-like oligoamine branches (Scheme 3). Because the terminal amines remain free instead of being part of the subsequent amide bond as for the linear shaped oligomers, in these comb oligomers each artificial amino acid provides one additional protonatable amine. Besides this benefit a distinct change in carrier topology is achieved with the new strategy.

The carrier assembly was performed in two different ways. First, a convergent approach was tested, where a building block was assembled, consisting of lysine protected with Fmoc at the α-N amino group and the Boc-protected cationic building block conjugated to the ε-N

amino group (Scheme 3). Coupling these building blocks eight times led to the final comb oligomers.

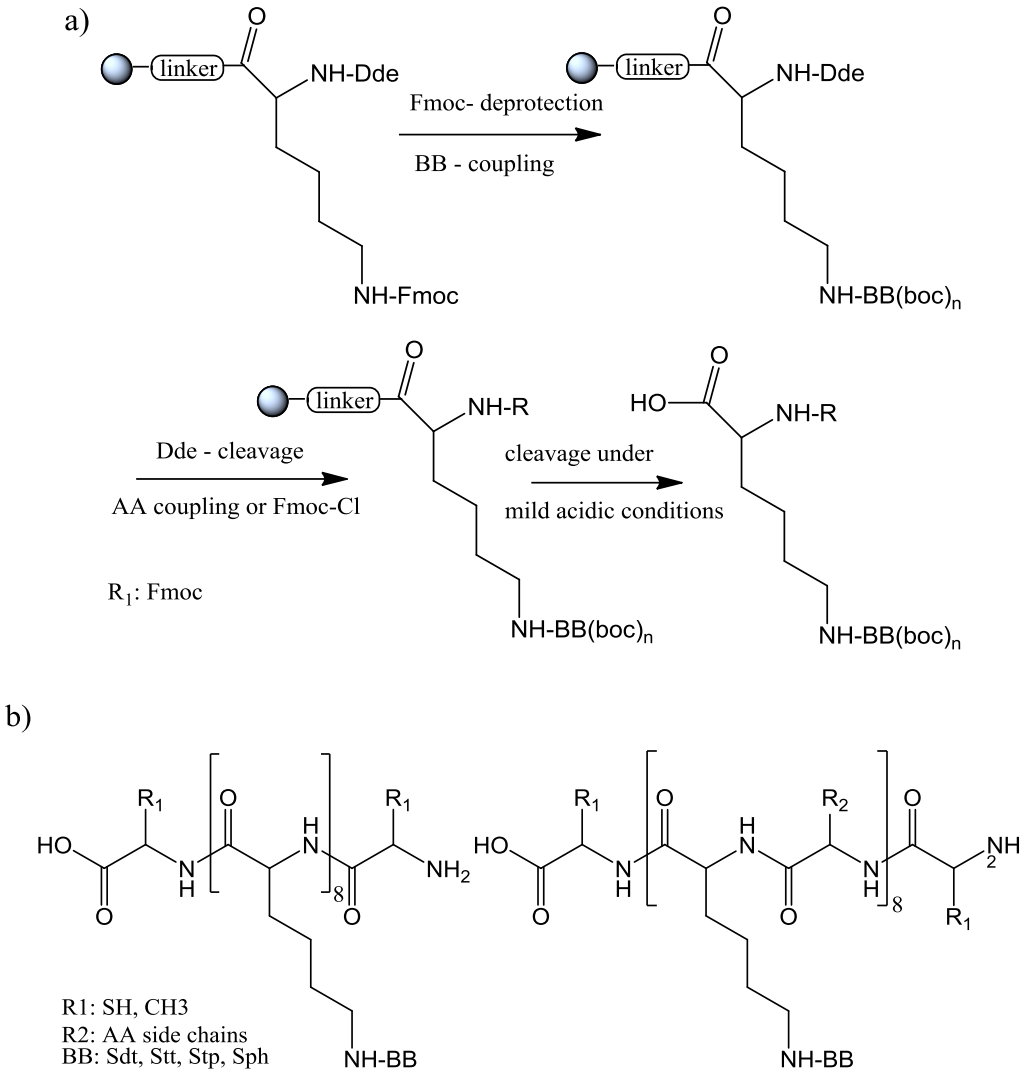

Scheme 3. a) Synthesis of the protected building blocks used for the comb structure synthesis with the convergent strategy. b) Structures of the synthesized comb structures. AA = amino acid; exact structures are depicted in

The second synthesis strategy was to assemble the backbone first, using Fmoc-Lys(Dde)-OH. In a subsequent step the Dde protection group is cleaved and finally the cationic building block was coupled to the free ε-N amino groups of the lysines, forming eight branches.

The convergent coupling strategy at room temperature was quite inefficient due to the large size of the building block, which probably led to steric hindrance. After the first three coupling steps, the coupling times had to be prolonged tremendously up to 3 h and double or triple couplings became necessary. With the aim of solving these problems an automated synthesizer was acquired and established for this application. Using this method, double

couplings of 8 min at 75 °C for the backbone assembly and “comb attachment” led to successful synthesis. Analytical data (Figure 19 a-c) and transfection efficiency (Figure 19 d) show that both approaches yield suitable products, but as the automated synthesis is much less time-consuming, it was preferentially used.

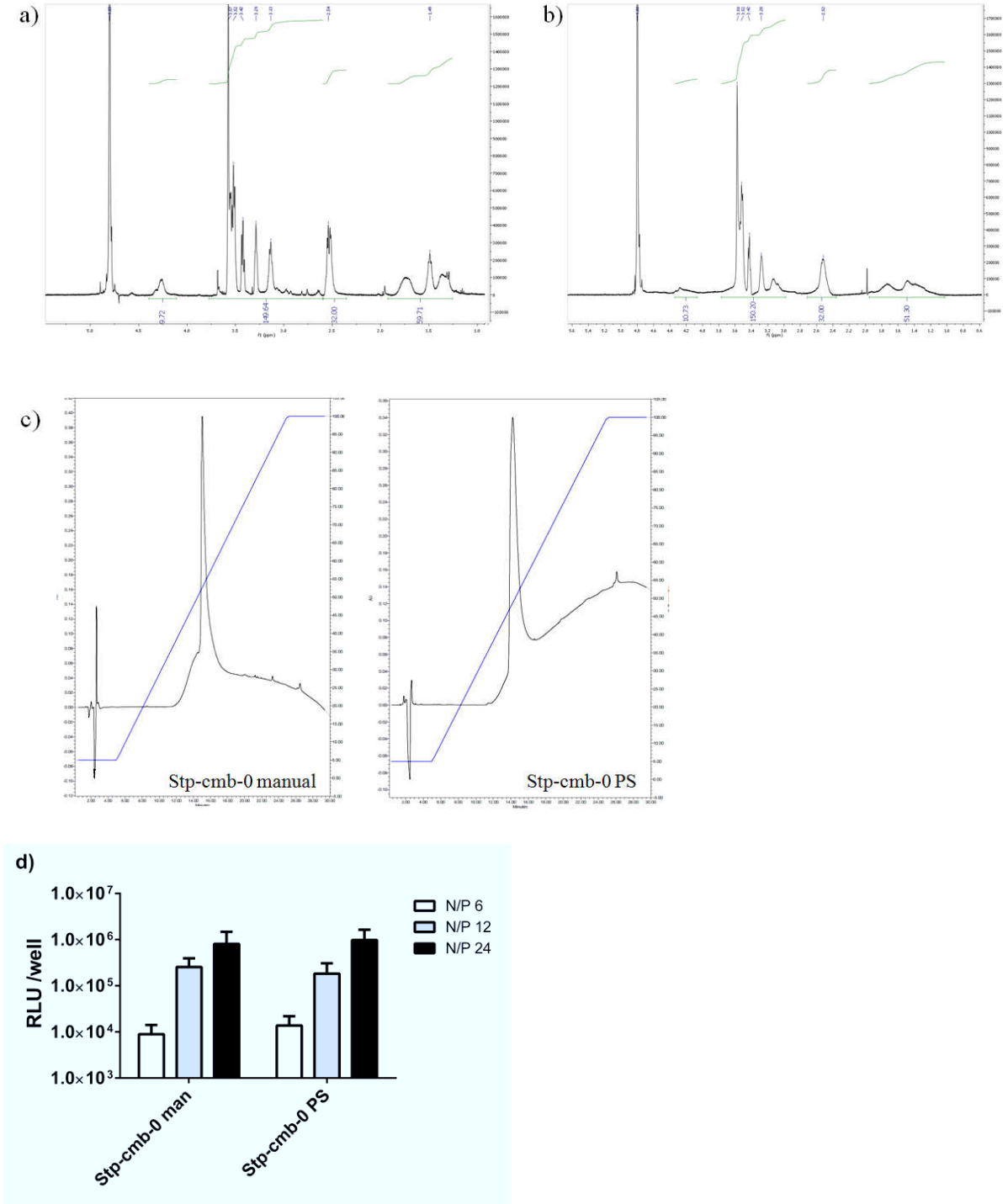

Figure 19. a) ^{1}H-NMR spectra in D_2O of Stp-cmb-0 synthesized with the automatic peptide synthesizer. b) ^{1}H-NMR spectra in D_2O of Stp-cmb-0 synthesized manually. c) RP-HPLC chromatogramm (5 % to 100 % ACN in 20 min) of Stp-cmb-0 synthesized manually and with the

peptide synthesizer d) Luciferase gene transfer of Stp-cmb-0 synthesized manually (man) and with peptide synthesizer (PS) tested with pCMVLuc in Neuro2A cells. Part d) was performed by Petra Kos (PhD thesis LMU, 2014).

Initial studies of comb structures with four repeating lysine units had shown only low pDNA transfection efficiency (Figure 20). Increasing the number to eight branches improved the biological performance so that this number was chosen for the design of all subsequent comb structures.

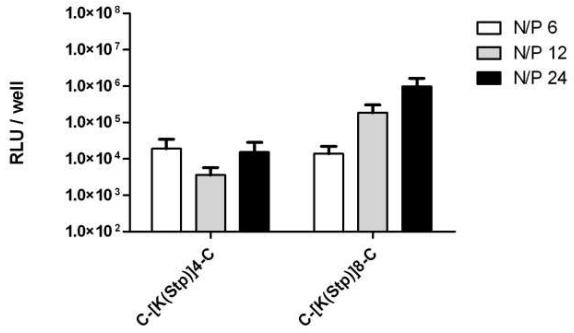

Figure 20. Comparison of the activity of comb structures with 4 and 8 Stp-modified lysine units in the luciferase gene transfer assay tested with pCMVLuc in Neuro2A cells at N/P ratios 6, 12 and 24. The experiment was performed by Petra Kos (PhD thesis LMU, 2014).

4.3.2 Incorporation of different functionalities (Cys, His, Trp, Ala, β-Ala)

From previous work in the Wagner Lab [63, 132] it is known that terminal cysteines serve as useful carrier modifications. The oxidation of thiol groups leads to disulfide formation during polyplex formation and stabilizes the complexes via crosslinking. In the present work comb oligomers with 8 branches, one carrying terminal cysteines and another one terminal alanine residues as a control, were compared. The higher stability (Figure 21) and transfection efficiency (Figure 22) confirms the benefit of cysteines also for the comb structures. Therefore, the cysteine-modification was maintained in the course of further carrier optimization.

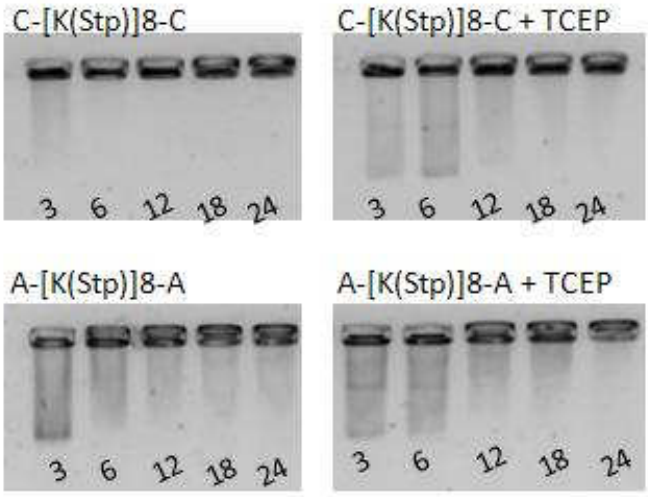

Figure 21. Comparison of pDNA binding of the cysteine-modified comb structure C-[K(Stp)]8-C and the alanine-modified control structure with and without 30 min TCEP incubation after polyplex formation at increasing N/P ratios as indicated.

To vary the distance between the comb branches, different natural amino acids were incorporated in the oligolysine backbone (Scheme 3b). Alanine was used to investigate a possible spacer effect as well as β-alanine, which extends the comb backbone by providing one methylene unit more than the typical α- amino acids and might therefore also change the 3D structure of the oligomer. Tryptophane was introduced as an example for an aromatic, hydrophobic amino acid, which might be beneficial for polyplex stabilization. Histidine was incorporated as a spacer amino acid because the imidazole group with a pK_A value around 6 is known to contribute to the endosomal escape via the proton sponge effect during endosome acidification [137].

The introduction of an alanine spacer had a slightly positive effect on transfection efficiency but did not greatly influence other biophysical and biological properties compared to the structures without spacer amino acid (see chapter 4.4.). In contrast, the introduction of β-alanine led to decreased transfection efficiency (Figure 22), most likely due to reduced DNA complexation ability (Figure 23). The incorporation of tryptophane or histidine both enhanced the transfection efficiency. For further detailed investigations of structure-activity relationships by the attachment of diaminoethane building blocks of different length (see Chapter 4.3.3) and the direct comparison to linear control sequences (see Chapter 4.4) three structures were chosen from the comb structure library. All three structures have terminal cysteine modifications, one without spacer amino acid (cmb-0), one with alanine spacer (cmb-A) and one with histidine spacer (cmb-H).

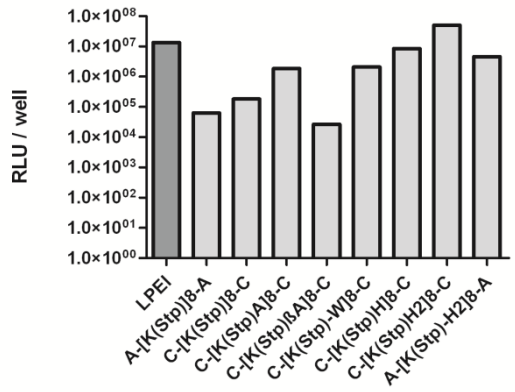

Figure 22. Luciferase reporter gene expression after transfection using cysteine- or alanine-modified Stp comb structures containing different spacer amino acids tested with pCMVLuc pDNA at N/P 12 in Neuro2A cells. The experiment was performed by Petra Kos (PhD thesis LMU, 2014).

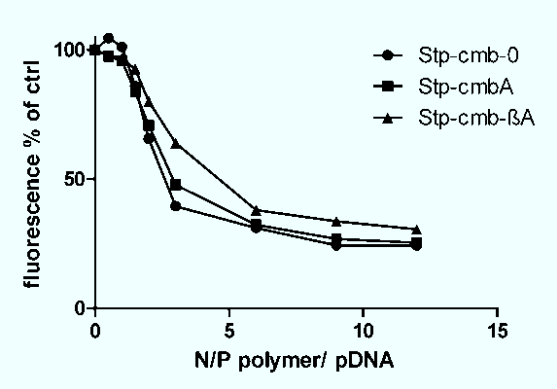

Figure 23. Comparison of pDNA binding ability of Stp-cmb-0, Stp-cmb-A and Stp-cmb-βA comb structures determined by EtBr exclusion assay at increasing N/P ratios.

4.3.3 Application of building blocks with different number of ethylenamine repeating units

Carrier synthesis and design

The previously obtained results emphasized the potential for pDNA delivery of a small library of comb structure oligomers with the Stp building block. To provide further confirmation and gain new insights in structure-activity relationships, three further building blocks, Sdt, Stt, and Sph with differing numbers of amino ethylene units were attached to the oligolysine backbone, without spacer, with alanine spacer or histidine spacer (Scheme 3b). A list of all structures is presented in Table 5.

Building block	Compound Id	Sequence	Code	Protonatable amines
Sdt comb (2 prot N)	632	C-[K(Sdt)]$_8$-C	Sdt-cmb-0	17
	633	C-[A-K(Sdt)]$_8$-C	Sdt-cmb-A	17
	634	C-[H-K(Sdt)]$_8$-C	Sdt-cmb-H	17
Stt comb (3 prot N)	635	C-[K(Stt)]$_8$-C	Stt-cmb-0	25
	636	C-[A-K(Stt)]$_8$-C	Stt-cmb-A	25
	637	C-[H-K(Stt)]$_8$-C	Stt-cmb-H	25
Stp comb (4 prot N)	622	C-[K(Stp)]$_8$-C	Stp-cmb-0	33
	551	C-[A-K(Stp)]$_8$-C	Stp-cmb-A	33
	552	C-[H-K(Stp)]$_8$-C	Stp-cmb-H	33
Sph comb (5 prot N)	629	C-[K(Sph)]$_8$-C	Sph-cmb-0	41
	630	C-[A-K(Sph)]$_8$-C	Sph-cmb-A	41
	631	C-[H-K(Sph)]$_8$-C	Sph-cmb-H	41
Stp linear (3 prot N)	625	C-(Stp-K)$_8$-C	Stp-lin-0	33
	626	C-(A-Stp-K)$_8$-C	Stp-lin-A	33
	628	C-(H-Stp-K)$_8$-C	Stp-lin-H	33
Sph linear (4 prot N)	648	C-(Sph-K)$_8$-C	Sph-lin-0	41
	649	C-(A-Sph-K)$_8$-C	Sph-lin-A	41
	650	C-(H-Sph-K)$_8$-C	Sph-lin-H	41

Table 5. Sequences of comb and linear structures written from N- to C-terminus and the corresponding codes used throughout the text. Cmb= comb, lin= linear, 0= no spacer amino acid, A= alanine spacer, H= histidine spacer, prot N= number of protonatable nitrogens per building block.

Biophysical properties

Testing the pDNA binding characteristics of the comb oligomers with the agarose gel shift assay demonstrated complete pDNA complexation ability at N/P ratio of 6 and higher for all oligomers with Stt, Stp and Sph building block (Figure 24). The Sdt oligomers with only two protonatable amines per comb unit showed the weakest binding which was complete only at N/P 12 and higher. As exception, the histidine containing Sdt structure, showed complete binding already at N/P 3. These findings were verified in the EtBr exclusion assay, where the Sdt oligomers showed the lowest fluorescence decrease independent of the spacer (Figure 25). Stt and Sph oligomers compacted the pDNA to a similar extent, while for the Stp sequences an enhanced pDNA condensation ability could be observed. This was less pronounced for the structures without spacer molecule.

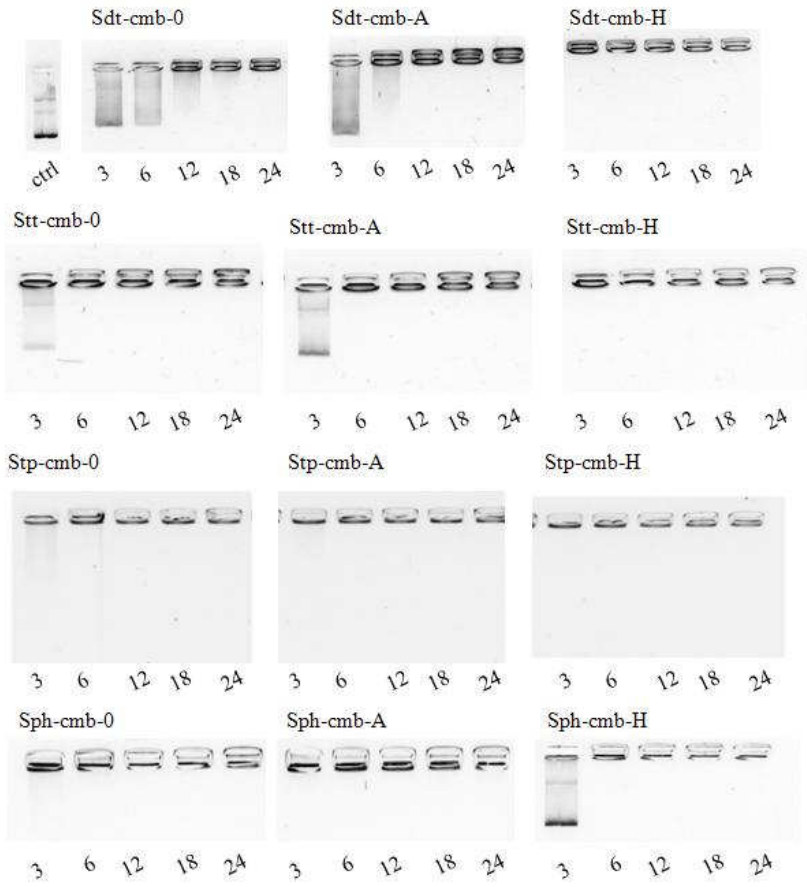

Figure 24. pDNA binding ability of Sdt, Stt, Stp and Sph comb structures determined by agarose gel shift assay at increasing N/P ratios as indicated.

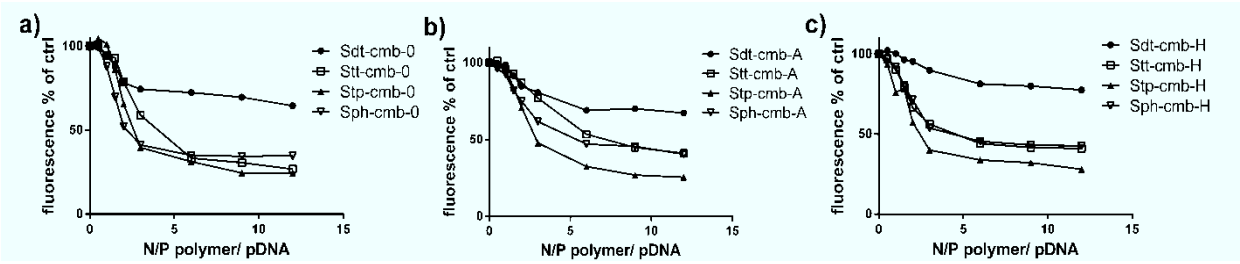

Figure 25. EtBr exclusion assay of DNA polyplexes of Sdt, Stt, Stp and Sph comb structures without spacer (a), alanine spacer (b) and histidine spacer (c) at increasing N/P ratios.

Particle sizes measured with DLS greatly differed depending on the length of the ethylenamine building block (Table 6). Oligomers consisting of the shortest, less protonated building block formed the biggest DNA particles. Sdt oligomers without spacer formed aggregates of about 2 µm. Sdt oligomers with Ala and His spacer formed particles of about 600 and 400 nm, which are still more than 3- and 2- fold bigger than particles formed with structures containing the other building blocks of increasing length. With sizes between 170 and 260 nm also the Stt oligomers produced DNA particles clearly bigger than the Stp and Sph oligomers. For Stp oligomers the smallest particles in a range between 100 and 140 nm

were observed. They display the highest zeta potential between 27 and 35 mV (Table 6). Overall a tendency of decreasing DNA particle size with increasing number of ethylenamine units was observed.

	Z-average [nm]	PDI	Zeta potential [mV]
Sdt-cmb-0	2128,7 ± 147,7	0,861	14,5 ± 0,3
Sdt-cmb-A	607,7 ± 18,7	0,394	17,9 ± 0,2
Sdt-cmb-H	444,0 ± 35,3	0,353	16,2 ± 0,6
Stt-cmb-0	175,3 ± 12,9	0,291	10,0 ± 0,8
Stt-cmb-A	259,3 ± 3,7	0,184	4,2 ± 0,1
Stt-cmb-H	255,6 ± 23,2	0,277	12,8 ± 1,2
Stp-cmb-0	136,4 ± 4,0	0,354	27,8 ± 0,1
Stp-cmb-A	103,6 ± 8,7	0,309	34,2 ± 0,5
Stp-cmb-H	102,5 ± 9,8	0,319	28,9 ± 0,5
Sph-cmb-0	109,5 ± 5,4	0,138	26,0 ± 0,1
Sph-cmb-A	132,3 ± 3,5	0,244	23,8 ± 0,7
Sph-cmb-H	167,3 ± 17,6	0,371	18,3 ± 1,5

Table 6. Particle sizes and zeta potential of Sdt, Stt, Stp and Sph comb structure polyplexes with pDNA at N/P ratio 12 obtained by DLS measurement.

The buffer capacity of the oligomers (Figure 26) was measured by alkalimetric titration at the pH range between 5.0 and 7.4. This range represents the physiologically relevant acidification from pH 7.4 in the extracellular compartment to pH 5.0 in the endosome. Clear differences in the buffer capacity could be found for the comb structures with increasing number of protonatable amines. The Sdt oligomers with only two protonatable amines per branch exhibited by far the highest buffering capacity (Figure 26 a). Stt oligomers with three protonatable amines per branches displayed the lowest buffering capacity for the structures without spacer and Ala spacer. Increasing the number to four protonatable amines led to an increase in the total buffer capacity between 5.0 and 7.4, whereas a further extension to five protonatable amines per branch, which can be found in the Sph structures, resulted in a small decrease in the buffer capacity. Regardless of the building block, the histidine containing oligomers showed the highest total buffer capacity in the pH range between 5.0 and 7.4.

On closer examination of the differential buffer capacities in the relevant pH range, two different buffering profiles are revealed (Figure 26 b-d). Sdt and Stp containing oligomers

with 2 and 4 protonatable amines per branch have the maximum buffer capacity between pH 5.5 and 6.5, while Stt and Sph sequences with 3 or 5 protonatable amines in row exhibit their maximum capacity between 6.5 and 7.4 (Figure 26 b, c). Only for the histidine containing structures discrepancies from this trend are observed. This was predictable due to an additive buffering effect of histidine around the pH of 6 (Figure 26 d).

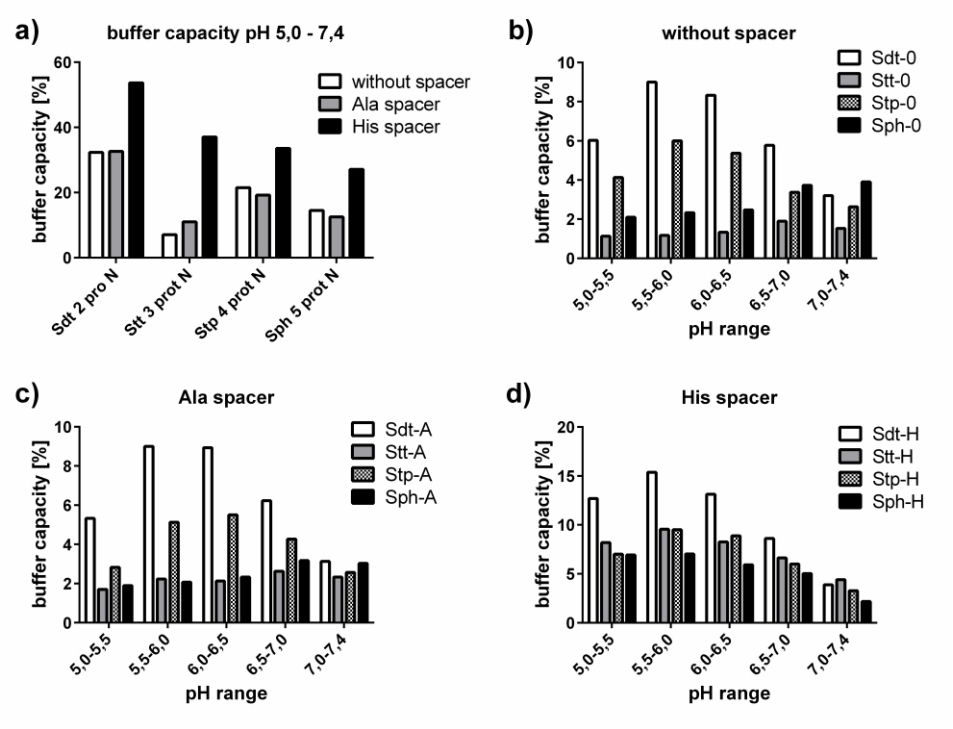

Figure 26. Buffer capacity of comb-type oligomers. a) Total buffer capacity of Sdt, Stt, Stp and Sph comb structures measured in the pH range of 5.0 and 7.4 b) – d) Differential buffer capacities between pH 5.0 and 7.4 b) without spacer, c) with Ala spacer and d) with His spacer.

Cellular uptake and gene transfer

The cellular uptake of the comb oligomers with different length of ethylenamine building blocks was investigated in Neuro2A cells (Figure 27). Polyplexes formed with Stt, Stp and Sph oligomers displayed a similar uptake rate independent of the spacer. In the case of the Sdt oligomers without spacer the polyplexes were not internalized by the cells. For the Ala- and His- containing Sdt structures only a small subpopulation of cells did not internalize any particles. The greater fraction of cells showed similar fluorescence intensities as observed for the Stt, Stp and Sph oligomers in the flow cytometric analysis.

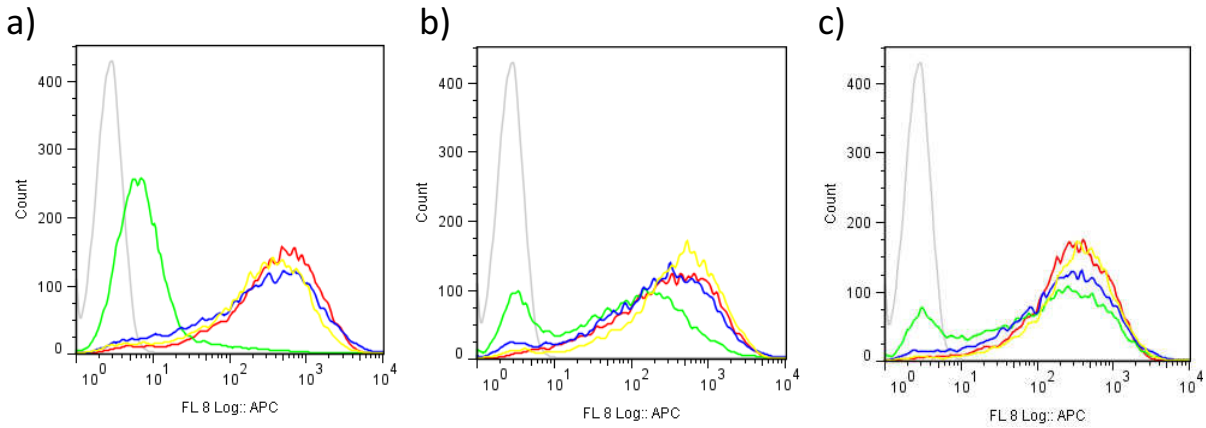

Figure 27. Cellular uptake of Cy5-labeled DNA/oligomer complexes at N/P 12 determined by flow cytometry in Neuro2A cells. Comb-shaped oligomers a) without spacer, b) with Ala spacer and c) with His spacer; oligomers containing Sdt = green, Stt = blue, Stp = yellow and Sph = red. X-axis represents the intensity of the Cy5 signal and "Count" the number of cell counts with according fluorescence signal after appropriate gating. The experiment was performed by Petra Kos (PhD thesis LMU, 2014).

Initial testings of luciferase pDNA transfection efficiency in Neuro2A cells revealed that the Stp-containing comb structures modulate the highest gene transfer among the tested building blocks (Figure 28). Histidine-containing oligomers displayed the greatest gene transfer efficiency in each group. Except for the Stt oligomers, also the Ala spacer resulted in a higher gene expression compared to the structures without spacer. The best performing sequence, Stp-cmb-H, at the N/P ratio of 6 exceeded LPEI 26-fold at its most effective, non-toxic concentration (Figure 29).

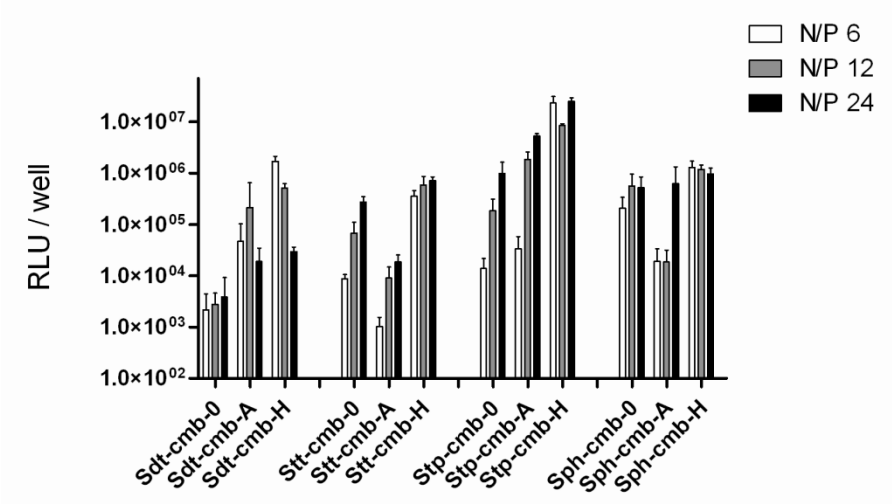

Figure 28. Luciferase gene transfer of all Sdt, Stt, Stp and Sph comb structures tested with pCMVLuc pDNA in Neuro2A cells. The experiment was performed by Petra Kos (PhD thesis LMU, 2014).

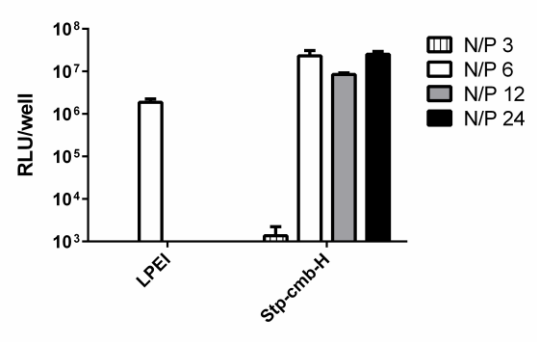

Figure 29. Comparison of luciferase gene transfer of linear PEI at N/P 6 and Stp-cmb-H at different N/P ratios. The experiment was performed by Petra Kos (PhD thesis LMU, 2014).

To examine cytotoxicity, MTT assays were performed at different N/P ratios in parallel to the luciferase assay in Neuro2A cells. The metabolic activity values yielded between 80 and 110 % after pDNA transfection (Figure 30), indicating that none of the oligomers displayed severe toxicity under the tested conditions.

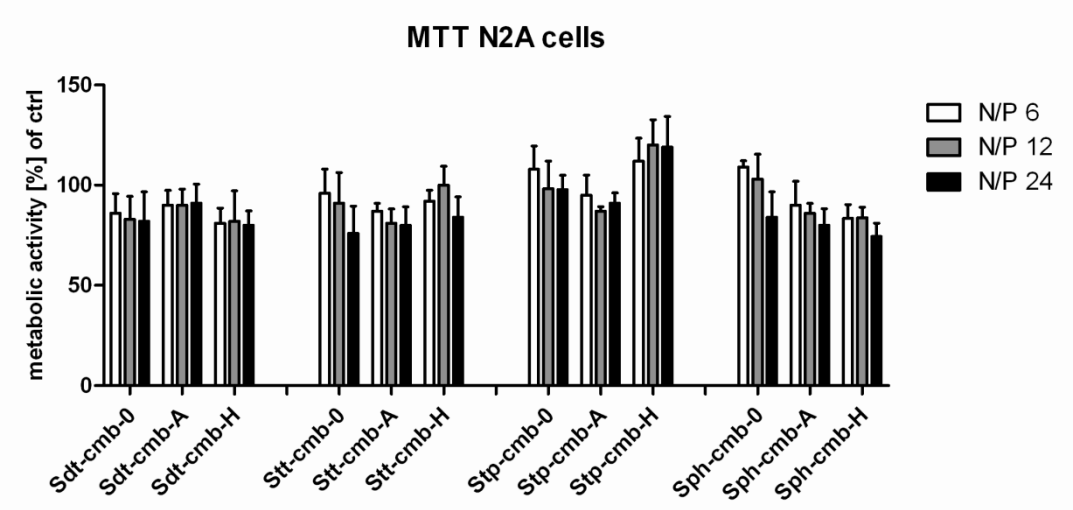

Figure 30. Metabolic activity determined with the MTT assay in Neuro2A cells of a) Sdt, Stt, Stp and Sph comb structures and b) Stp and Sph linear structures. The experiment was performed by Petra Kos (PhD thesis LMU, 2014).

4.3.4 Introduction of a functionalization site using the Dde-Alloc orthogonality

In the present work the orthogonality of the Fmoc- and Dde-protecting group was exploited for the assembly of comb-type oligomers. Among all synthesized comb structures, Stp-cmb-H turned out to be the most effective one for pDNA delivery, clearly exceeding the transfection efficiency of LPEI. Nevertheless, thinking ahead towards therapeutical applications the need for carrier optimization arises, for example in terms of specific tumor targeting. In this context, the extension of the orthogonality by introducing a further

protecting group is of great interest. Exploiting this synthetic diversity, as a proof of concept a PEG-conjugated folic acid (FolA) targeting ligand was attached to the Stp-cmb-H, illustrating the possible options of comb structure functionalization. The resulting structure C-K(PEG-FolA)-[H-K(Stp)]$_8$-C (Stp-cmb-H-PEG-FolA) is depicted in (Scheme 4). The Allyloxycarbonyl (Alloc) protecting group for amines can be removed by reduction with palladium catalysts and therefore does not interfere with the base- or acid-driven protective group removal [138]. Whereas the cleavage of Alloc in the presence of Dde can be done without any precaution, the Dde cleavage with hydrazine in the presence of Alloc is performed in the presence of a high excess of allyl alcohol to prevent the premature cleavage [130]. Because the cleavage of the Alloc group is much more time-consuming, this protection strategy was chosen only for one lysine, which was used for the attachment of the targeting ligand. The eight other lysine residues were protected with Dde and were used for the attachment of the diaminoethane building blocks for comb assembly (Scheme 5). In addition, for investigation of the folic acid-mediated targeting effect a control sequence carrying acetylation instead of the targeting ligand was synthesized analogously.

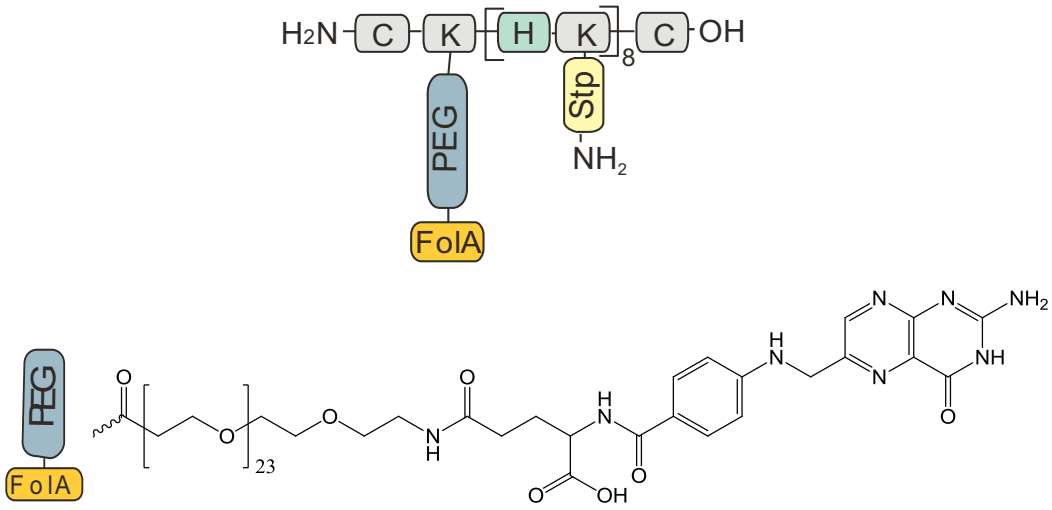

Scheme 4. Structure of the comb structure with targeting ligand synthesized with the Dde-Alloc strategy.

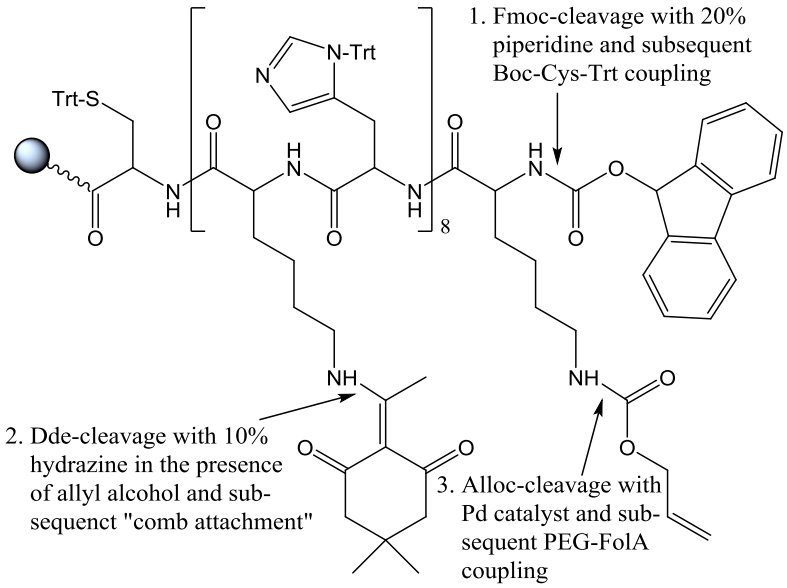

Scheme 5. Last synthesis steps of the targeted comb structure Stp-cmb-H-PEG-FolA, showing the structure of the three orthogonal protecting groups Fmoc, Dde and Alloc and the order of their cleavage.

The NMR spectrum of the targeted comb structure, Stp-cmb-H-PEG-FolA, proves the identity and the presence of the PEG-linked Folic acid (Figure 31). Nevertheless, the presence of peaks belonging to the Fmoc protecting group, indicate difficulties (incomplete Fmoc removal) in the synthesis. Also in the HPLC chromatogram a small fraction of Fmoc-containing product can be detected for the FolA-targeted oligomer but the chromatogram of the control sequence with acetate demonstrates that the applied synthesis conditions are suitable to obtain products of a higher level of purity (Figure 32).

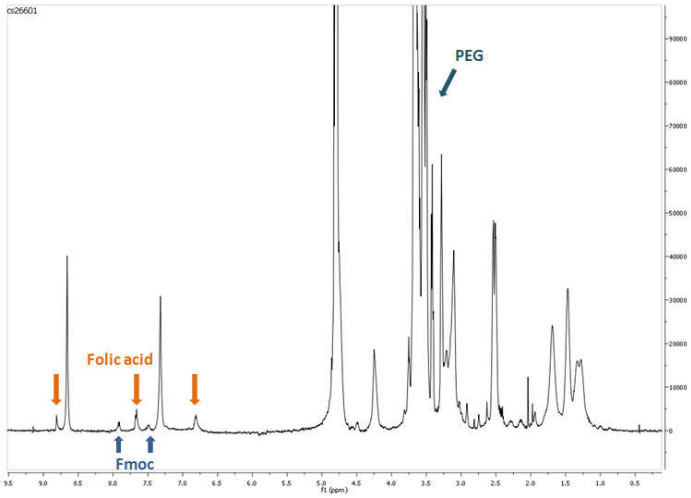

Figure 31. ^{1}H-NMR spectrum of Stp-cmb-H-PEG-FolA in D_2O verifying the successful attachment of the PEG-FolA ligand.

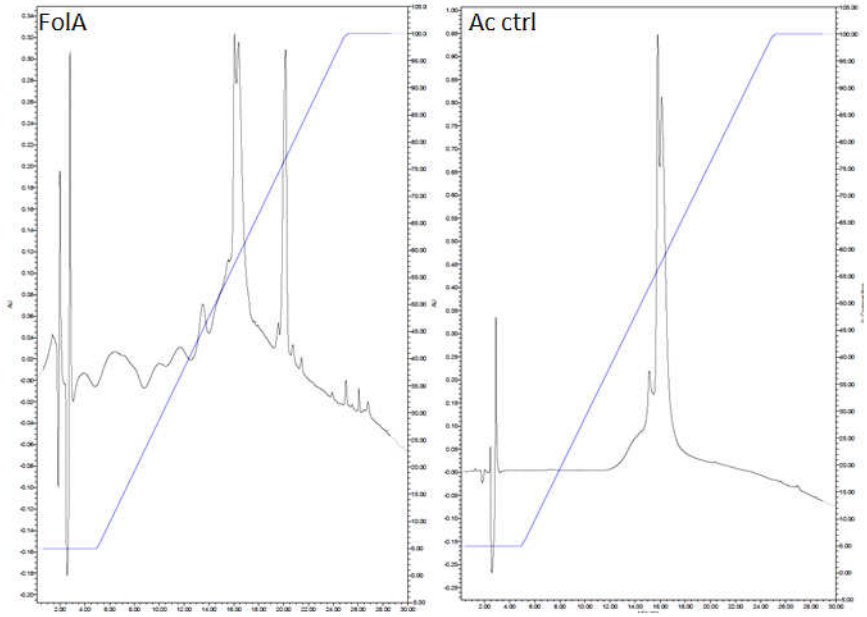

Figure 32. HPLC chromatograms of Stp-cmb-H-PEG-FolA (=FolA) and Stp-cmb-H-PEG-Acetate (=Ac ctrl) recorded on a RP SunFire C18 column.

The successful PEG-shielding is demonstrated by an increase of size of pDNA polyplexes of the comb structures with PEG-ligand (FolA and Ac ctrl) compared to the original unmodified oligomer, as well as the simultaneous decrease of the zeta potential, measured by DLS (Figure 33). Despite the PEGylation, which may hinder the electrostatic binding of the oligomer and the nucleic acid to some extent, both PEGylated structures display complete DNA binding in the agarose gel shift assay at N/P 6 and higher (Figure 34). Finally, the functionality of the FolA-targeted ligand was shown by efficient DNA delivery in FolA receptor-overexpressing KB cells. The specific uptake via the FolA receptor can be concluded from the lack of gene transfer of the control sequence with PEG-shielding, hampering the unspecific uptake (Figure 35).

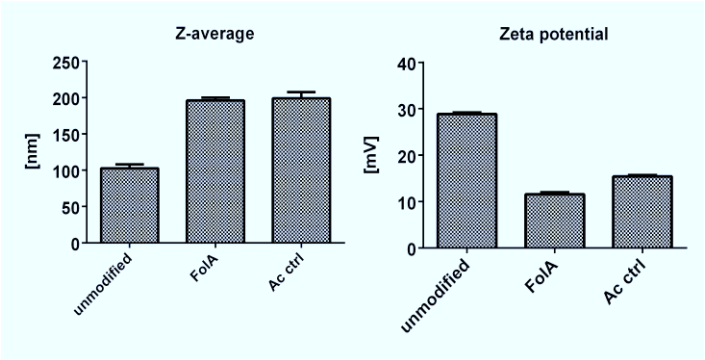

Figure 33. Size (indicated as Z-average) and zeta potential of FolA (= Stp-cmb-H-PEG-FolA) and Ac ctrl (= Stp-cmb-H-PEG-acetate) pDNA polyplexes at N/P 12 determined by DLS.

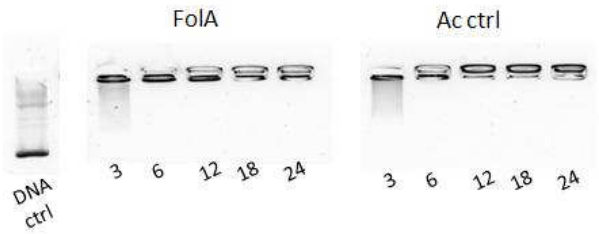

Figure 34. DNA binding of FolA (= Stp-cmb-H-PEG-FolA) and Ac ctrl (= Stp-cmb-H-PEG-acetate) at increasing N/P ratios determined by agarose gel shift assay.

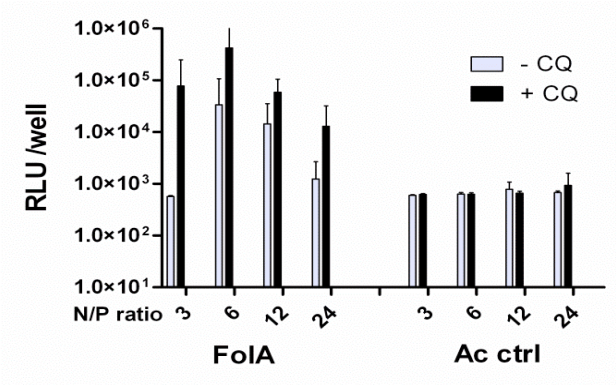

Figure 35. Luciferase gene transfer of FolA (= Stp-cmb-H-PEG-FolA) and Ac ctrl (= Stp-cmb-H-PEG-acetate) pDNA polyplexes tested in FolA-receptor overexpressing KB cells at increasing N/P ratios without or with addition of the endolysosomotropic molecule chloroquine (CQ). The experiment was performed by Petra Kos (PhD thesis LMU, 2014).

4.4 Comparison of comb and linear topology of oligomers for pDNA delivery

The results shown in Chapter 4.3 revealed that the comb topology may provide effective carriers for pDNA delivery. In the following, the most promising sequences, which were those bearing Stp or Sph branches, were compared to corresponding linear structures containing the identical type and numbers of amino acids, but with the Stp or Sph building blocks attached to the α-amino group of lysine instead of the corresponding ε-amino group of the oligomer backbone. Therefore, the total number of protonatable amines remains the same in both carrier types, but the lengths of oligomer backbone strongly differ.

4.4.1 Biophysical characterization: DNA condensation, particle size and buffer capacity

The pDNA complexation ability of the branched and linear oligomers was examined at different N/P ratios using the agarose gel shift assay. While the comb structures showed partial DNA binding at N/P 3 and complete binding at N/P 6 and higher (Figure 24) the linear Stp and Sph sequences showed already complete DNA binding at N/P 3 (Figure 36). To investigate the influence of the N/P ratio on the binding capability in more detail, an EtBr

exclusion assay was performed increasing the N/P ratio in steps of 0.5 from N/P 0 to 2 and bigger steps up to N/P 12 (Figure 37). Except for the Stp containing structures with Ala spacer, all linear structures showed a better DNA condensation ability compared to the corresponding comb structures. This effect was less pronounced for the structures with histidine spacer (Stp-lin-H vs. Stp-cmb-H). The results are in agreement with the data obtained in the gel shift assay and demonstrate an advantageous DNA binding for the linear structures. However, both comb- and linear-type structures are able to form stable polyplexes with pDNA at N/P ratios higher than 5.

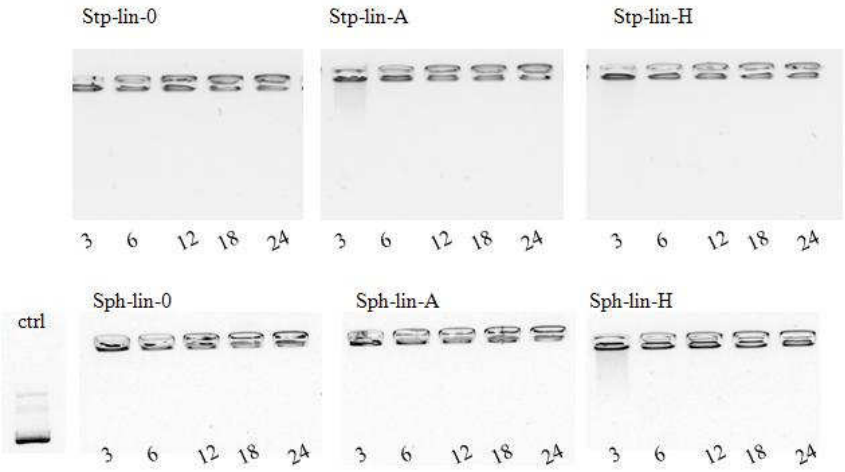

Figure 36. pDNA binding ability of Stp and Sph linear structures determined by agarose gel shift assay at increasing N/P ratios as indicated.

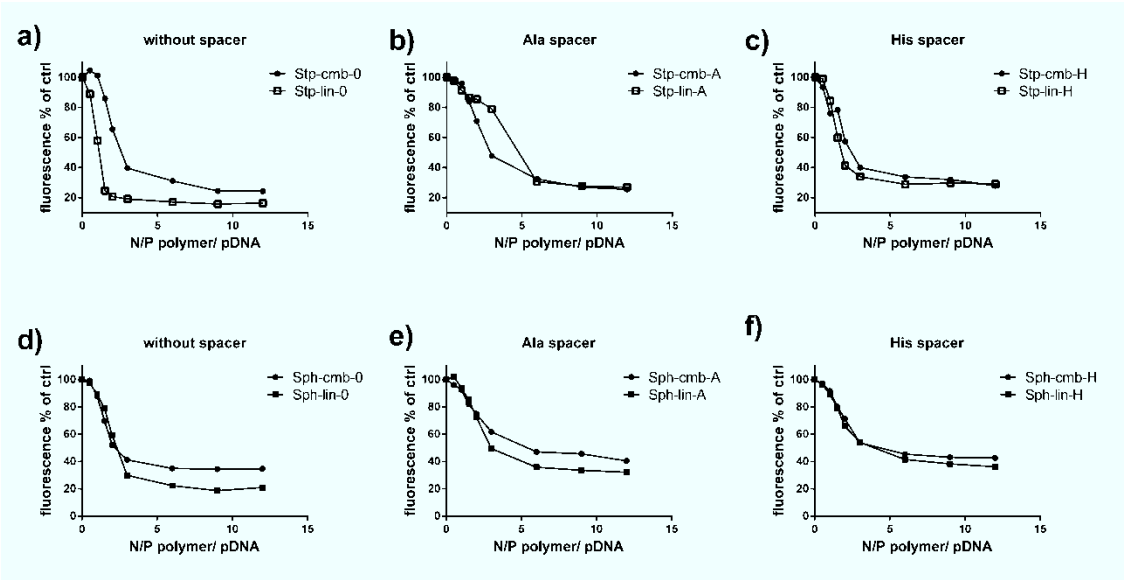

Figure 37. EtBr exclusion assay of Stp (a-c) and Sph (d-f) comb structures and corresponding linear structures with increasing N/P ratios by stepwise addition of the oligomer to pDNA solution at pH 7.4. a), d) without spacer b), e) Ala spacer c), f) His spacer

Particle size and zeta potential of oligomer/pDNA complexes were determined at N/P 12 by DLS (Table 7). The mean sizes of the polyplexes of the Stp comb type structures were about 100 to 130 nm (Table 6). Polyplex sizes were quite similar for the linear structures with a range between 85 and 135 nm. For Sph-containing structures slightly bigger sizes were observed, in the range of 100 to 170 nm for the comb structures and 115 to 130 nm for the linear structures, but revealing again no significant differing effect of the topology on the polyplex size. Independent of the building block, the zeta potential of comb structures without spacer or Ala spacer displayed a slightly higher zeta potential than the corresponding linear structure. The zeta potential was quite similar for His-containing structures (Table 7).

	Z-average [nm]	PDI	Zeta potential [mV]
Stp-lin-0	112,9 ± 12,9	0,359	26,2 ± 0,8
Stp-lin-A	85,8 ± 3,9	0,226	26,0 ± 0,4
Stp-lin-H	131,6 ± 3,6	0,314	28,7 ± 0,4
Sph-lin-0	117,4 ± 12,2	0,195	14,6 ± 3,7
Sph-lin-A	127,9 ± 4,0	0,276	12,4 ± 0,6
Sph-lin-H	125,3 ± 3,4	0,313	21,8 ± 0,3

Table 7. Particle sizes (indicated as Z-average), polydispersity index (PDI) and zeta potential (ZP) of oligomer/pDNA complexes at N/P 12 measured by DLS.

Comparing the differential buffer capacities between pH 5.0 and 7.4 in detail, a clear difference in the buffering profiles became obvious (Figure 38). For Stp oligomers with four protonatable amines in the comb type and three in the linear type, all comb structures displayed the highest buffer capacity between pH 5.0 and 6.5, whereas the maximum buffer capacity of the linear oligomers was observed between pH 6.5 and 7.4 (Figure 38 a, b). An opposite effect could be observed for the Sph oligomers, where four protonatable amines are provided in the linear structures and five in the comb structures. Here the linear oligomers demonstrated a clearly higher buffer capacity between pH 5.0 and 6.5, whereas the highest buffer capacity of the comb oligomers was observed between pH 6.5 and 7.4 (Figure 38 d, e). As histidine enhances the buffer capacity at pH 6, an additive effect at this pH could be observed for the histidine-containing oligomers, so that the already high buffer capacity at this pH was further increased for the Stp comb and Sph linear structures,

whereas the Stp linear and Sph comb structures consequently showed a broader buffer capacity over the whole pH range from 5.0 to 7.4 (Figure 38 c, f).

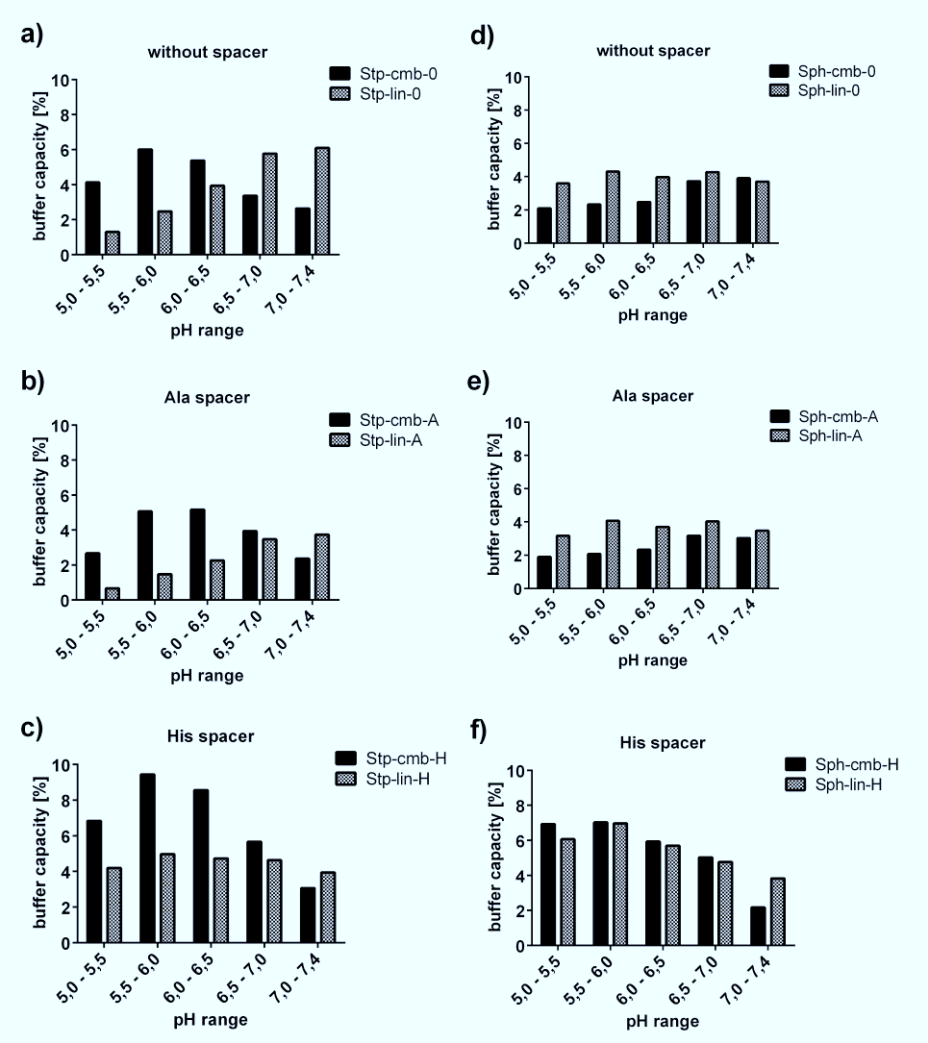

Figure 38. Comparison of differential buffer capacities of Stp- and Sph-based comb and linear structures between pH 5.0 and 7.4. a) Stp oligomers without spacer, b) Stp oligomers with Ala spacer, c) Stp oligomers with His spacer, d) Sph oligomers without spacer, e) Sph oligomers with Ala spacer, f) Sph oligomers with His spacer.

4.4.2 Biological evaluation: Cellular association, intracellular uptake, gene transfer and cytotoxicty

To compare the biological efficiency of the Stp and Sph comb and linear oligomers, the cellular association of polyplexes was investigated in Neuro2A cells (Figure 39). After one hour at 0 °C, the linear structures displayed a higher amount of polyplexes bound to the cells. After four hours of incubation, the cellular association was similar for comb and linear structures.

Next the intracellular uptake of polyplexes was investigated after four hours at 37 °C (Figure 40). Interestingly and independent of the ethylene amine building block and the spacer amino acid, the comb type structures displayed higher intracellular uptake rates than their linear counterparts. Cellular uptake was already higher for the comb structures than the linear structures after one hour and approximately 3- to 4-fold higher for the Stp combs and 5- to 11-fold for the Sph combs after four hours.

The reasons for the discrepancy between cell association and intracellular uptake, and the differing effect of oligomers topology remain unclear. Simple biophysical properties such as zeta potential can be ruled out as dominating parameters. In the case of Stp-cmb-A, Sph-cmb-0 and Sph-cmb-A the zeta potential of the comb structures was higher than for the linear structures, which correlates with their enhanced cellular internalization. However, for the other examined structure pairs the measured zeta potential was similar but the enhanced uptake was still observed.

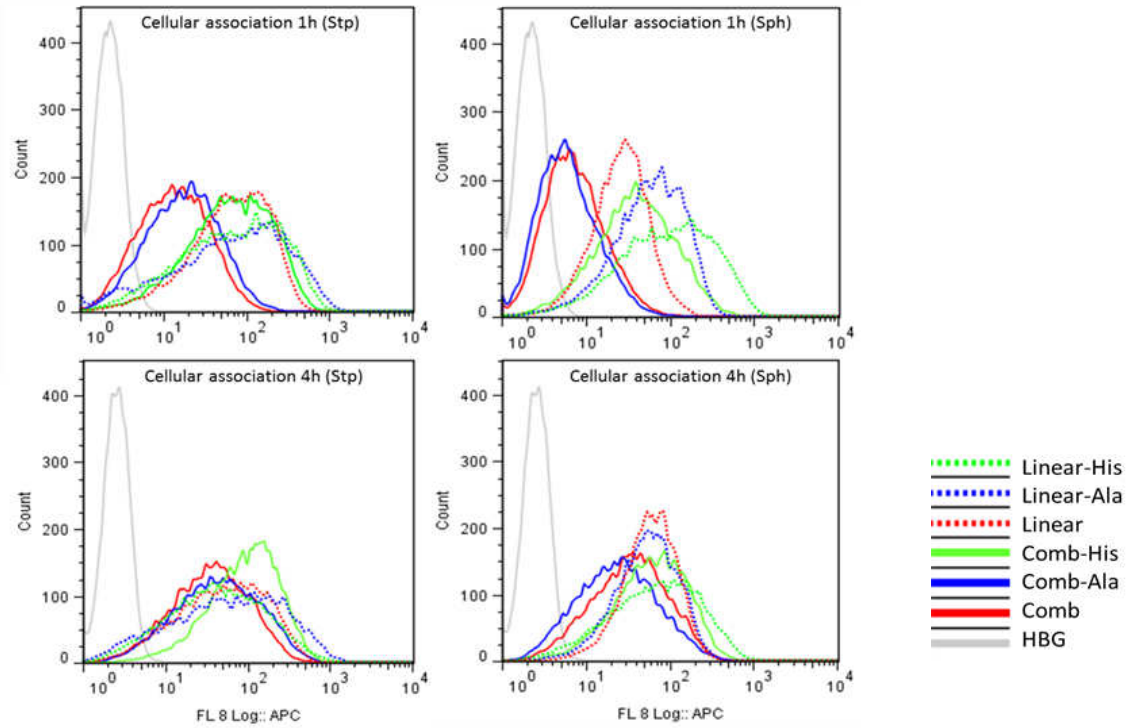

Figure 39. Cellular association of Cy5-labeled DNA/oligomer complexes at N/P 12 after one or four hours with Stp or Sph oligomers determined by flow cytometry in Neuro2A cells. Comb structures are displayed with solid lines, linear structures with dotted lines. Without spacer = red, Ala spacer = blue and His spacer = green. X-axis represents the intensity of the Cy5 signal and "Count" the number of cell counts with according fluorescence signal after appropriate gating. The experiment was performed by Petra Kos (PhD thesis LMU, 2014).

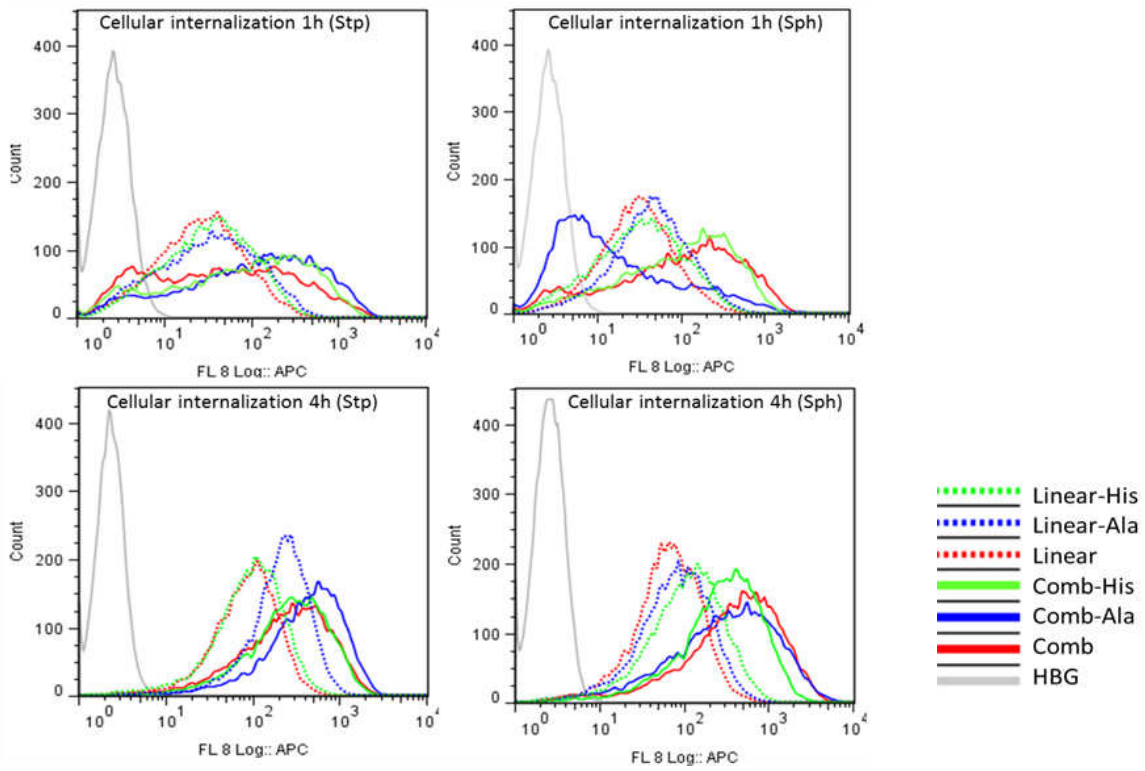

Figure 40. Cellular internalization of Cy5-labeled DNA/oligomer complexes at N/P 12 after one or four hours with Stp or Sph oligomers determined by flow cytometry in Neuro2A cells. Comb structures are displayed with solid lines, linear structures with dotted lines. Without spacer = red, Ala spacer = blue and His spacer = green. X-axis represents the intensity of the Cy5 signal and "Count" the number of cell counts with according fluorescence signal after appropriate gating. The experiment was performed by Petra Kos (PhD thesis LMU, 2014).

The oligomers were compared in their pDNA transfection efficiency (Figure 41). For Stp oligomers, the gene transfer levels of the comb type oligomers were 7- to up to 340-fold higher compared to the linear structures (Figure 41 a). The histidine-containing oligomers displayed the greatest gene transfer efficiency. Evaluation of the pDNA transfection efficiency of Sph comb and linear structures also revealed some higher gene transfer efficiency of the comb type oligomers, but compared to the Stp oligomers this effect was less pronounced (Figure 41 b).

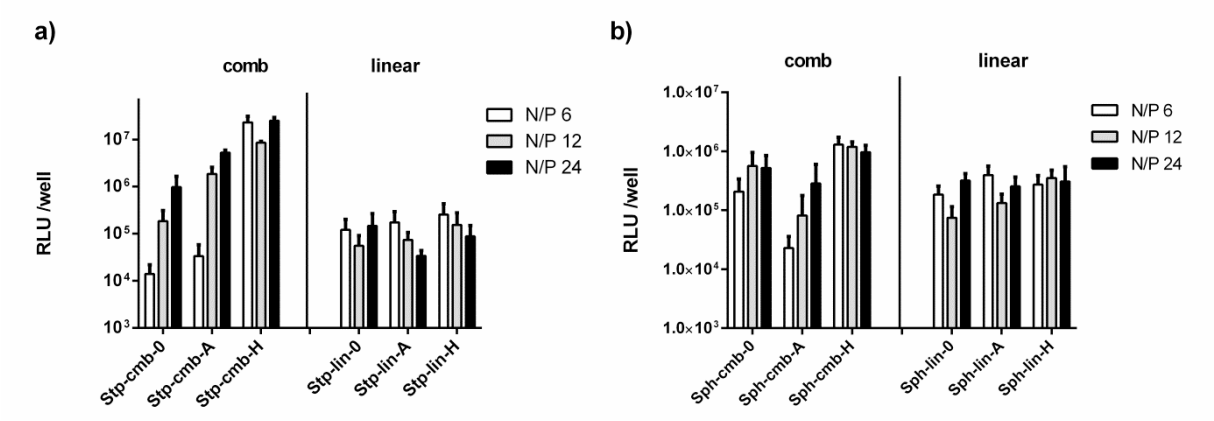

Figure 41. Luciferase gene transfer by comb versus linear carriers. a) Stp and b) Sph oligomers tested with pCMVLuc pDNA in Neuro2A cells at N/P ratios 6, 12 and 24. The experiment was performed by Petra Kos (PhD thesis LMU, 2014).

As already demonstrated for the Stp and Sph comb structures (Figure 30) also the linear structures displayed mean values of around 80 to 100 % metabolic aciticty in the MTT assay at different N/P ratios indicating no severe cytotoxicity under the tested conditions (Figure 42).

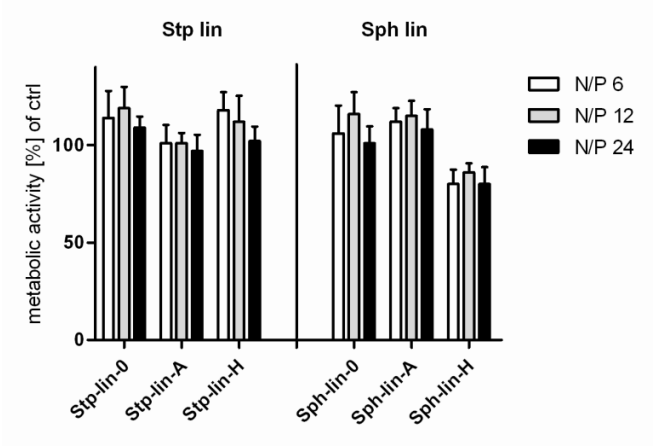

Figure 42. Metabolic activity determined with the MTT assay in Neuro2A cells of Stp and Sph linear structures. The experiment was performed by Petra Kos (PhD thesis LMU, 2014).

5 DISCUSSION

5.1 Evaluation of linear oligo(ethanamino)amide carriers of increasing molecular weight for pDNA delivery and comparison to linear PEI

In the present work optimized microwave-assisted solid-phase supported synthesis and the artificial amino acids succinyl-tetraethylene pentamine (Stp) [61] or succinyl-pentaethylene hexamine (Sph) [66, 68] were applied for the assembly of well-defined linear peptide-like carriers for pDNA delivery. The artificial amino acids as well as the transfection agent PEI [25, 139-141] contain the diaminoethane motif. This protonatable repeat unit is responsible for the favorable transfection properties, mediating electrostatic binding with pDNA and additional protonation capacity upon cell entry into endolysosomal compartments [127, 142-145]. The gold standard linear PEI (LPEI), containing approximately 500 (±200) protonatable nitrogens [146], obviously has a far larger average polymer size than previously synthesized Stp oligomers. In addition both Stp and Sph oligomers differ from LPEI by an amide-bonded succinic acid linker after every fifth or sixth ethanamino unit. To address the question whether longer linear Stp or Sph oligomers can mimic LPEI in transfection, the effect of increasing the MW of linear oligo(ethanamino)amides on pDNA mediated gene transfer and cytotoxicity was investigated. Beyond a critical oligomer size - indeed the diaminoethane motif containing building blocks (Stp or Sph) enable efficient gene transfer without need for further functional modifications.

DNA complexation studies using agarose gel shift and EtBr based assays showed improved binding characteristics with increasing number of Stp units. In agreement with previous studies [111] an oligomer with 5 Stp did not show any pDNA binding. The longer the synthesized Stp chain, the better pDNA binding was observed. This polyplex stabilization can be attributed to multivalent electrostatic interactions between the pDNA with oligomers carrying more positive charges per molecule. Interestingly, comparison of the oligomer containing 30 Stp units (MW 8.3 kDa) with the same molecule carrying two terminal cysteines for further disulfide-based stabilization did not reveal any differences in polyplex stabilization and dissociation. This contrasts previous findings with a wide spectrum of smaller oligomers where the cysteine modification displayed an essential contribution to polyplex stabilization [63, 132]. Similarly, the effect of substituting Stp for Sph, which

resulted in enhanced pDNA complexation in studies using oligomers with lower number of building block units [66, 68], was attenuated in the case of the long oligomers with 20 or 30 Stp (or Sph) units per oligomer. Stp chain interruption by β-alanine incorporation, as it was implemented in the $[Stp5\text{-}ßA]_6$-W oligomer, clearly diminished the pDNA binding ability. This finding points out that not only the MW and number of positive charges, but also the charge density plays an important role for the electrostatic interaction of the polycation with the polyanionic nucleic acid. The results of the binding and polyplex stability assays are in accordance with the measurements of the particle sizes, indicating that only at a certain length threshold (> 10 Stp units) the Stp oligomers are able to form compact nanosized particles with pDNA.

Endosomal protonation is a key prerequisite for the transfection activity of PEI [25, 139-141]. Both the number of protonatable amines in a row in one diaminoethane building block [66] as well as the number of repeated building block units might influence the buffering profile. Measurement of the buffer capacities of Stp oligomers with increasing length, Sph oligomers and LPEI resulted in very similar values of around 15-20 % differential protonation between pH 5.0 and 7.4, independent of the molecular weight. Previous findings that Sph analogs (with 4 protonatable amines in a row) displayed improved endosomal buffering compared to Stp oligomers (with 3 protonatable amines in a row) are most likely only applicable to smaller oligomers with lower amount of building block units and might not apply for these longer structures with 20 or more units. The gene transfer experiments show a clear increase of transfection efficiency with increasing MW. Interestingly, Stp15-W with a MW of around 4.3 kDa exceeded the LPEI transfection level but only at the highest tested N/P ratio of 24. Stp30-W, containing 91 protonatable nitrogens, displayed a greater gene transfer than LPEI already at N/P ratio 3, indicating the excellent capability of these carrier systems for pDNA delivery. As Stp40-W achieved similar pDNA transfection levels but did not exceed the performance of Stp30-W, we assume that an optimum length was reached at around 30 units and further elongation does not result in a greater benefit. Also the cysteine-terminated Stp30-W analog did not further increase luciferase expression levels, confirming that for these long Stp oligomers the disulfide bond-mediated polyplex stabilization does not provide a benefit. According to the findings that exchanging Stp for Sph did not significantly alter the buffering capacity and DNA complexation ability of the oligomers Sph20-W and Sp30-W, also the luciferase gene transfer was at the same high level as for the original Stp

oligomers. The observation that the Stp30-W analog with β-alanine incorporation after every fifth Stp unit clearly reduced the gene transfer activity, underlines the influence of the microstructure of the oligomers, especially the charge density determining the nucleic acid binding ability.

Since the cytotoxicity of the cationic polymer PEI is one of the major concerns for the use as a carrier for gene delivery, the comparison between LPEI and the new Stp oligomers is particularly relevant. PEI is known to cause toxic effects by versatile mechanisms such as cytosolic and mitochondrial membrane damage as well as necrotic-like and apoptotic changes [123, 124, 147-149]. The CellTiter®Glo cytotoxicity assay revealed an at least 10-fold reduction of toxicity for the transfection-competent Stp oligomers in comparison to the commonly used LPEI. Cytotoxicity correlates with MW. Not only the lower MW of Stp30-W, but also the succinate spacer between the oligoamine units may contribute to the favorable biocompatibility of the Stp oligomers over standard PEIs. In fact, previous work demonstrated about 10-fold reduced toxicity of randomly branched PEI 25 kDa upon partial amidation with propionic or succinic acid [46].

5.2 Characterization of oligo(ethanamino)amides by capillary electrophoresis and Taylor dispersion analysis

The application of CE to sequence-defined oligo(ethanamino)amides of increasing length by our collaboration partners (Xiaoyun Jin, Dr. Laurent Leclercq, Prof. Dr. Hervé Cottet, U, Montpellier) turned out to be a useful tool for the analytical characterization of the electrophoretic behavior, providing new insights into charge and size distribution as well as possible interactions between the oligomers and their environment.

Electropherograms in acetic acid show a high electrophoretic mobility for all oligomers, as it can be expected due to the high extent of protonation at the low pH. Furthermore, it can be recognized that the dependence of mobility on molar mass for evenly charged small polyelectrolytes is non monotonous. These results are consistent with previous findings revealing that small oligomers (MW < 2000) present a larger range of increasing mobility with increasing chain length, whereas charged molecules of intermediate MW (2000 – 20000) display a slightly decreased mobility [150]. The increase of mobility with molar mass, typical for MWs of < 2000, is due to hydrodynamic coupling. Comparing a dimer and a monomer, the charge is multiplied by two while the friction coefficient of the dimer is less

than twice the friction coefficient of the monomer. Therefore the mobility that results from the ratio of charge to friction increases from monomer to dimer. This is true for oligomers with MW of ~1000-2000. For higher MWs, the mobility tends to decrease slowly for two reasons. First, there is a screening of the previously described hydrodynamic coupling effect by the friction of the counter ions. For that reason the friction coefficient tends to become proportional to the MW. The other reason is the occurrence of counter ion condensation, this means ion pair formation decreasing the effective charge. For higher molar mass (typically above MW 20 000), the mobility is independent of the size since both effective charge and friction are proportional to the MW. Cottet *et al.* showed that a change from rod-like to coil conformation accompanies the observation of an intermediate oligomer size with maximum mobility and the following slight decrease until a constant mobility is reached for oligomers or polymers of high MW [150].

A similar pattern becomes apparent for the less acidic α-aminocaproic acid. The decreasing electrophoretic mobility with increasing oligomer length, observed in both buffer solutions (acetic acid and α-aminocaproic acid), can be explained by counter ion condensation and screening of the hydrodynamic coupling that increases the frictional coefficient. However, inversed correlation was observed in HEPES buffer, meaning increased mobility with increasing oligomer length. This abnormal behavior might be explained by specific interactions of HEPES with the oligomer, which at the applied pH of 7.4 offers both cationic charges for electrostatic interactions and unprotonated domains for hydrophobic interactions or hydrogen bond formation. Interaction with HEPES seems to be much stronger with the smallest oligomers, leading to lower mobilities.

Application of CGE by addition of dextran was expected to show a size-dependant electrophoretic mobility. In a gel of 5 % dextran, the mobility of all oligomers was significantly decreased and peak broadening was observed likely due to higher resolution in molar mass. The desired effect of better resolution with a higher dextran concentration of 10 % was not observed because at this high dextran concentration peak broadening occured and the results were hardly repeatable. Interactions of the large dextran molecules with the oligomers have to be taken into account as possible reasons. Application of other polymers for gel formation should be considered in the future to improve the size-based separation of the oligomers.

The opposing correlations between the electrophoretic mobility and the MW of the analyzed oligomers, which were observed in the buffer systems of differing pH values, demonstrate the complexity of the possible interactions that can occure between the oligomers and the surrounding buffer components. The observed changes of the electrophoretic mobility at different pH values allow assumptions on possible conformations, which could be adopted by the oligomers in dependence of their protonation status and thus their cationic charge density.

Similar findings were made in TDA, which was used for determination of the hydrodynamic radius of the oligomers. First measurements in HBG buffer resulted in quite small R_h values, which can be attributed to repulsive interactions with the high concentrated glucose lowering the apparent diffusion coefficient. This presumption was verified by much higher radius (1.94 nm instead of 0.78 nm for Stp30-W) in HEPES buffer without glucose. The expected correlation of increasing hydrodynamic radius with increasing MW could be shown for the oligomers with 10, 20 and 30 Stp units, but the longest oligomer with 40 units displayed a smaller size, similar to the oligomer consisting of 20 Stp units. This aberration could be a consequence of a higher proportion of small impurities in the sample leading to a lower average size for the Stp40-W sample. It might be also explained by a conformational change at a certain length modifying the size of the oligomer.

A further interesting aspect in regard to conformational considerations is to set the R_h value, determined by TDA experiments, in relation to the contour length, which can be estimated with the exact oligomer structure and the length of chemical bonds. The assumption that the oligomer Stp30-W has a contour length of around 50 nm, is based on the knowledge of the contour length of one diaminoethane unit of polyethylenimine in a semiprotonated state (0.29 nm) [127] and the contour length of the amino acid backbone (0.38nm) [151]. In relation to the determined diameter of 3.88 nm (determined in HEPES pH 7.3 in TDA) it is almost 13-fold larger, which allows the conclusion that the linear oligomers adopt a rather coiled form in solution and still leaves the question open, how such a long structure can be condensed to such a small diameter. The reason for the appearance of two populations of different sizes in some of the buffer solutions also remains unclear but can most likely be explained by different conformational assemblies, although to a certain extent polydispersity cannot be excluded.

Assessing the variation of the hydrodynamic radius at different pH values, an increase of R_h values could be observed at acidic pH below 2. This effect is in accordance with the knowledge of a conformational change from the entangled gauche conformation in the unprotonated and semiprotonated state of PEI, to the stretched, antiperiplanar conformation in the fully protonated state, resulting in an increase of the contour length from 0.29 nm to 0.38 nm [152].

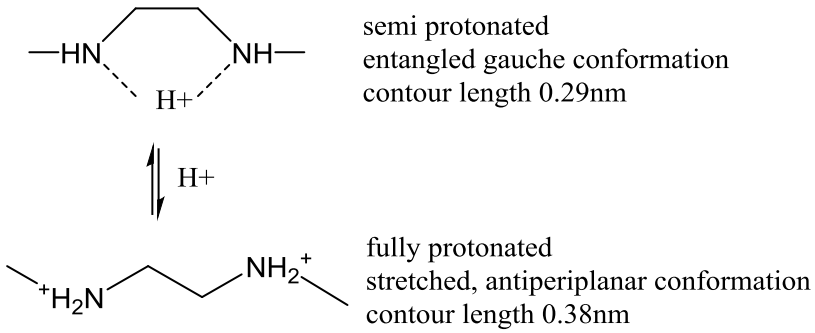

Figure 43. Conformational change of the diaminoethane motif in dependence of the protonation state. Modified from Wagner [127] and Ziebarth & Wang [153].

Although the results obtained by CE and TDA experiments are still in a preliminary state, they demonstrate the suitability of these sophisticated techniques to characterize oligo(ethanamino)amide carriers and get new insights in their behavior as polycationic species. Leclercq *et al* recently combined TDA and CE for analysis of polyelectrolyte complexes [154]. Application of this method for polyplex characterization opens up the possibility to determine the charge stoichiometry of the polycationic carrier and the polyanionic nucleic acid. In case of polydisperse samples, it could furthermore elucidate which population associates preferentially to the DNA and help to quantify the fraction of excess free oligomer in the polyplex. The determination of different sizes of disulfide-linked di-, oligo- or polymers would present a further interesting aspect, providing deeper insights in the physicochemical properties of the polyplexes, which help to further optimize the carrier systems.

5.3 Optimization of comb-like oligomers for pDNA delivery

Based on the knowledge of structure-activity relationships of an already existing library of sequence-defined cationic carriers for pDNA delivery [111], new comb-like structures were designed and synthesized by attaching the artificial amino acid Stp to an oligolysine backbone and inserting different natural amino acids between the lysines in the backbone

(Scheme 3b). Several of the obtained structures containing the spacer amino acids alanine, beta-alanine, histidine or tryptophane with or without terminal cysteines were screened for DNA transfection efficiency. Based on these results, three structures were chosen for further carrier optimization. As previously reported for linear structures [63, 68, 111] also for the comb structures the terminal cysteines demonstrated beneficial stabilization of polyplexes by means of disulfide formation and were therefore maintained in the synthesis of additional structures. The knowledge that histidine enhances endosomal release due to a beneficial buffering profile, which could be confirmed by the observed increase of transfection efficiency also for the comb structures, led to the selection of a histidine-containing structure. Corresponding control sequences with an alanine spacer for the determination of the specific histidine effect as well as without any spacer molecule, to visualize a possible spacer effect, completed the selection. Based on these three backbone structures a small library of twelve oligomers was synthesized via attachment of the four artificial amino acids Sdt, Stt, Stp and Sph (differing in the numbers of cationizable nitrogens from two to five) to the oligolysine backbone. The biophysical properties of the oligomers and their performance in biological application were then compared. In analyses of comb oligomers with the different oligoamino acid building blocks, the ability of DNA complexation was investigated by EtBr assay. The weakest DNA binding was revealed for Sdt oligomers, implying that these structures might be the less suitable ones amongst the tested carriers. Consistent with the weak DNA binding, pH titrations revealed a less protonated state at pH 7.4 and therefore potentially less electrostatic interactions with the negatively charged DNA. Sdt structures were not able to form small and stable particles. The formation of big aggregates of around 2 µm for Sdt-cmb-0 may account for the very low cellular uptake. Also polyplexes with Sdt-cmb-A and Sdt-cmb-H displayed rather large particle sizes and only a small fraction of cells internalized. Nevertheless, some transfection efficiency was observed for the Sdt oligomers in the luciferase assay. A possible reason might be an improved endosomal release based on effective endosomal buffering and protonation. Sdt comb oligomers display the highest buffer capacity between pH 5.0 and 7.4 amongst the tested oligomers. In contrast, Stt oligomers showed the worst buffering capacity. The particle sizes were around 2- fold higher compared to the polyplexes formed with the Stp structures. The latter ones resulted in the smallest particles with the highest positive zeta potential.

Together with the high buffering capacity the beneficial nanoparticle characteristics mark the Stp comb structures as potent carriers for gene delivery.

The best-performing oligomer in terms of DNA transfection, Stp-cmb-H, was chosen as an exemplary structure in order to demonstrate the potential of further functionalization of comb-type structures. Taking advantage of the orthogonality of the Dde and Alloc protecting group, the ε-amino groups of the oligolysine backbone can be specifically modified with different “comb arms” at defined positions. As a proof of this concept a comb structure was synthesized resembling Stp-cmb-H but carrying one additional lysine to which a folic acid-bearing PEG-ligand was attached. Although the complex synthetic procedure requires further optimization, the suitability of the strategy and the benefit of the functionalization were demonstrated.

5.4 Comparison of comb and linear topology of oligomers for pDNA delivery

To investigate which properties can be attributed to the specific comb topology, linear control Stp sequences were synthesized and directly compared in terms of biophysical properties and biological performance. To further explore to which extent the different behavior is a consequence of the topology or an effect of the variation of the protonatable ethylenamine building block length, the same comparison was performed with the Sph-containing comb and linear structures.

Superior pDNA binding of the histidine-free linear structures was displayed by the EtBr assay, whereas for the histidine-containing structures a similar pDNA condensation ability of linear and comb structures could be observed, both in case of Stp and Sph based oligomers. A possible explanation is that histidine also contributes to the pDNA complexation ability and polyplex stabilization of these structures, therefore mitigating the difference in performance of comb and linear type. Furthermore, the tests revealed that at N/P 12 the DNA condensation was complete for all oligomers, so that this N/P ratio was used for further studies aimed at comparing particle size, zeta potential, cellular uptake and association.

A most prominent distinction of comb and linear structures was found in the buffer capacity at the physiological relevant pH range between 5.0 and 7.4. Kataoka *et al.* proposed the so-called “odd-even effect”, reporting that polymers with side chains consisting of an even number of protonatable amino ethylene units provide high buffer capacity in this pH range

and therefore a high transfection efficiency, while polymers with odd-numbered amino ethylene side chains display low buffer capacity and hence also low transfection efficiency. This assumption is based on the fact that changes in protonation from pH 7.4 to pH 5.0 occur for even-numbered structures, while electrostatic repulsion prohibits further protonation for odd-numbered structures, resulting in a lower buffer capacity. This model is confirmed in the current study by the comparison of the buffering capacity of Sdt, Stt, Stp and Sph building blocks. Sdt and Stp-containing comb structures with even-numbered protonatable amines show a higher buffer capacity than the odd-numbered Stt and Sph containing structures. Nevertheless, only partial accordance with the hypothetical model can be found in the comparison of comb and linear topology. Stp units in the comb sequences provide four protonatable amines (even number) and in the linear structures only three (odd number). Therefore the total buffer capacity should be higher for the comb structures, while in comparison of the Sph combs (five protonatable amines = odd number) with Sph linear structures (four protonatable amines = even number) the linear structures were expected to provide a higher total buffer capacity. The fact that free amines of the lysine in the linear structures result in the same total number of protonatable amines in both structure types shows that not the total number, but the intramolecular localization plays a crucial role. In both cases, comparing Stp and Sph comb and linear structures, a similar total buffer capacity between pH 5.0 and 7.4 was found. However, a modified “odd-even rule” becomes apparent with regard to the buffering profile. The results clearly demonstrate that an odd number of protonatable amines in row leads to a maximum buffer capacity in the pH range from 6.5 to 7.4 and an even number of protonatable amines results in a maximum buffer capacity at pH 5.0 to 6.5. Especially the higher buffer capacity from pH 5.0 to 6.5, which corresponds to the endosomal pH, may be contributing to an enhanced endosomal release. These findings give deeper insight into this phenomenon and contribute to understanding the superior performance in gene transfer of structures with higher buffering capacity at the relevant pH range. Remarkably, for all types of carriers the histidine-containing sequences displayed the highest gene transfer consistent with the general notion that an increased buffer and protonation capacity at endosomal pH may enhance endosomal escape (‘proton sponge effect’) and gene transfer. According to these results in terms of buffer capacity, the Stp building block is more beneficial when using it in the comb topology.

The comb and linear topology resulted in a further clear difference in regard to cellular association and internalization. In the cell association assay performed by incubation at 0 °C (to block internalization), after one hour the polyplexes formed with linear structures showed an increased cell association compared to the comb structures. After four hours the measured cell binding of polyplexes of comb and linear sequences was similar. Surprisingly, all Stp and Sph comb structures displayed an enhanced cellular uptake in comparison to their linear counterparts. This trend was observed already at one hour incubation time and was clearly visible after four hours. As no remarkable differences could be observed for the size and zeta potential of comb and linear structures, these studies clearly demonstrate that the uptake process is considerably influenced by the carrier topology. Whether the oligomer topology alters the nanoparticle surface exposed in cellular interaction, or whether the different free oligomers trigger cell uptake processes in a different manner, remains to be investigated. These observations are in agreement with other studies showing that nanoparticle shape and surface can have influence on the cellular uptake and binding on the cell surface.

Interestingly, the different transfection efficiencies of oligomers without spacer or with alanine spacer indicate that not only the total amount of cationic charges and buffering may be important, but also the orientation and distance of the charged domains, which is changing the charge density and hence several biophysical properties.

6 SUMMARY

Despite considerable success in the use of viral vectors for gene delivery, limitations in connection with the potential for immune reactions and insertional mutagenesis shifted the attention towards the application of synthetic carriers with lipids, polymers and peptides as most prominent examples. Among the cationic polymers, linear polyethylenimine (LPEI) is still a prevalent standard reagent for DNA transfection. A huge number of modifications have so far been applied in order to improve the properties of this carrier in terms of effectivity and cytotoxicity with partial success, but the eminent drawback of its polydisperse nature remains a major concern for a potential use in the clinics.

In the current doctoral study novel sequence-defined oligo(ethanamino)amide carriers were assembled by solid-phase peptide synthesis (SPPS). Artificial oligoamino acids such as succinyl-tetraethylene pentamine (Stp) or succinyl-pentaethylene hexamine (Sph) were combined with various natural amino acids in defined sequence and topology. The monodispersity and precision of the synthesized oligomers allowed the systematic study of clear structure-activity relations, such as the effect of increasing MW or backbone topology on the most relevant parameters for gene transfer, including pDNA binding, polyplex stabilization, cell uptake, endosomal buffering, transfection efficiency and cytotoxicity.

In the first part the step by step elongation of precise linear oligo(ethanamino)amides synthesized via SPPS was carried out. The expectation was that containing only the diaminoethane motif but no other functional domains, these oligomers should ideally mimic a kind of defined low molecular weight “LPEI” and thereby overcome the major obstacles of polydispersity and cytotoxicity. Moreover the high gene transfer activity should be maintained or even enhanced. The applied strategy demonstrated the influence of increasing MW and allowed to determine an optimum carrier length of 30 Stp units (representing 90 protonatable nitrogens). This gene carrier based on the diaminoethane motif showed six-fold higher transfection efficiency and ten-fold lower cytotoxicity than the conventionally used LPEI.

In the second part of this thesis the effect of topological changes on specific carrier properties for pDNA delivery was investigated. By means of SPPS a new comb topology was designed, where several different artificial amino acids containing the diaminoethane motif

were attached to a lysine backbone. Different spacer amino acids (alanine, beta alanine, histidine) were introduced to the lysine backbone and distinct effects could be attributed to them. The most profitable modification was the insertion of histidine, which enhanced the endosomal buffering due to its protonation of the imidazole group at the physiological relevant pH 6. Consequently, the transfection efficiency was significantly increased emphasizing the endosomal release as a crucial step among the hurdles of nucleic acid delivery. In the next step the most efficient comb oligomers were directly compared to linear control sequences to derive more detailed structure-activity relationships and to show the explicit effect of the topology. This direct comparison revealed that a change in topology of sequence-defined oligoamino acid-based pDNA carriers from linear to comb-like design resulted in a distinct change in buffer capacity profile of oligomers and intracellular uptake of corresponding pDNA polyplexes. For the Sph oligomers the linear structures showed an increased buffer capacity at endosomal pH, but the comb structures displayed a higher cellular uptake. These two opposing trends resulted in an only slightly higher transfection efficiency of the comb structures. For the Stp oligomers, the comb structures displayed the favorable endosomal buffering profile and mediated an enhanced cellular uptake. This additive comb benefit contributed to a strongly enhanced efficacy of Stp combs for pDNA delivery, determining them as promising candidates for further applications.

In summary, this doctoral study points out the relevance of two criteria – size and topology – for the design of oligomer carriers for nucleic acid delivery. The option of designing precise sequence-controlled structures offers the opportunity of deriving detailed structure-activity relationships. In the future, combining the gained knowledge of the systematic sequence variation and modification could allow designing an ideal carrier, comprising most essential features – stability during the delivery process, cargo release at the desired place of action and biocompatibility – that are crucial for the therapeutical use of synthetic carriers for nucleic acid delivery.

7 REFERENCES

[1] J. Rosenecker, S. Huth, C. Rudolph, Gene therapy for cystic fibrosis lung disease: current status and future perspectives, Curr Opin Mol Ther, 8 (2006) 439-445.
[2] M. Cavazzana-Calvo, S. Hacein-Bey, B.G. de Saint, F. Gross, E. Yvon, P. Nusbaum, F. Selz, C. Hue, S. Certain, J.L. Casanova, P. Bousso, F.L. Deist, A. Fischer, Gene therapy of human severe combined immunodeficiency (SCID)-X1 disease, Science, 288 (2000) 669-672.
[3] M. Grossman, S.E. Raper, K. Kozarsky, E.A. Stein, J.F. Engelhardt, D. Muller, P.J. Lupien, J.M. Wilson, Successful ex vivo gene therapy directed to liver in a patient with familial hypercholesterolaemia, Nat Genet, 6 (1994) 335-341.
[4] E.H. Szybalska, W. Szybalski, Genetics of human cell line. IV. DNA-mediated heritable transformation of a biochemical trait, Proc Natl Acad Sci U S A, 48 (1962) 2026-2034.
[5] S. Rogers, P. Pfuderer, Use of viruses as carriers of added genetic information, Nature, 219 (1968) 749-751.
[6] A. Fire, S. Xu, M.K. Montgomery, S.A. Kostas, S.E. Driver, C.C. Mello, Potent and specific genetic interference by double-stranded RNA in Caenorhabditis elegans, Nature, 391 (1998) 806-811.
[7] S.M. Elbashir, J. Harborth, W. Lendeckel, A. Yalcin, K. Weber, T. Tuschl, Duplexes of 21-nucleotide RNAs mediate RNA interference in cultured mammalian cells, Nature, 411 (2001) 494-498.
[8] R.C. Lee, R.L. Feinbaum, V. Ambros, The C. elegans heterochronic gene lin-4 encodes small RNAs with antisense complementarity to lin-14, Cell, 75 (1993) 843-854.
[9] D.P. Bartel, MicroRNAs: target recognition and regulatory functions, Cell, 136 (2009) 215-233.
[10] D.P. Bartel, MicroRNAs: genomics, biogenesis, mechanism, and function, Cell, 116 (2004) 281-297.
[11] J. Mattes, M. Yang, P.S. Foster, Regulation of microRNA by antagomirs: a new class of pharmacological antagonists for the specific regulation of gene function?, Am J Respir Cell Mol Biol, 36 (2007) 8-12.
[12] K. Germer, M. Leonard, X. Zhang, RNA aptamers and their therapeutic and diagnostic applications, Int J Biochem Mol Biol, 4 (2013) 27-40.
[13] T.C. Chu, K.Y. Twu, A.D. Ellington, M. Levy, Aptamer mediated siRNA delivery, Nucleic Acids Res, 34 (2006) e73.
[14] E.W. Ng, A.P. Adamis, Anti-VEGF aptamer (pegaptanib) therapy for ocular vascular diseases, Ann N Y Acad Sci, 1082 (2006) 151-171.
[15] J.W. Engels, Gene silencing by chemically modified siRNAs, N Biotechnol, 30 (2013) 302-307.
[16] J. Elmen, H. Thonberg, K. Ljungberg, M. Frieden, M. Westergaard, Y. Xu, B. Wahren, Z. Liang, H. Orum, T. Koch, C. Wahlestedt, Locked nucleic acid (LNA) mediated improvements in siRNA stability and functionality, Nucleic Acids Res, 33 (2005) 439-447.
[17] J.H. Jeong, H. Mok, Y.K. Oh, T.G. Park, siRNA conjugate delivery systems, Bioconjug Chem, 20 (2009) 5-14.

[18] Y. Ikeda, K. Taira, Ligand-targeted delivery of therapeutic siRNA, Pharm Res, 23 (2006) 1631-1640.
[19] A. Amantana, P.L. Iversen, Pharmacokinetics and biodistribution of phosphorodiamidate morpholino antisense oligomers, Curr Opin Pharmacol, 5 (2005) 550-555.
[20] S.L. Ginn, I.E. Alexander, M.L. Edelstein, M.R. Abedi, J. Wixon, Gene therapy clinical trials worldwide to 2012 - an update, J Gene Med, 15 (2013) 65-77.
[21] F.M. Veronese, G. Pasut, PEGylation, successful approach to drug delivery, Drug Discov Today, 10 (2005) 1451-1458.
[22] R. Duncan, The dawning era of polymer therapeutics, Nat Rev Drug Discov, 2 (2003) 347-360.
[23] S. Xu, B.Z. Olenyuk, C.T. Okamoto, S.F. Hamm-Alvarez, Targeting receptor-mediated endocytotic pathways with nanoparticles: rationale and advances, Adv Drug Deliv Rev, 65 (2013) 121-138.
[24] C. Pichon, L. Billiet, P. Midoux, Chemical vectors for gene delivery: uptake and intracellular trafficking, Curr Opin Biotechnol, 21 (2010) 640-645.
[25] O. Boussif, F. Lezoualc'h, M.A. Zanta, M.D. Mergny, D. Scherman, B. Demeneix, J.P. Behr, A versatile vector for gene and oligonucleotide transfer into cells in culture and in vivo: polyethylenimine, Proc Natl Acad Sci U S A, 92 (1995) 7297-7301.
[26] L. Vannucci, M. Lai, F. Chiuppesi, L. Ceccherini-Nelli, M. Pistello, Viral vectors: a look back and ahead on gene transfer technology, New Microbiol, 36 (2013) 1-22.
[27] P.L. Felgner, Y. Barenholz, J.P. Behr, S.H. Cheng, P. Cullis, L. Huang, J.A. Jessee, L. Seymour, F. Szoka, A.R. Thierry, E. Wagner, G. Wu, Nomenclature for synthetic gene delivery systems, Hum Gene Ther, 8 (1997) 511-512.
[28] K. Gao, L. Huang, Nonviral methods for siRNA delivery, Mol Pharm, 6 (2009) 651-658.
[29] J. Schafer, S. Hobel, U. Bakowsky, A. Aigner, Liposome-polyethylenimine complexes for enhanced DNA and siRNA delivery, Biomaterials, 31 (2010) 6892-6900.
[30] S. Spagnou, A.D. Miller, M. Keller, Lipidic carriers of siRNA: differences in the formulation, cellular uptake, and delivery with plasmid DNA, Biochemistry, 43 (2004) 13348-13356.
[31] D. Castanotto, J.J. Rossi, The promises and pitfalls of RNA-interference-based therapeutics, Nature, 457 (2009) 426-433.
[32] L.C. Gomes-da-Silva, N.A. Fonseca, V. Moura, M.C. Pedroso de Lima, S. Simoes, J.N. Moreira, Lipid-based nanoparticles for siRNA delivery in cancer therapy: paradigms and challenges, Acc Chem Res, 45 (2012) 1163-1171.
[33] M.A. A. Cervantes, J. Tabernero, J. R. Infante, P. LoRusso, G. Shapiro, L. G. Paz-Ares, R. Falzone, J. Hill, J. Cehelsky, A. White, I. Toudjarska, D. Bumcrot, R. Meyers, G. Hinkle, N. Svrzikapa, D. W. Sah, A. Vaishnaw, J. Gollob, H. A. Burris, Phase I dose-escalation study of ALN-VSP02, a novel RNAi therapeutic for solid tumors with liver involvement, in: ASCO Annual Meeting, Chicago, 2011.
[34] F. Lori, J. Trocio, N. Bakare, L.M. Kelly, J. Lisziewicz, DermaVir, a novel HIV immunisation technology, Vaccine, 23 (2005) 2030-2034.
[35] M.W. Konstan, P.B. Davis, J.S. Wagener, K.A. Hilliard, R.C. Stern, L.J. Milgram, T.H. Kowalczyk, S.L. Hyatt, T.L. Fink, C.R. Gedeon, S.M. Oette, J.M. Payne, O. Muhammad, A.G. Ziady, R.C. Moen, M.J. Cooper, Compacted DNA nanoparticles administered to the nasal

mucosa of cystic fibrosis subjects are safe and demonstrate partial to complete cystic fibrosis transmembrane regulator reconstitution, Hum Gene Ther, 15 (2004) 1255-1269.
[36] M.A. Mintzer, E.E. Simanek, Nonviral vectors for gene delivery, Chem Rev, 109 (2009) 259-302.
[37] E. Wagner, K. Zatloukal, M. Cotten, H. Kirlappos, K. Mechtler, D.T. Curiel, M.L. Birnstiel, Coupling of adenovirus to transferrin-polylysine/DNA complexes greatly enhances receptor-mediated gene delivery and expression of transfected genes, Proc Natl Acad Sci U S A, 89 (1992) 6099-6103.
[38] K. Zatloukal, E. Wagner, M. Cotten, S. Phillips, C. Plank, P. Steinlein, D.T. Curiel, M.L. Birnstiel, Transferrinfection: a highly efficient way to express gene constructs in eukaryotic cells, Ann N Y Acad Sci, 660 (1992) 136-153.
[39] T. Nomura, K. Yasuda, T. Yamada, S. Okamoto, R.I. Mahato, Y. Watanabe, Y. Takakura, M. Hashida, Gene expression and antitumor effects following direct interferon (IFN)-gamma gene transfer with naked plasmid DNA and DC-chol liposome complexes in mice 889, Gene Ther, 6 (1999) 121-129.
[40] E. Wagner, Functional Polymer Conjugates for Medicinal Nucleic Acid Delivery, Adv. Polymer Sci, 247 (2012) 1-30.
[41] S. Schreiber, E. Kampgen, E. Wagner, D. Pirkhammer, J. Trcka, H. Korschan, A. Lindemann, R. Dorffner, H. Kittler, F. Kasteliz, Z. Kupcu, A. Sinski, K. Zatloukal, M. Buschle, W. Schmidt, M. Birnstiel, R.E. Kempe, T. Voigt, H.A. Weber, H. Pehamberger, R. Mertelsmann, E.B. Brocker, K. Wolff, G. Stingl, Immunotherapy of metastatic malignant melanoma by a vaccine consisting of autologous interleukin 2-transfected cancer cells: outcome of a phase I study, Hum Gene Ther, 10 (1999) 983-993.
[42] M.E. Davis, The first targeted delivery of siRNA in humans via a self-assembling, cyclodextrin polymer-based nanoparticle: from concept to clinic, Mol Pharm, 6 (2009) 659-668.
[43] M.E. Davis, J.E. Zuckerman, C.H. Choi, D. Seligson, A. Tolcher, C.A. Alabi, Y. Yen, J.D. Heidel, A. Ribas, Evidence of RNAi in humans from systemically administered siRNA via targeted nanoparticles, Nature, 464 (2010) 1067-1070.
[44] E. Wagner, D. Curiel, M. Cotten, Delivery of drugs, proteins and genes into cells using transferrin as a ligand for receptor-mediated endocytosis, Adv Drug Del Rev, 14 (1994) 113-136.
[45] U.K. Laemmli, Characterization of DNA condensates induced by poly(ethylene oxide) and polylysine, Proc Natl Acad Sci U S A, 72 (1975) 4288-4292.
[46] A. Zintchenko, A. Philipp, A. Dehshahri, E. Wagner, Simple Modifications of Branched PEI Lead to Highly Efficient siRNA Carriers with Low Toxicity, Bioconjug Chem, 19 (2008) 1448-1455.
[47] R.K. Oskuee, A. Philipp, A. Dehshahri, E. Wagner, M. Ramezani, The impact of carboxyalkylation of branched polyethylenimine on effectiveness in small interfering RNA delivery, J Gene Med, 12 (2010) 729-738.
[48] L. Tauhardt, K. Kempe, K. Knop, E. Altuntas, M. Jäger, S. Schubert, D. Fischer, U.S. Schubert, Linear Polyethyleneimine: Optimized Synthesis and Characterization – On the Way to ‘‘Pharmagrade’’ Batches, Macromol Chem Phys, 212 (2011) 1918–1924.

[49] J.F. Lutz, M. Ouchi, D.R. Liu, M. Sawamoto, Sequence-controlled polymers, Science, 341 (2013) 1238149.
[50] C. Troiber, E. Wagner, Nucleic Acid Carriers Based on Precise Polymer Conjugates, Bioconj Chem, 22 (2011) 1737-1752.
[51] D. Schaffert, E. Wagner, Gene therapy progress and prospects: synthetic polymer-based systems, Gene Ther, 15 (2008) 1131-1138.
[52] J.H. Lee, Y.B. Lim, J.S. Choi, Y. Lee, T.I. Kim, H.J. Kim, J.K. Yoon, K. Kim, J.S. Park, Polyplexes assembled with internally quaternized PAMAM-OH dendrimer and plasmid DNA have a neutral surface and gene delivery potency, Bioconjug Chem, 14 (2003) 1214-1221.
[53] M.L. Patil, M. Zhang, S. Betigeri, O. Taratula, H. He, T. Minko, Surface-modified and internally cationic polyamidoamine dendrimers for efficient siRNA delivery, Bioconjug Chem, 19 (2008) 1396-1403.
[54] P. Kos, C. Scholz, E.E. Salcher, A. Herrmann, E. Wagner, Gene Transfer with Sequence-Defined Oligo(ethanamino)amides Bioreducibly Attached to a Propylenimine Dendrimer Core, Pharm Nanotech, 1 (2013) 269-281.
[55] T. Lehto, K. Kurrikoff, U. Langel, Cell-penetrating peptides for the delivery of nucleic acids, Expert Opin Drug Deliv, 9 (2012) 823-836.
[56] T. Lehto, O.E. Simonson, I. Mager, K. Ezzat, H. Sork, D.M. Copolovici, J.R. Viola, E.M. Zaghloul, P. Lundin, P.M. Moreno, M. Mae, N. Oskolkov, J. Suhorutsenko, C.I. Smith, S.E. Andaloussi, A peptide-based vector for efficient gene transfer in vitro and in vivo, Mol Ther, 19 (2011) 1457-1467.
[57] T.B. Wyman, F. Nicol, O. Zelphati, P.V. Scaria, C. Plank, F.C. Szoka, Jr., Design, synthesis, and characterization of a cationic peptide that binds to nucleic acids and permeabilizes bilayers, Biochemistry, 36 (1997) 3008-3017.
[58] S.E. Andaloussi, T. Lehto, I. Mager, K. Rosenthal-Aizman, Oprea, II, O.E. Simonson, H. Sork, K. Ezzat, D.M. Copolovici, K. Kurrikoff, J.R. Viola, E.M. Zaghloul, R. Sillard, H.J. Johansson, F. Said Hassane, P. Guterstam, J. Suhorutsenko, P.M. Moreno, N. Oskolkov, J. Halldin, U. Tedebark, A. Metspalu, B. Lebleu, J. Lehtio, C.I. Smith, U. Langel, Design of a peptide-based vector, PepFect6, for efficient delivery of siRNA in cell culture and systemically in vivo, Nucleic Acids Res, 39 (2011) 3972-3987.
[59] L. Crombez, G. Aldrian-Herrada, K. Konate, Q.N. Nguyen, G.K. McMaster, R. Brasseur, F. Heitz, G. Divita, A new potent secondary amphipathic cell-penetrating peptide for siRNA delivery into mammalian cells, Mol Ther, 17 (2009) 95-103.
[60] H. Michiue, A. Eguchi, M. Scadeng, S.F. Dowdy, Induction of in vivo synthetic lethal RNAi responses to treat glioblastoma, Cancer Biol Ther, 8 (2009) 2306-2313.
[61] D. Schaffert, N. Badgujar, E. Wagner, Novel Fmoc-polyamino acids for solid-phase synthesis of defined polyamidoamines, Org Lett, 13 (2011) 1586-1589.
[62] P. Kos, E. Wagner, Polymers for siRNA Delivery: Combining precision with multifunctionality, Chim Oggi - Chemistry Today 31 (2013) 6-10.
[63] D. Schaffert, C. Troiber, E.E. Salcher, T. Frohlich, I. Martin, N. Badgujar, C. Dohmen, D. Edinger, R. Klager, G. Maiwald, K. Farkasova, S. Seeber, K. Jahn-Hofmann, P. Hadwiger, E. Wagner, Solid-phase synthesis of sequence-defined T-, i-, and U-shape polymers for pDNA and siRNA delivery, Angew Chem Int Ed Engl, 50 (2011) 8986-8989.

[64] T. Fröhlich, D. Edinger, R. Kläger, C. Troiber, E. Salcher, N. Badgujar, I. Martin, D. Schaffert, A. Cengizeroglu, P. Hadwiger, H.-P. Vornlocher, E. Wagner, Structure–activity relationships of siRNA carriers based on sequence-defined oligo (ethane amino) amides, J Control Release, 160 (2012) 532-541.
[65] C. Dohmen, T. Frohlich, U. Lachelt, I. Rohl, H.-P. Vornlocher, P. Hadwiger, E. Wagner, Defined Folate-PEG-siRNA Conjugates for Receptor-specific Gene Silencing, Mol Ther Nucleic Acids, 1 (2012) e7.
[66] U. Lachelt, P. Kos, F.M. Mickler, A. Herrmann, E.E. Salcher, W. Rodl, N. Badgujar, C. Brauchle, E. Wagner, Fine-tuning of proton sponges by precise diaminoethanes and histidines in pDNA polyplexes, Nanomedicine, 1 (2014) 35-44.
[67] C. Troiber, D. Edinger, P. Kos, L. Schreiner, R. Klager, A. Herrmann, E. Wagner, Stabilizing effect of tyrosine trimers on pDNA and siRNA polyplexes, Biomaterials, 34 (2013) 1624-1633.
[68] E.E. Salcher, P. Kos, T. Frohlich, N. Badgujar, M. Scheible, E. Wagner, Sequence-defined four-arm oligo(ethanamino)amides for pDNA and siRNA delivery: Impact of building blocks on efficacy, J Control Release, 164 (2012) 380-386.
[69] C. Dohmen, D. Edinger, T. Frohlich, L. Schreiner, U. Lachelt, C. Troiber, J. Radler, P. Hadwiger, H.P. Vornlocher, E. Wagner, Nanosized Multifunctional Polyplexes for Receptor-Mediated SiRNA Delivery, ACS Nano, 6 (2012) 5198-5208.
[70] I. Martin, C. Dohmen, C. Mas-Moruno, C. Troiber, P. Kos, D. Schaffert, U. Lachelt, M. Teixido, M. Gunther, H. Kessler, E. Giralt, E. Wagner, Solid-phase-assisted synthesis of targeting peptide-PEG-oligo(ethane amino)amides for receptor-mediated gene delivery, Org Biomol Chem, 10 (2012) 3258-3268.
[71] K. Lu, Q.P. Duan, L. Ma, D.X. Zhao, Chemical strategies for the synthesis of peptide-oligonucleotide conjugates, Bioconjug Chem, 21 (2010) 187-202.
[72] H.C. Kolb, M.G. Finn, K.B. Sharpless, Click Chemistry: Diverse Chemical Function from a Few Good Reactions, Angewandte Chemie International Edition, 40 (2001) 2004-2021.
[73] E.M. Sletten, C.R. Bertozzi, From mechanism to mouse: a tale of two bioorthogonal reactions, Acc Chem Res, 44 (2011) 666-676.
[74] J. Willibald, J. Harder, K. Sparrer, K.K. Conzelmann, T. Carell, Click-modified anandamide siRNA enables delivery and gene silencing in neuronal and immune cells, J Am Chem Soc, 134 (2012) 12330-12333.
[75] P. Dawson, T. Muir, I. Clark-Lewis, S. Kent, Synthesis of proteins by native chemical ligation, Science, 266 (1994) 776-779.
[76] J.B. Blanco-Canosa, P.E. Dawson, An efficient Fmoc-SPPS approach for the generation of thioester peptide precursors for use in native chemical ligation, Angew Chem Int Ed Engl, 47 (2008) 6851-6855.
[77] J. Li, C. Fan, H. Pei, J. Shi, Q. Huang, Smart drug delivery nanocarriers with self-assembled DNA nanostructures, Adv Mater, 25 (2013) 4386-4396.
[78] V.J. Schuller, S. Heidegger, N. Sandholzer, P.C. Nickels, N.A. Suhartha, S. Endres, C. Bourquin, T. Liedl, Cellular immunostimulation by CpG-sequence-coated DNA origami structures, ACS Nano, 5 (2011) 9696-9702.
[79] H. Lee, A.K. Lytton-Jean, Y. Chen, K.T. Love, A.I. Park, E.D. Karagiannis, A. Sehgal, W. Querbes, C.S. Zurenko, M. Jayaraman, C.G. Peng, K. Charisse, A. Borodovsky, M. Manoharan, J.S. Donahoe, J. Truelove, M. Nahrendorf, R. Langer, D.G. Anderson, Molecularly self-

assembled nucleic acid nanoparticles for targeted in vivo siRNA delivery, Nat Nanotechnol, 7 (2012) 389-393.
[80] E.O. Fischer, E., Synthesis of the derivatives of some dipeptides, Ber Deutsch Chem Ges, 36 (1903) 2106-2116.
[81] V. Du Vigneaud, Ressler, C., Swan, J.M., Roberts, C.W. and Katsoyannis, P.G., The synthesis of oxytocin, J Am Chem Soc, 76 (1954) 3115–3121.
[82] R.B. Merrifield, Solid Phase Peptide Synthesis. I. The Synthesis of a Tetrapeptide, Journal of the American Chemical Society, 85 (1963) 2149-2154.
[83] G.Y.H. Louis A. Carpino 9-Fluorenylmethoxycarbonyl amino-protecting group, J Org Chem, 37 (1972) 3404-3409.
[84] L. Hartmann, E. Krause, M. Antonietti, H.G. Borner, Solid-phase supported polymer synthesis of sequence-defined, multifunctional poly(amidoamines), Biomacromolecules., 7 (2006) 1239-1244.
[85] L. Hartmann, S. Hafele, R. Peschka-Suss, M. Antonietti, H.G. Borner, Tailor-Made Poly(amidoamine)s for Controlled Complexation and Condensation of DNA, Chemistry, 14 (2008) 2025-2033.
[86] T. Frohlich, D. Edinger, R. Klager, C. Troiber, E. Salcher, N. Badgujar, I. Martin, D. Schaffert, A. Cengizeroglu, P. Hadwiger, H.P. Vornlocher, E. Wagner, Structure-activity relationships of siRNA carriers based on sequence-defined oligo (ethane amino) amides, J Control Release, 160 (2012) 532-541.
[87] Q.R. Chen, L. Zhang, S.A. Stass, A.J. Mixson, Branched co-polymers of histidine and lysine are efficient carriers of plasmids, Nucleic Acids Res, 29 (2001) 1334-1340.
[88] Q. Leng, P. Scaria, J. Zhu, N. Ambulos, P. Campbell, A.J. Mixson, Highly branched HK peptides are effective carriers of siRNA, J Gene Med, 7 (2005) 977-986.
[89] X.L. Wang, S. Ramusovic, T. Nguyen, Z.R. Lu, Novel polymerizable surfactants with pH-sensitive amphiphilicity and cell membrane disruption for efficient siRNA delivery, Bioconjug Chem, 18 (2007) 2169-2177.
[90] X.-L. Wang, R. Xu, Z.-R. Lu, A peptide-targeted delivery system with pH-sensitive amphiphilic cell membrane disruption for efficient receptor-mediated siRNA delivery, J Control Release, 134 (2009) 207-213.
[91] E. Wagner, M. Ogris, W. Zauner, Polylysine-based transfection systems utilizing receptor-mediated delivery, Adv Drug Deliv Rev, 30 (1998) 97-113.
[92] M. Meyer, A. Philipp, R. Oskuee, C. Schmidt, E. Wagner, Breathing life into polycations: functionalization with pH-responsive endosomolytic peptides and polyethylene glycol enables siRNA delivery, J Am Chem Soc, 130 (2008) 3272-3273.
[93] M.A. Wolfert, P.R. Dash, O. Nazarova, D. Oupicky, L.W. Seymour, S. Smart, J. Strohalm, K. Ulbrich, Polyelectrolyte vectors for gene delivery: influence of cationic polymer on biophysical properties of complexes formed with DNA 937, Bioconjug Chem, 10 (1999) 993-1004.
[94] K. Kunath, A. von Harpe, D. Fischer, H. Petersen, U. Bickel, K. Voigt, T. Kissel, Low-molecular-weight polyethylenimine as a non-viral vector for DNA delivery: comparison of physicochemical properties, transfection efficiency and in vivo distribution with high-molecular-weight polyethylenimine, J Control Release, 89 (2003) 113-125.

[95] D. Fischer, T. Bieber, Y. Li, H.P. Elsasser, T. Kissel, A novel non-viral vector for DNA delivery based on low molecular weight, branched polyethylenimine: effect of molecular weight on transfection efficiency and cytotoxicity, Pharm Res, 16 (1999) 1273-1279.
[96] S. Werth, B. Urban-Klein, L. Dai, S. Hobel, M. Grzelinski, U. Bakowsky, F. Czubayko, A. Aigner, A low molecular weight fraction of polyethylenimine (PEI) displays increased transfection efficiency of DNA and siRNA in fresh or lyophilized complexes, J Control Release, 112 (2006) 257-270.
[97] M.A. Gosselin, W. Guo, R.J. Lee, Efficient gene transfer using reversibly cross-linked low molecular weight polyethylenimine, Bioconjug Chem, 12 (2001) 989-994.
[98] M.L. Forrest, J.T. Koerber, D.W. Pack, A degradable polyethylenimine derivative with low toxicity for highly efficient gene delivery, Bioconjug Chem, 14 (2003) 934-940.
[99] Y.H. Kim, J.H. Park, M. Lee, T.G. Park, S.W. Kim, Polyethylenimine with acid-labile linkages as a biodegradable gene carrier, J Control Release, 103 (2005) 209-219.
[100] J. Kloeckner, S. Bruzzano, M. Ogris, E. Wagner, Gene carriers based on hexanediol diacrylate linked oligoethylenimine: effect of chemical structure of polymer on biological properties, Bioconjug Chem, 17 (2006) 1339-1345.
[101] M. Breunig, U. Lungwitz, R. Liebl, A. Goepferich, Breaking up the correlation between efficacy and toxicity for nonviral gene delivery, Proc Natl Acad Sci U S A, 104 (2007) 14454-14459.
[102] V. Knorr, V. Russ, L. Allmendinger, M. Ogris, E. Wagner, Acetal linked oligoethylenimines for use as pH-sensitive gene carriers, Bioconjug Chem, 19 (2008) 1625-1634.
[103] Q. Peng, Z. Zhong, R. Zhuo, Disulfide cross-linked polyethylenimines (PEI) prepared via thiolation of low molecular weight PEI as highly efficient gene vectors, Bioconjug Chem, 19 (2008) 499-506.
[104] Y. Wen, S. Pan, X. Luo, X. Zhang, W. Zhang, M. Feng, A biodegradable low molecular weight polyethylenimine derivative as low toxicity and efficient gene vector, Bioconjug Chem, 20 (2009) 322-332.
[105] L. Chen, H. Tian, J. Chen, X. Chen, Y. Huang, X. Jing, Multi-armed poly(L-glutamic acid)-graft-oligoethylenimine copolymers as efficient nonviral gene delivery vectors, J Gene Med, 12 (2010) 64-76.
[106] M. Hashemi, B.H. Parhiz, A. Hatefi, M. Ramezani, Modified polyethyleneimine with histidine-lysine short peptides as gene carrier, Cancer Gene Ther, 18 (2011) 12-19.
[107] M. Zheng, Y. Zhong, F. Meng, R. Peng, Z. Zhong, Lipoic acid modified low molecular weight polyethylenimine mediates nontoxic and highly potent in vitro gene transfection, Mol Pharm, 8 (2011) 2434-2443.
[108] G. Creusat, J.S. Thomann, A. Maglott, B. Pons, M. Dontenwill, E. Guerin, B. Frisch, G. Zuber, Pyridylthiourea-grafted polyethylenimine offers an effective assistance to siRNA-mediated gene silencing in vitro and in vivo, J Control Release, 157 (2012) 418-426.
[109] W.T. Godbey, K.K. Wu, A.G. Mikos, Size matters: molecular weight affects the efficiency of poly(ethylenimine) as a gene delivery vehicle 2, J Biomed Mater Res, 45 (1999) 268-275.

[110] B. Abdallah, A. Hassan, C. Benoist, D. Goula, J.P. Behr, B.A. Demeneix, A powerful nonviral vector for in vivo gene transfer into the adult mammalian brain: polyethylenimine 2, Hum Gene Ther, 7 (1996) 1947-1954.
[111] D. Schaffert, C. Troiber, E. Wagner, New Sequence-Defined Polyaminoamides with Tailored Endosomolytic Properties for Plasmid DNA Delivery, Bioconjug Chem, 23 (2012) 1157-1165.
[112] L. Wightman, R. Kircheis, V. Rossler, S. Carotta, R. Ruzicka, M. Kursa, E. Wagner, Different behavior of branched and linear polyethylenimine for gene delivery in vitro and in vivo, J Gene Med, 3 (2001) 362-372.
[113] A. Kwok, S.L. Hart, Comparative structural and functional studies of nanoparticle formulations for DNA and siRNA delivery, Nanomedicine, 7 (2011) 210-219.
[114] R. Wang, L. Zhou, Y. Zhou, G. Li, X. Zhu, H. Gu, X. Jiang, H. Li, J. Wu, L. He, X. Guo, B. Zhu, D. Yan, Synthesis and gene delivery of poly(amido amine)s with different branched architecture, Biomacromolecules, 11 (2010) 489-495.
[115] X. Sun, N. Zhang, Cationic polymer optimization for efficient gene delivery, Mini Rev Med Chem, 10 (2010) 108-125.
[116] J. Zhou, J. Wu, N. Hafdi, J.P. Behr, P. Erbacher, L. Peng, PAMAM dendrimers for efficient siRNA delivery and potent gene silencing, Chem Commun (Camb), (2006) 2362-2364.
[117] M.X. Tang, C.T. Redemann, F.C. Szoka, Jr., In vitro gene delivery by degraded polyamidoamine dendrimers, Bioconjug Chem, 7 (1996) 703-714.
[118] M.X. Tang, F.C. Szoka, The influence of polymer structure on the interactions of cationic polymers with DNA and morphology of the resulting complexes, Gene Ther, 4 (1997) 823-832.
[119] C. Lin, C.-J. Blaauboer, M.M. Timoneda, M.C. Lok, M. van Steenbergen, W.E. Hennink, Z. Zhong, J. Feijen, J.F.J. Engbersen, Bioreducible poly(amido amine)s with oligoamine side chains: Synthesis, characterization, and structural effects on gene delivery, J Control Release, 126 (2008) 166-174.
[120] H. Uchida, K. Miyata, M. Oba, T. Ishii, T. Suma, K. Itaka, N. Nishiyama, K. Kataoka, Odd-even effect of repeating aminoethylene units in the side chain of N-substituted polyaspartamides on gene transfection profiles, J Am Chem Soc, 133 (2011) 15524-15532.
[121] Y. Gao, Q. Yin, L. Chen, Z. Zhang, Y. Li, Linear cationic click polymers/DNA nanoparticles: in vitro structure-activity relationship and in vivo evaluation for gene delivery, Bioconjug Chem, 22 (2011) 1153-1161.
[122] P. Chollet, M.C. Favrot, A. Hurbin, J.L. Coll, Side-effects of a systemic injection of linear polyethylenimine-DNA complexes, J Gene Med, 4 (2002) 84-91.
[123] S.M. Moghimi, P. Symonds, J.C. Murray, A.C. Hunter, G. Debska, A. Szewczyk, A two-stage poly(ethylenimine)-mediated cytotoxicity: implications for gene transfer/therapy, Mol Ther, 11 (2005) 990-995.
[124] G. Grandinetti, N.P. Ingle, T.M. Reineke, Interaction of poly(ethylenimine)-DNA polyplexes with mitochondria: implications for a mechanism of cytotoxicity, Mol Pharm, 8 (2011) 1709-1719.
[125] L.E. Prevette, M.L. Lynch, T.M. Reineke, Amide spacing influences pDNA binding of poly(amidoamine)s, Biomacromolecules, 11 (2010) 326-332.

[126] K. Miyata, N. Nishiyama, K. Kataoka, Rational design of smart supramolecular assemblies for gene delivery: chemical challenges in the creation of artificial viruses, Chem Soc Rev, 41 (2012) 2562-2574.
[127] E. Wagner, Polymers for siRNA Delivery: Inspired by Viruses to be Targeted, Dynamic, and Precise, Acc Chem Res, 45 (2012) 1005-1013.
[128] I. Martin, C. Dohmen, C. Mas-Moruno, C. Troiber, P. Kos, D. Schaffert, U. Lachelt, M. Teixido, M. Günther, H. Kessler, E. Giralt, E. Wagner, Solid-phase-assisted synthesis of targeting peptide-PEG-oligo(ethane amino)amides for receptor-mediated gene delivery, Org Biomol Chem, 10 (2012) 3258-3268.
[129] D. Schaffert, M. Kiss, W. Rodl, A. Shir, A. Levitzki, M. Ogris, E. Wagner, Poly(I:C)-mediated tumor growth suppression in EGF-receptor overexpressing tumors using EGF-polyethylene glycol-linear polyethylenimine as carrier, Pharm Res, 28 (2011) 731-741.
[130] B.M. Rohwedder, Y; Dumy,P; Mutter,M, Hydrazinolysis of Dde: Complete orthogonality with Aloc protecting groups, Tetrahedron Lett, 39 (1998) 1175–1178.
[131] F. Wojcik, S. Mosca, L. Hartmann, Solid-phase synthesis of asymmetrically branched sequence-defined poly/oligo(amidoamines), J Org Chem, 77 (2012) 4226-4234.
[132] T. Fröhlich, D. Edinger, R. Kläger, C. Troiber, E. Salcher, N. Badgujar, I. Martin, D. Schaffert, A. Cengizeroglu, P. Hadwiger, H.P. Vornlocher, E. Wagner, Structure-activity relationships of siRNA carriers based on sequence-defined oligo (ethane amino) amides, J Control Release, (2012).
[133] A. Ibrahim, R. Meyrueix, G. Pouliquen, Y.P. Chan, H. Cottet, Size and charge characterization of polymeric drug delivery systems by Taylor dispersion analysis and capillary electrophoresis, Anal Bioanal Chem, 405 (2013) 5369-5379.
[134] H. Cottet, J.P. Biron, M. Martin, Taylor dispersion analysis of mixtures, Anal Chem, 79 (2007) 9066-9073.
[135] A. Hawe, W.L. Hulse, W. Jiskoot, R.T. Forbes, Taylor dispersion analysis compared to dynamic light scattering for the size analysis of therapeutic peptides and proteins and their aggregates, Pharm Res, 28 (2011) 2302-2310.
[136] U. Franzen, C. Vermehren, H. Jensen, J. Ostergaard, Physicochemical characterization of a PEGylated liposomal drug formulation using capillary electrophoresis, Electrophoresis, 32 (2011) 738-748.
[137] C. Pichon, C. Goncalves, P. Midoux, Histidine-rich peptides and polymers for nucleic acids delivery, Adv Drug Deliv Rev, 53 (2001) 75-94.
[138] N.A. Thieriet, J; Giralt,E; François Guibé,F; Albericio, F, Use of Alloc-amino acids in solid-phase peptide synthesis. Tandem deprotection-coupling reactions using neutral conditions, Tetrahedron Lett, 38 (1997) 7275–7278.
[139] P. Erbacher, T. Bettinger, E. Brion, J.L. Coll, C. Plank, J.P. Behr, J.S. Remy, Genuine DNA/polyethylenimine (PEI) complexes improve transfection properties and cell survival, J Drug Target, 12 (2004) 223-236.
[140] U. Lungwitz, M. Breunig, T. Blunk, A. Gopferich, Polyethylenimine-based non-viral gene delivery systems, Eur J Pharm Biopharm, 60 (2005) 247-266.
[141] S. Grosse, G. Thevenot, M. Monsigny, I. Fajac, Which mechanism for nuclear import of plasmid DNA complexed with polyethylenimine derivatives?, J Gene Med, 8 (2006) 845-851.

[142] A. Kichler, C. Leborgne, E. Coeytaux, O. Danos, Polyethylenimine-mediated gene delivery: a mechanistic study, J Gene Med, 3 (2001) 135-144.
[143] G. Creusat, A.S. Rinaldi, E. Weiss, R. Elbaghdadi, J.S. Remy, R. Mulherkar, G. Zuber, Proton sponge trick for pH-sensitive disassembly of polyethylenimine-based siRNA delivery systems, Bioconjug Chem, 21 (2010) 994-1002.
[144] A. Akinc, M. Thomas, A.M. Klibanov, R. Langer, Exploring polyethylenimine-mediated DNA transfection and the proton sponge hypothesis, J Gene Med, 7 (2005) 657-663.
[145] Y. Yue, F. Jin, R. Deng, J. Cai, Y. Chen, M.C. Lin, H.F. Kung, C. Wu, Revisit complexation between DNA and polyethylenimine - Effect of uncomplexed chains free in the solution mixture on gene transfection, J Control Release, 155 (2011) 67-76.
[146] V. Russ, H. Elfberg, C. Thoma, J. Kloeckner, M. Ogris, E. Wagner, Novel degradable oligoethylenimine acrylate ester-based pseudodendrimers for in vitro and in vivo gene transfer, Gene Ther, 15 (2008) 18-29.
[147] D. Fischer, Y. Li, B. Ahlemeyer, J. Krieglstein, T. Kissel, In vitro cytotoxicity testing of polycations: influence of polymer structure on cell viability and hemolysis, Biomaterials, 24 (2003) 1121-1131.
[148] G. Grandinetti, A.E. Smith, T.M. Reineke, Membrane and nuclear permeabilization by polymeric pDNA vehicles: efficient method for gene delivery or mechanism of cytotoxicity?, Mol Pharm, 9 (2012) 523-538.
[149] A. Hall, A.K. Larsen, L. Parhamifar, K.D. Meyle, L.P. Wu, S.M. Moghimi, High resolution respirometry analysis of polyethylenimine-mediated mitochondrial energy crisis and cellular stress: Mitochondrial proton leak and inhibition of the electron transport system, Biochim Biophys Acta, 1827 (2013) 1213-1225.
[150] H. Cottet, P. Gareil, O. Theodoly, C.E. Williams, A semi-empirical approach to the modeling of the electrophoretic mobility in free solution: application to polystyrenesulfonates of various sulfonation rates, Electrophoresis, 21 (2000) 3529-3540.
[151] H.P. Erickson, Reversible unfolding of fibronectin type III and immunoglobulin domains provides the structural basis for stretch and elasticity of titin and fibronectin, Proc Natl Acad Sci U S A, 91 (1994) 10114-10118.
[152] E. Wagner, Polymers for siRNA Delivery: Inspired by Viruses to be Targeted, Dynamic, and Precise, Acc Chem Res, (2011) doi: 10.1021/ar2002232.
[153] J.D. Ziebarth, Y. Wang, Understanding the protonation behavior of linear polyethylenimine in solutions through Monte Carlo simulations, Biomacromolecules, 11 (2010) 29-38.
[154] L. Leclercq, H. Cottet, Fast characterization of polyelectrolyte complexes by inline coupling of capillary electrophoresis to Taylor dispersion analysis, Anal Chem, 84 (2012) 1740-1743.

8 APPENDIX

8.1 Abbreviatons

AA	Amino acid
ACN	Acetonitrile
Alloc	Allyloxycarbonyl
AMD	Age-related macular degeneration
AVET	Adenovirus-enhanced transferrinfection
boc	*Tert*- butyloxycarbonyl
bp	Base pair
brPEI	Branched polyethylenimine
CE	Capillary electrophoresis
cmb	Comb
CMV	Cytomegalovirus
CpG	Cytosine phosphatidyl guanine
CPP	Cell-penetrating peptide
CQ	Chloroquine
Da	Dalton
DAPI	4',6-diamidino-2-phenylindole
DBU	1,8-diazabicycloundec-7-ene
DCM	Dichloromethane
DCVC	Dry column vacuum chromatography
Dde	N-(1-(4,4-dimethyl-2,6-dioxocyclohexylidene)ethyl)
DETA	Diethylene triamine
DHB	Dihydroxy benzoic acid
DIPEA	Diisopropylethylamine
DLS	Dynamic light scattering
DMBA	Dimethyl-barbituric acid
DMEM	Dulbecco´s modified eagle´s medium
DMF	Dimethylformamide
DNA	Deoxyribonucleic acid
dsRNA	Double-stranded RNA
EDTA	Ethylenediamine tetraacetic acid
EHCO	N-(1-aminoethyl)iminobis[N-(oleicyl-cyteinyl-histinyl-1-Aminoethyl)propionamide]
EPR	Enhanced permeability and retention
ESI	Electrospray ionization
EtBr	Ethidium bromide
EtOH	Ethanol
FCS	Fetal calf serum
FDA	Food and Drug Administration
Fmoc	9-Fluorenylmethyloxycarbonyl
FolA	Folic acid
HBG	HEPES buffered glucose
HBTU	2-(1H-benzotriazole-1-yl)-1,1,3,3-tetramethyluronium hexafluorophosphate

HEPES	N-(2-hydroxyethyl)piperazine-N´-(2-ethanesulfonic acid)
HOAc	Acetic acid
HOBt	1-hydroxybenzotriazole
HPC	Hydroxypropylcellulose
HPLC	High-performance liquid chromatography
IEX	Ion exchange
lin	Linear
LNA	Locked nucleic acid
LMW	Low molecular weight
LPEI	Linear polyethylenimine
Luc	Luciferase
MALDI-TOF	Matrix assisted laser desorption ionization – time of flight
MeOH	Methanol
miRNA	MicroRNA
mRNA	Messenger RNA
MS	Mass spectrometry
MTBE	*Tert*-butyl methylether
MTT	Methylthiazolyldiphenyl-tetrazolium bromide
MW	Molecular weight
N/P	(protonable) nitrogens/phosphates
NCL	Native chemical ligation
NEM	N-ethylmorpholine
NMP	N-methylpyrrolidone
NMR	Nuclear magnetic resonance
Npys	3-nitropyridylsulfenyl
ODN	Oligodeoxynucleotide
PAA	Polyamidoamine
PAMAM	Poly(amidoamine) dendrimer
PDI	Polydispersity index
pDNA	Plasmid DNA
PEG	Polyethylene glycol
pCMVLuc	Plasmid encoding firefly luciferase under the control of CMV promotor
PEHA	Pentaethylene hexamine
PEI	Polyethylenimine
PLL	Poly(L-lysine)
PMO	Phosphorodiamidate morpholino oligomer
PPI	Polypropylenimine
PyBOP	Benzotriazol-1-yl-oxytripyrrolidinophosphonium hexafluorophosphate
Pys	Pyridylsulfenyl
RISC	RNA-induced silencing complex
RLU	Relative light units
RNA	Ribonucleic acid
RNAi	RNA interference
RP-HPLC	Reversed phase high-performance liquid chromatography
RPMI	Cell culture medium developed in the Roswell Park Memorial Institute
RT	Room temperature
SCID	Severe combined immunodeficiency
SD	Standard deviation

Sdt	Succinyl-diethylentriamine
SEC	Size exclusion chromatography
siRNA	Small interfering RNA
SNALP	Stabilized nucleic acid lipid particle
Sph	Succinyl-pentaethylenhexamine
SPPS	Solid-phase peptide synthesis
Stp	Succinyl-tetraethylenpentamine
Stt	Succinyl-triethylentetramine
TBE	Tris-boric acid-EDTA buffer
TCEP	Tris(2-carboxyethyl)phosphine
TDA	Taylor dispersion analysis
TEA	Triethylamine
TEPA	Tetraethylene pentamine
TETA	Triethylene tetramine
TFA	Trifluoroacetic acid
TFE	Trifluoroethanol
THF	Tetrahydrofuran
TIS	Triisopropylsilane
TLC	Thin layer chromatography
TP-10	Transportan-10
UV	Ultra violett
VEGF	Vascular endothelial growth factor

8.2 List of all oligomers

8.2.1 Long linear oligo(ethanamino)amide carriers

Compound Id	Sequence	Calculated molecular weight	Detected molecular weight[a]	Protonatable amines
681	Stp5-W	1561,02	1566,6[b]	16
643	Stp10-W	2917,82	2939,7[c]	31
644	Stp15-W	4274,61	4294,9[c]	46
645	Stp20-W	5650,56	n.d.[d]	61
554	Stp30-W	8345,0	n.d.[d]	91
555	Stp40-W	11058,59	-	121
556	$[Stp5\text{-}\beta A]_6$-W	8876,51	-	91
682	C-Stp30-W-C	8551,29	-	91
683	Sph20-W	6492,77	-	81
684	Sph30-W	9637,04	-	121

[a] determined by MALDI-TOF mass analysis, [b] $[M+H]^+$ [c] $[M+Na]^+$ [d] n.d. = not detectable

8.2.2 Comb structure oligomers

Compound Id	Sequence	Code	Calculated molecular weight	Protonatable amines
545	C-[K(Stp)]$_4$-C	-	1822,43	13
547	C-[H-K(Stp)]$_4$-C	-	2370,98	13
623	A-[K(Stp)]$_8$-A	-	3356,42	25
627	C-[βA-K(Stp)]$_8$-C	Stp-cmb- βA	3989,18	25
621	C-[W-K(Stp)]$_8$-C	Stp-cmb-W	4910,23	25
686	A-[H_2-K(Stp)]$_8$-A	-	5550,65	25
553	C-[H_2-K(Stp)]$_8$-C	-	5614,78	25
687	C-[H_2-K(Stp)]$_{12}$-C	-	8340,09	37
632	C-[K(Sdt)]$_8$-C	Sdt-cmb-0	2731,47	17
633	C-[A-K(Sdt)]$_8$-C	Sdt-cmb-A	3300,09	17
634	C-[H-K(Sdt)]$_8$-C	Sdt-cmb-H	3828,58	17
635	C-[K(Stt)]$_8$-C	Stt-cmb-0	3076,01	25
636	C-[A-K(Stt)]$_8$-C	Stt-cmb-A	3644,63	25
637	C-[H-K(Stt)]$_8$-C	Stt-cmb-H	4173,13	25
622	C-[K(Stp)]$_8$-C	Stp-cmb-0	3420,55	33
551	C-[A-K(Stp)]$_8$-C	Stp-cmb-A	3989,18	33
552	C-[H-K(Stp)]$_8$-C	Stp-cmb-H	4517,67	33
629	C-[K(Sph)]$_8$-C	Sph-cmb-0	3765,1	41
630	C-[A-K(Sph)]$_8$-C	Sph-cmb-A	4333,72	41
631	C-[H-K(Sph)]$_8$-C	Sph-cmb-H	4862,21	41

8.2.3 Linear control sequences

Compound Id	Sequence	Code	Molecular weight [g/mol]	Protonatable amines
625	C-(Stp-K)$_8$-C	Stp-lin-0	3420,55	33
626	C-(A-Stp-K)$_8$-C	Stp-lin-A	3989,18	33
628	C-(H-Stp-K)$_8$-C	Stp-lin-H	4517,67	33
648	C-(Sph-K)$_8$-C	Sph-lin-0	3765,1	41
649	C-(A-Sph-K)$_8$-C	Sph-lin-A	4333,72	41
650	C-(H-Sph-K)$_8$-C	Sph-lin-H	4862,21	41

8.3 Analytical data

8.3.1 NMR spectra

^{1}H-NMR spectra were recorded either at 400 or 500 MHz in deuterium oxide.

Id:681 Sequence: Stp5-W

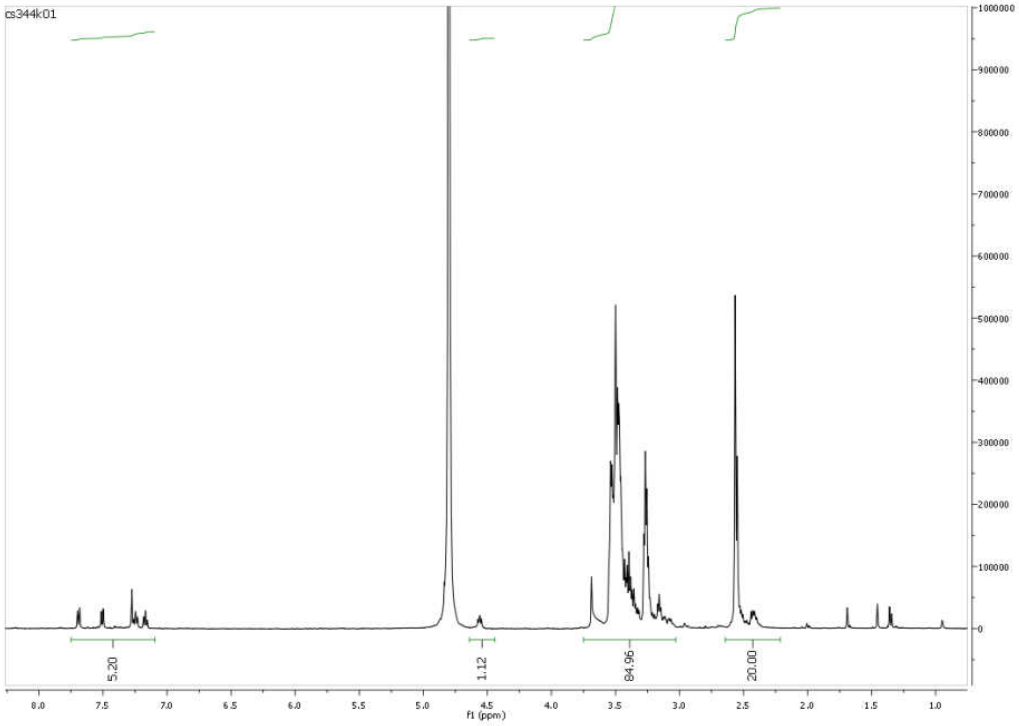

δ (ppm): 2.3 -2.7 (m, 20H, -CO-CH2-CH2-CO-), 2.7 -3.0 (m, 2H, βH tryptophane), 3.0-3.8 (m, 80H, -CH2- Tepa), 4.5-4.6 (m, 1H, αH tryptophane), 7.1-7.7 (m, 5H aromatic H, tryptophane)

Id:643 Sequence: Stp10-W

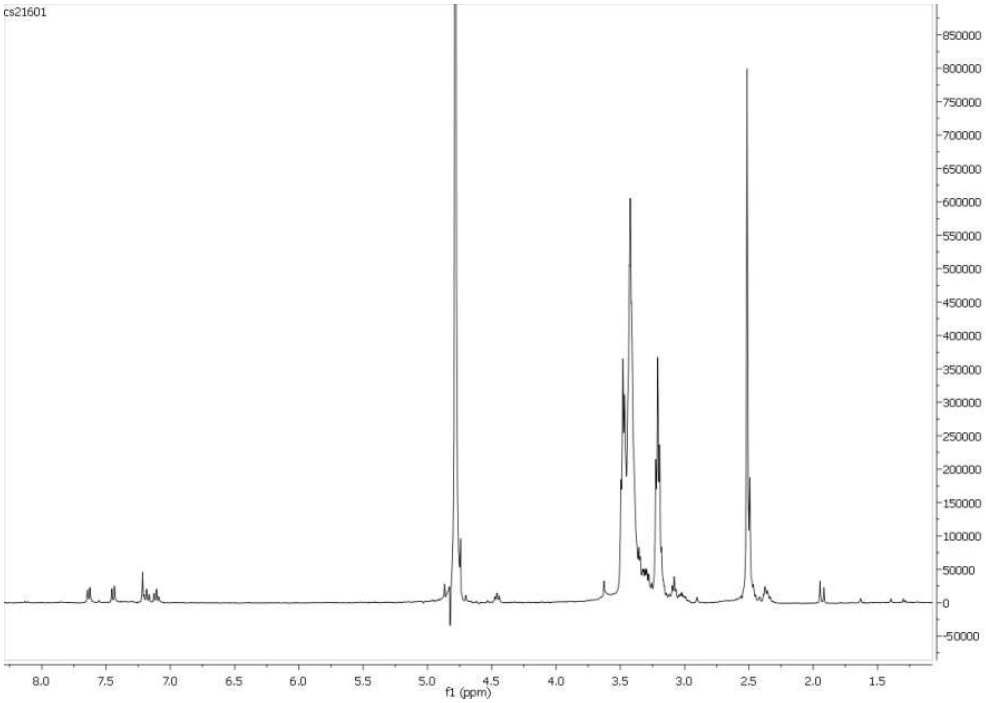

Id:644 Sequence: Stp15-W

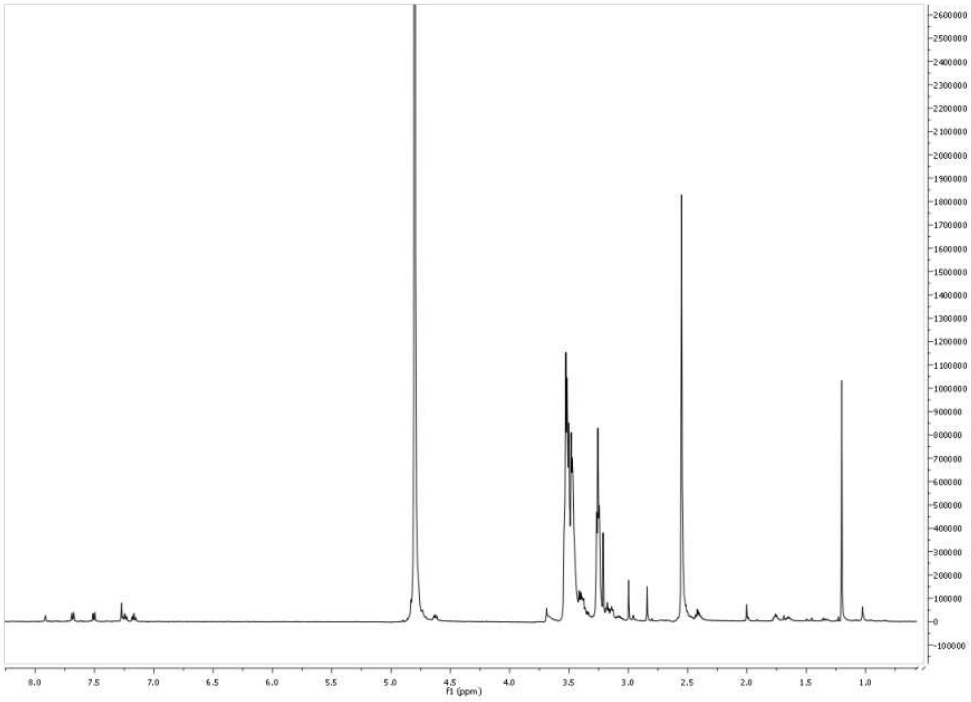

Id:645 Sequence: Stp20-W

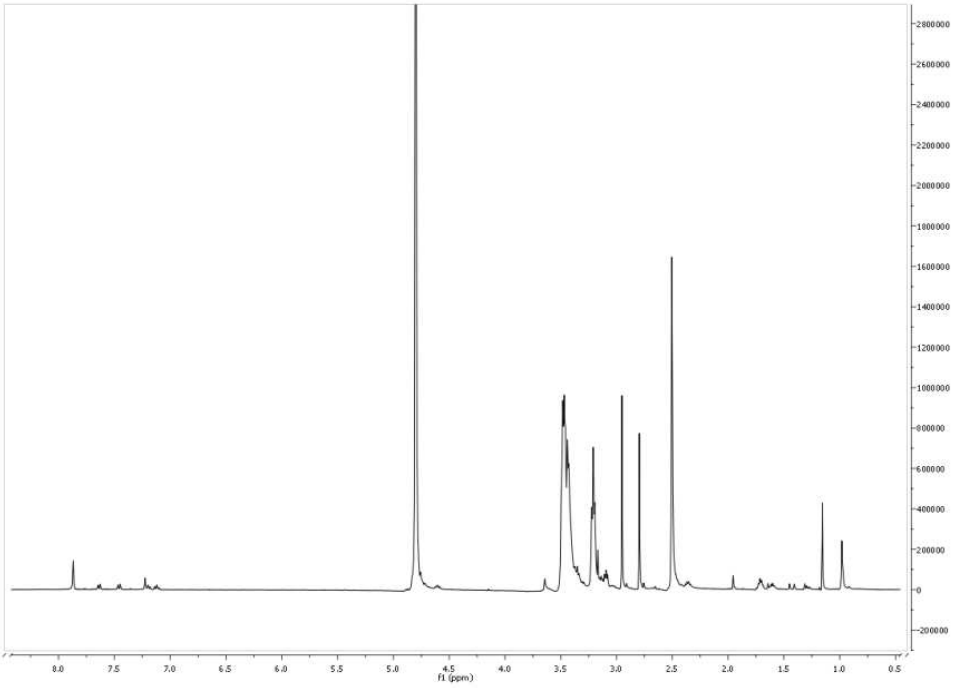

Id:554 Sequence: Stp30-W

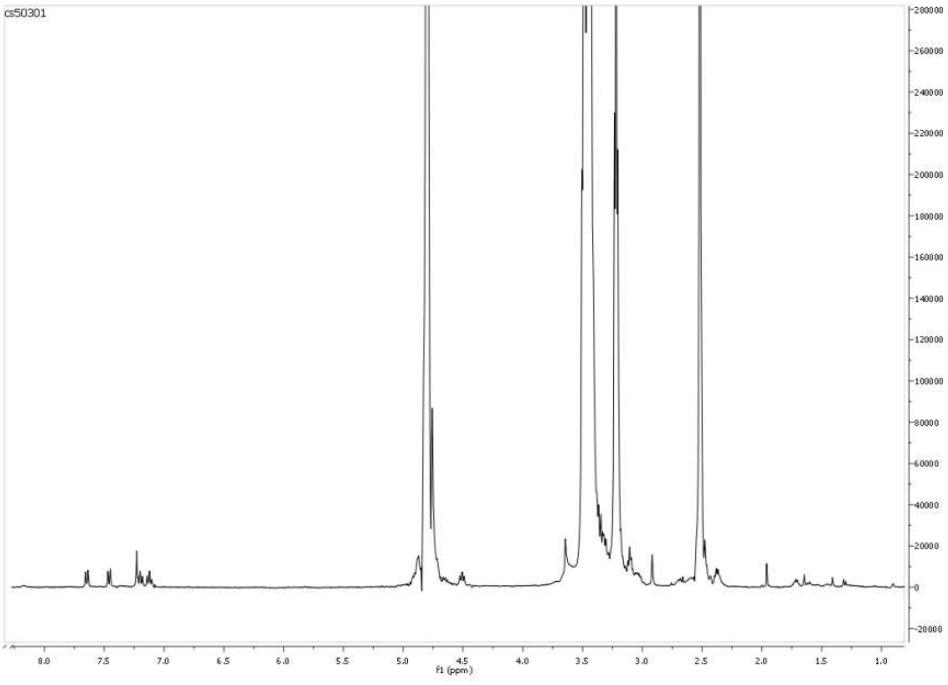

Id:555 Sequence: Stp40-W

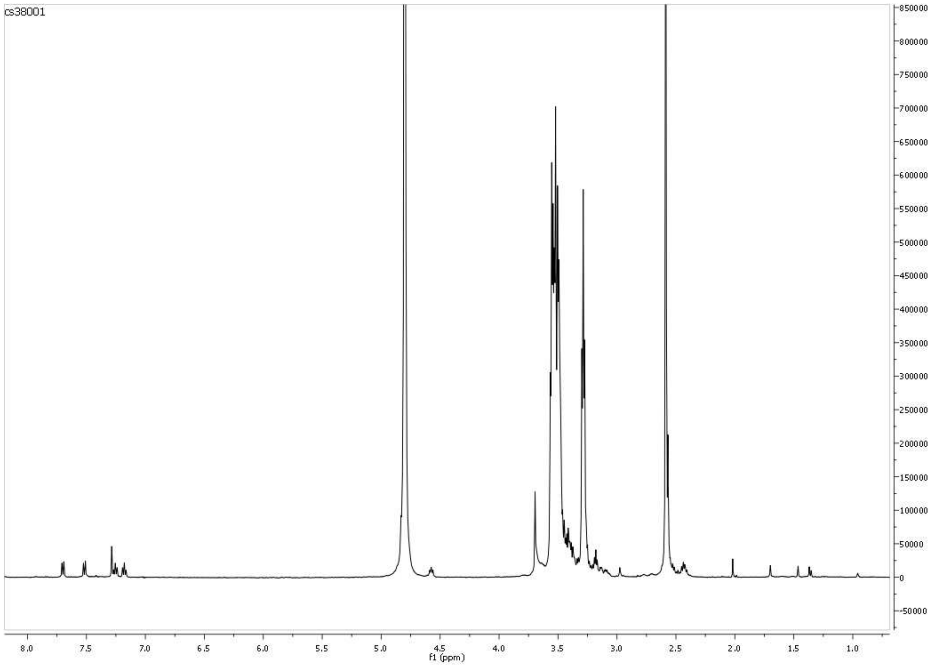

Id:556 Sequence: [Stp5-βA]$_5$-W

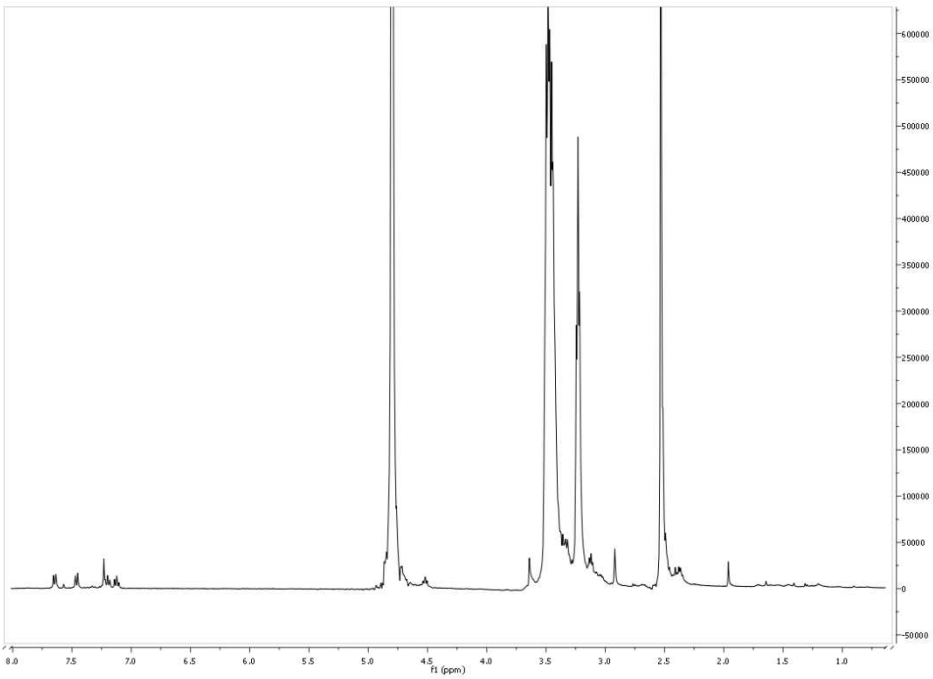

Id:682 Sequence: C-Stp30-W-C

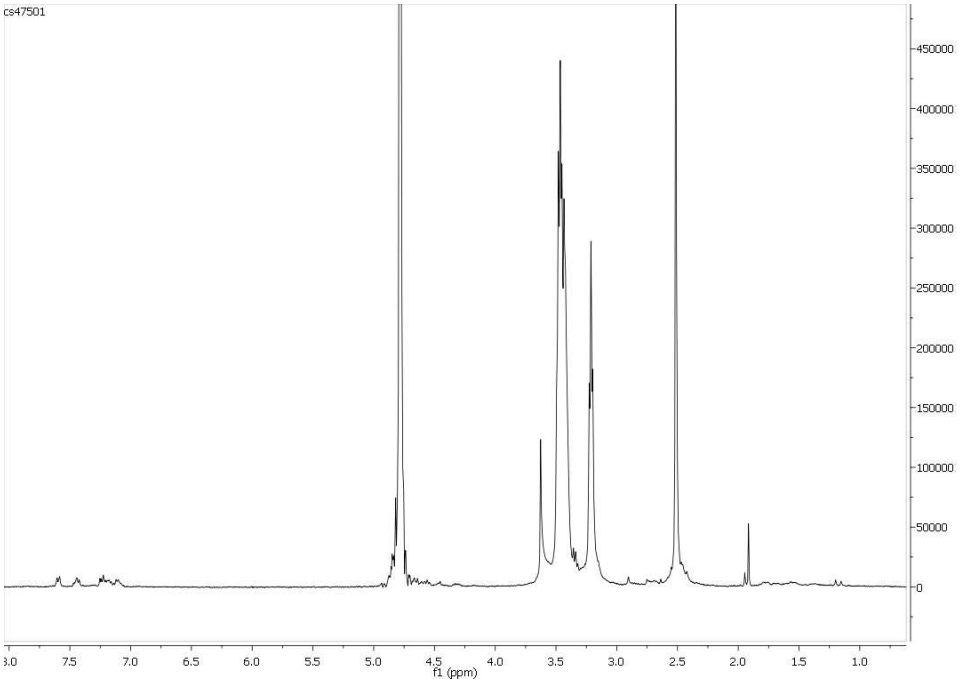

Id:683 Sequence: Sph20-W

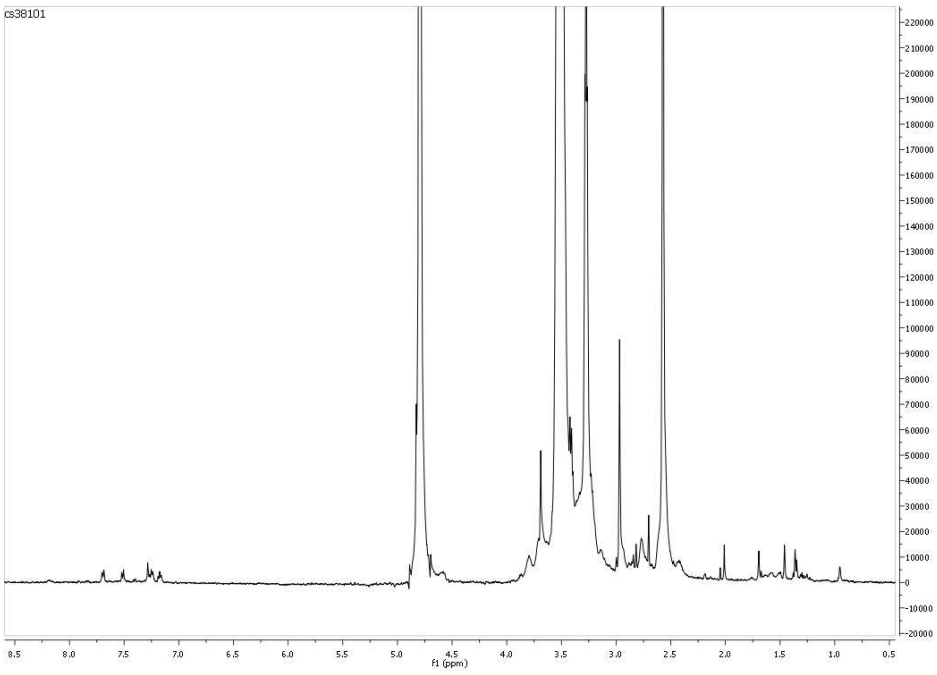

Id:684 Sequence: Sph30-W

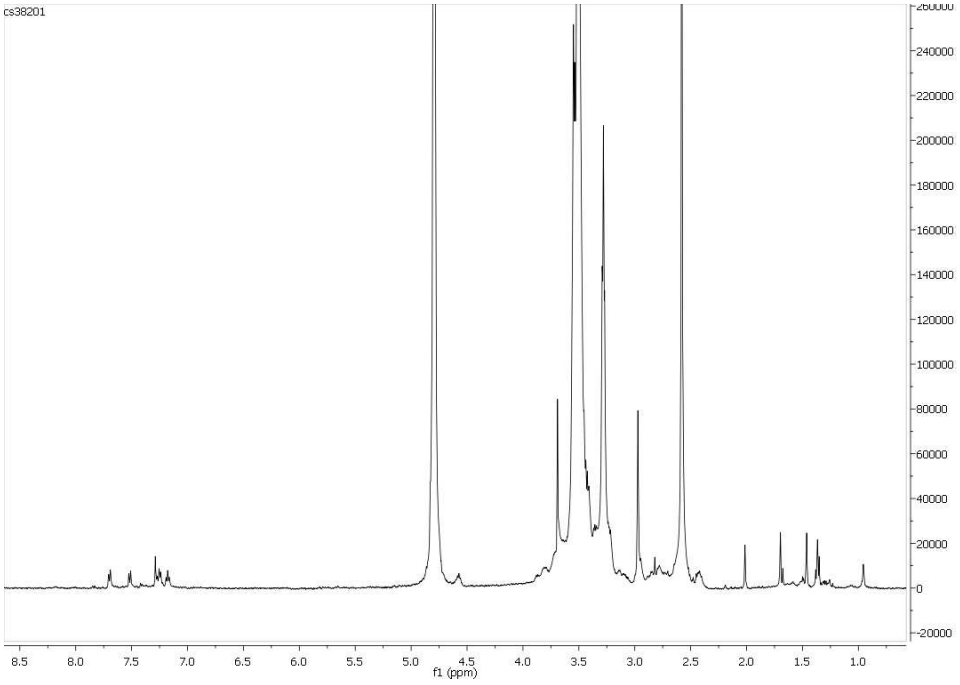

NMR spectra of Boc-protected diaminoethane motif containing building blocks

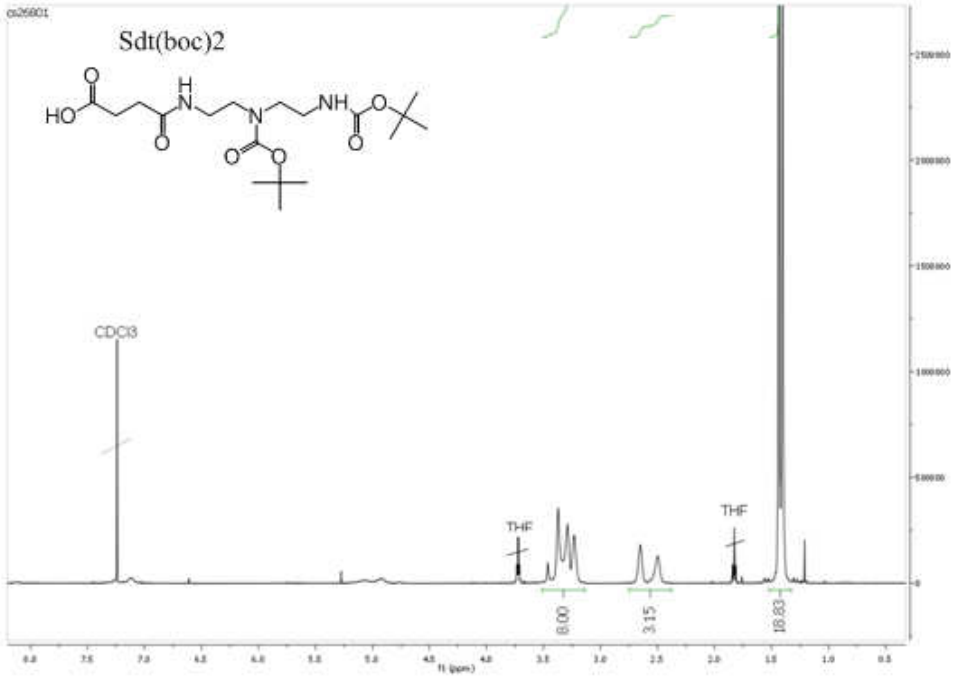

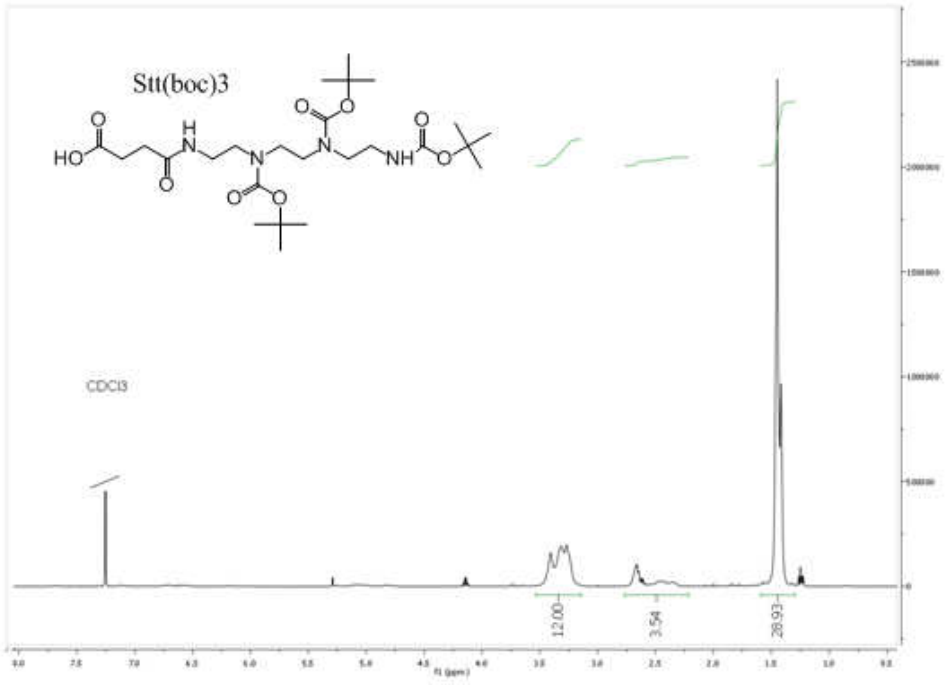
Stt(boc)3
CDCl3
12.00
3.54
28.93

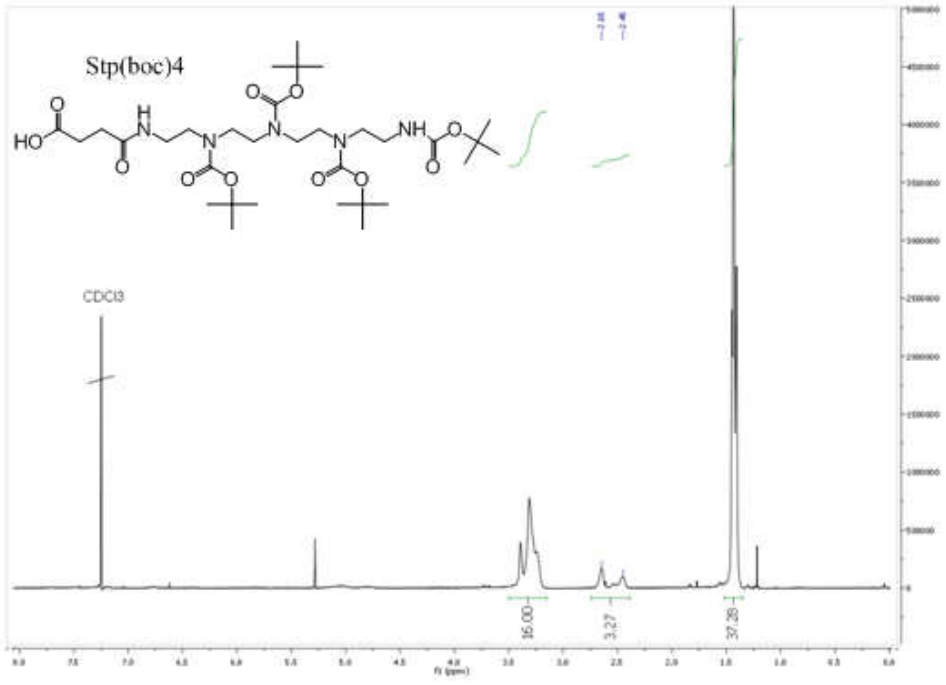
Stp(boc)4
CDCl3
16.00
3.27
37.28

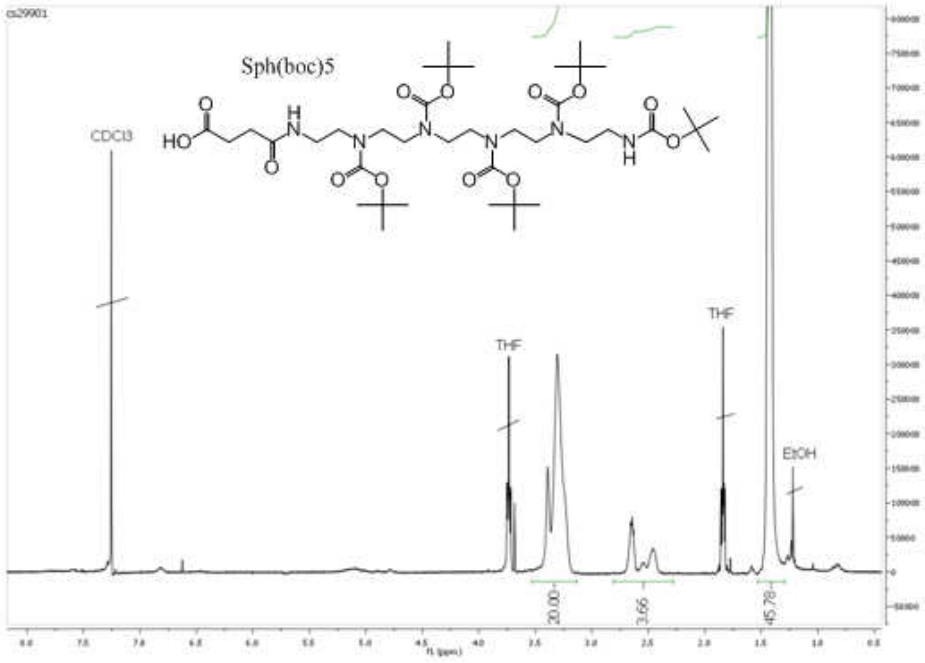

Id: 545 Sequence: C-[K(Stp)]$_4$-C

δ (ppm): 1.0 -1.8 (m, 24H, βγδH lysine), 2.4 -2.6 (m, 16H, -CO-CH2-CH2-CO-), 2.6 -3.1 (m, 12H, εH lysine, βH cysteine), 3.1-3.6 (m, 64H, -CH2- Tepa), 4.0-4.6 (m, 6H, αH lysine, cysteine)

Id: 626 Sequence: A-[K(Stp)]$_8$-A

δ (ppm): 1.0 -1.8 (m, 64H, βγδH lysine, βH alanine), 2.4 -2.6 (m, 32H, -CO-CH2-CH2-CO-), 2.6 -3.1 (m, 16H, εH lysine), 3.1-3.6 (m, 128H, -CH2- Tepa), 4.0-4.6 (m, 10H, αH lysine, alanine)

Id: 627 Sequence: C-[βA-K(Stp)]$_8$-C

δ (ppm): 1.0 -1.8 (m, 48H, βγδH lysine), 2.4 -2.6 (m, 48H, -CO-CH2-CH2-CO-, αH β-alanine), 2.6 -3.1 (m, 36H, εH lysine, βH cysteine, βH β-alanine), 3.1-3.6 (m, 128H, -CH2- Tp), 4.0-4.6 (m, 10H, αH lysine, cysteine)

Id: 621 Sequence: C-[W-K(Stp)]$_8$-C

δ (ppm): 1.0 -1.8 (m, 48H, βγδH lysine), 2.4 -2.6 (m, 32H, -CO-CH2-CH2-CO-), 2.6 -3.1 (m, 36H, εH lysine, βH cysteine, βH tryptophane), 3.1-3.6 (m, 128H, -CH2- Tepa), 4.0-4.6 (m, 16H, αH lysine, cysteine, tryptophane), 7.1-7.7 (m, 40H aromatic H, tryptophane)

Id: 686 Sequence: A-[H_2-K(Stp)]$_8$-A

δ (ppm): 1.0 -1.8 (m, 54H, βγδH lysine, βH alanine), 2.4 -2.6 (m, 32H, -CO-CH2-CH2-CO-), 2.6 -3.1 (m, 48H, εH lysine, βH histidine), 3.1-3.6 (m, 128H, -CH2- Tepa), 4.0-4.6 (m, 18H, αH lysine, histidine, alanine)

Id: 553 Sequence: C-[H_2-K(Stp)]$_8$-C

δ (ppm): 1.0 -1.8 (m, 48H, βγδH lysine), 2.4 -2.6 (m, 32H, -CO-CH2-CH2-CO-), 2.6 -3.1 (m, 52H, εH lysine, βH cysteine, βH histidine), 3.1-3.6 (m, 128H, -CH2- Tepa), 4.0-4.6 (m, 26H, αH lysine, cysteine, histidine), 7.3-7.5 (s,16H histidine), 8.6-8.7 (s, 16H histidine)

Id: 632 Sequence: C-[K(Sdt)]$_8$-C

δ (ppm): 1.0 -1.8 (m, 48H, βγδH lysine), 2.4 -2.6 (m, 32H, -CO-CH2-CH2-CO-), 2.6 -3.1 (m, 20H, εH lysine, βH cysteine), 3.1-3.6 (m, 64H, -CH2- Deta), 4.0-4.6 (m, 10H, αH lysine, cysteine)

Id: 633 Sequence: C-[A-K(Sdt)]$_8$-C

δ (ppm): 1.0 -1.8 (m, 72H, βγδH lysine, βH alanine), 2.4 -2.6 (m, 32H, -CO-CH2-CH2-CO-), 2.6 -3.1 (m, 20H, εH lysine, βH cysteine), 3.1-3.6 (m, 64H, -CH2- Deta), 4.0-4.6 (m, 18H, αH lysine, cysteine, alanine)

Id: 634 Sequence: C-[H-K(Sdt)]$_8$-C

δ (ppm): 1.0 -1.8 (m, 48H, βγδH lysine), 2.4 -2.6 (m, 32H, -CO-CH2-CH2-CO-), 2.6 -3.1 (m, 36H, εH lysine, βH cysteine, βH histidine), 3.1-3.6 (m, 64H, -CH2- Deta), 4.0-4.6 (m, 18H, αH lysine, cysteine, histidine), 7.3-7.5 (s, 8H histidine), 8.6-8.7 (s, 8H histidine)

Id: 635 Sequence: C-[K(Stt)]$_8$-C

δ (ppm): 1.0 -1.8 (m, 48H, βγδH lysine), 2.4 -2.6 (m, 32H, -CO-CH2-CH2-CO-), 2.6 -3.1 (m, 20H, εH lysine, βH cysteine), 3.1-3.6 (m, 96H, -CH2- Teta), 4.0-4.6 (m, 10H, αH lysine, cysteine)

Id: 636 Sequence: C-[A-K(Stt)]$_8$-C

δ (ppm): 1.0 -1.8 (m, 72H, βγδH lysine, βH alanine), 2.4 -2.6 (m, 32H, -CO-CH2-CH2-CO-), 2.6 -3.1 (m, 20H, εH lysine, βH cysteine), 3.1-3.6 (m, 96H, -CH2- Teta), 4.0-4.6 (m, 18H, αH lysine, cysteine, alanine)

Id: 637 Sequence: C-[H-K(Stt)]$_8$-C

δ (ppm): 1.0 -1.8 (m, 48H, βγδH lysine), 2.4 -2.6 (m, 32H, -CO-CH2-CH2-CO-), 2.6 -3.1 (m, 36H, εH lysine, βH cysteine, βH histidine), 3.1-3.6 (m, 96H, -CH2- Teta), 4.0-4.6 (m, 18H, αH lysine, cysteine, histidine), 7.3-7.5 (s, 8H histidine), 8.6-8.7 (s, 8H histidine)

Id: 622 Sequence: C-[K(Stp)]$_8$-C

δ (ppm): 1.0 -1.8 (m, 48H, βγδH lysine), 2.4 -2.6 (m, 32H, -CO-CH2-CH2-CO-), 2.6 -3.1 (m, 20H, εH lysine, βH cysteine), 3.1-3.6 (m, 128H, -CH2- Tepa), 4.0-4.6 (m, 10H, αH lysine, cysteine)

Id: 551 Sequence: C-[A-K(Stp)]$_8$-C

δ (ppm): 1.0 -1.8 (m, 72H, βγδH lysine, βH alanine), 2.4 -2.6 (m, 32H, -CO-CH2-CH2-CO-), 2.6 -3.1 (m, 20H, εH lysine, βH cysteine), 3.1-3.6 (m, 128H, -CH2- Tepa), 4.0-4.6 (m, 18H, αH lysine, cysteine, alanine)

Id: 552 Sequence: C-[H-K(Stp)]$_8$-C

δ (ppm): 1.0 -1.8 (m, 48H, βγδH lysine), 2.4 -2.6 (m, 32H, -CO-CH2-CH2-CO-), 2.6 -3.1 (m, 36H, εH lysine, βH cysteine, βH histidine), 3.1-3.6 (m, 128H, -CH2- Tepa), 4.0-4.6 (m, 18H, αH lysine, cysteine, histidine), 7.3-7.5 (s, 8H histidine), 8.6-8.7 (s, 8H histidine)

Id: 629 Sequence: C-[K(Sph)]$_8$-C

δ (ppm): 1.0 -1.8 (m, 48H, βγδH lysine), 2.4 -2.6 (m, 32H, -CO-CH2-CH2-CO-), 2.6 -3.1 (m, 20H, εH lysine, βH cysteine), 3.1-3.6 (m, 160H, -CH2- Peha), 4.0-4.6 (m, 10H, αH lysine, cysteine)

Id: 630 Sequence: C-[A-K(Sph)]$_8$-C

δ (ppm): 1.0 -1.8 (m, 72H, βγδH lysine, βH alanine), 2.4 -2.6 (m, 32H, -CO-CH2-CH2-CO-), 2.6 -3.1 (m, 20H, εH lysine, βH cysteine), 3.1-3.6 (m, 160H, -CH2- Peha), 4.0-4.6 (m, 18H, αH lysine, cysteine, alanine)

Id: 631 Sequence: C-[H-K(Sph)]$_8$-C

δ (ppm): 1.0 -1.8 (m, 48H, βγδH lysine), 2.4 -2.6 (m, 32H, -CO-CH2-CH2-CO-), 2.6 -3.1 (m, 36H, εH lysine, βH cysteine, βH histidine), 3.1-3.6 (m, 160H, -CH2- Peha), 4.0-4.6 (m, 18H, αH lysine, cysteine, histidine), 7.3-7.5 (s, 8H histidine), 8.6-8.7 (s, 8H histidine)

Id: 625 Sequence: C-(Stp-K)$_8$-C

δ (ppm): 1.0 -1.8 (m, 48H, βγδH lysine), 2.4 -2.6 (m, 32H, -CO-CH2-CH2-CO-), 2.6 -3.1 (m, 20H, εH lysine, βH cysteine), 3.1-3.6 (m, 128H, -CH2- Tepa), 4.0-4.6 (m, 10H, αH lysine, cysteine)

Id: 626 Sequence: C-(A-Stp-K)$_8$-C

δ (ppm): 1.0 -1.8 (m, 72H, βγδH lysine, βH alanine), 2.4 -2.6 (m, 32H, -CO-CH2-CH2-CO-), 2.6 -3.1 (m, 20H, εH lysine, βH cysteine), 3.1-3.6 (m, 128H, -CH2- Tepa), 4.0-4.6 (m, 18H, αH lysine, cysteine, alanine)

Id: 628 Sequence: C-(H-Stp-K)$_8$-C

δ (ppm): 1.0 -1.8 (m, 48H, βγδH lysine), 2.4 -2.6 (m, 32H, -CO-CH2-CH2-CO-), 2.6 -3.1 (m, 36H, εH lysine, βH cysteine, βH histidine), 3.1-3.6 (m, 128H, -CH2- Tepa), 4.0-4.6 (m, 18H, αH lysine, cysteine, histidine), 7.3-7.5 (s, 8H imidazole of histidine), 8.6-8.7 (s, 8H histidine)

Id: 648 Sequence: C-(Sph-K)$_8$-C

δ (ppm): 1.0 -1.8 (m, 48H, βγδH lysine), 2.4 -2.6 (m, 32H, -CO-CH2-CH2-CO-), 2.6 -3.1 (m, 20H, εH lysine, βH cysteine), 3.1-3.6 (m, 160H, -CH2- Peha), 4.0-4.6 (m, 10H, αH lysine, cysteine)

Id: 649 Sequence: C-(A-Sph-K)$_8$-C

δ (ppm): 1.0 -1.8 (m, 72H, βγδH lysine, βH alanine), 2.4 -2.6 (m, 32H, -CO-CH2-CH2-CO-), 2.6 -3.1 (m, 20H, εH lysine, βH cysteine), 3.1-3.6 (m, 160H, -CH2- Peha), 4.0-4.6 (m, 18H, αH lysine, cysteine, alanine)

Id: 650 Sequence: C-(H-Sph-K)$_8$-C

δ (ppm): 1.0 -1.8 (m, 48H, βγδH lysine), 2.4 -2.6 (m, 32H, -CO-CH2-CH2-CO-), 2.6 -3.1 (m, 36H, εH lysine, βH cysteine, βH histidine), 3.1-3.6 (m, 160H, -CH2- Peha), 4.0-4.6 (m, 18H, αH lysine, cysteine, histidine), 7.3-7.5 (s, 8H histidine), 8.6-8.7 (s, 8H histidine)

8.3.2 Additional HPLC chromatograms of long linear Stp and Sph oligo(ethanamino)amides, comb structure oligomers and linear control sequences

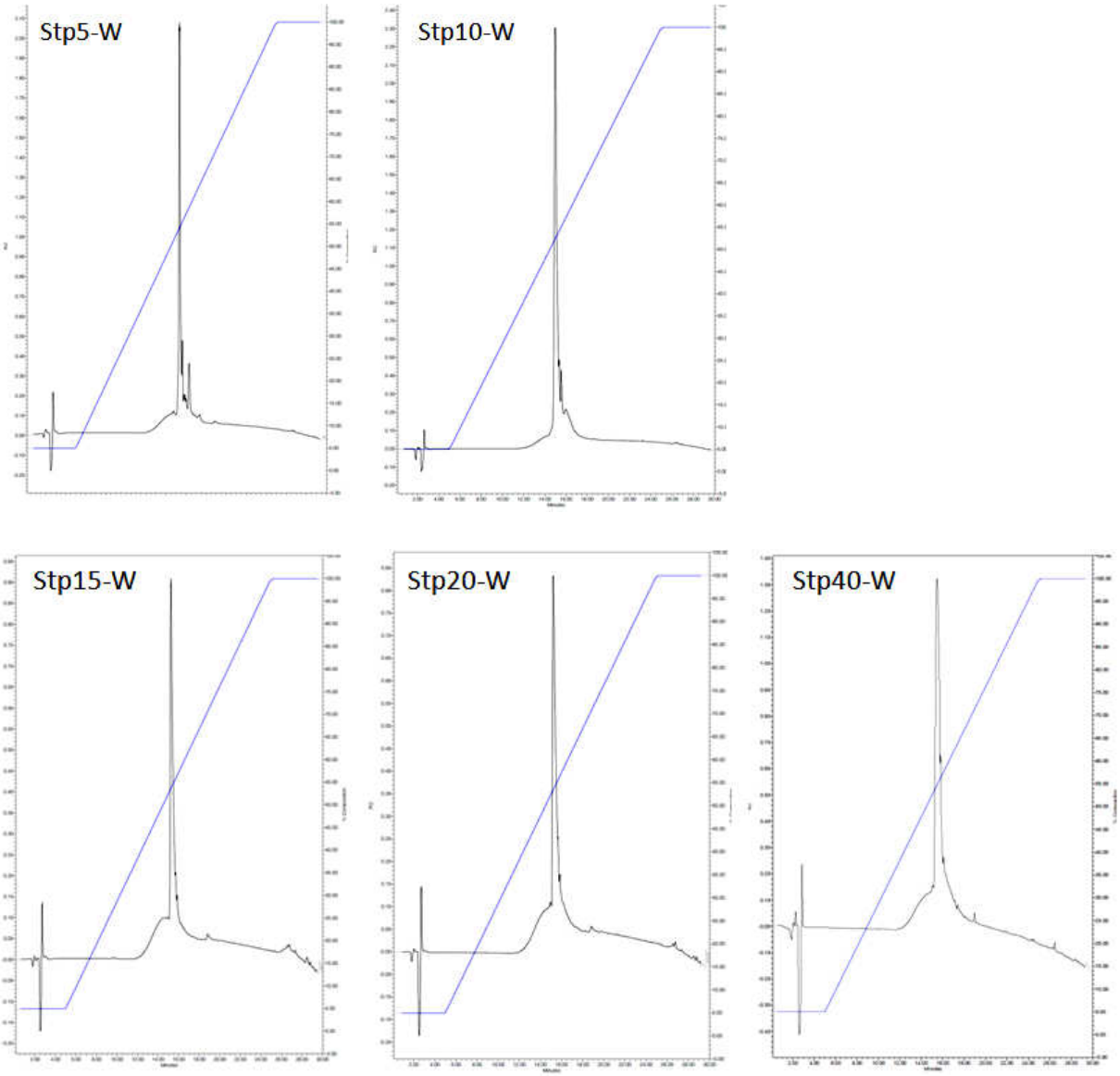

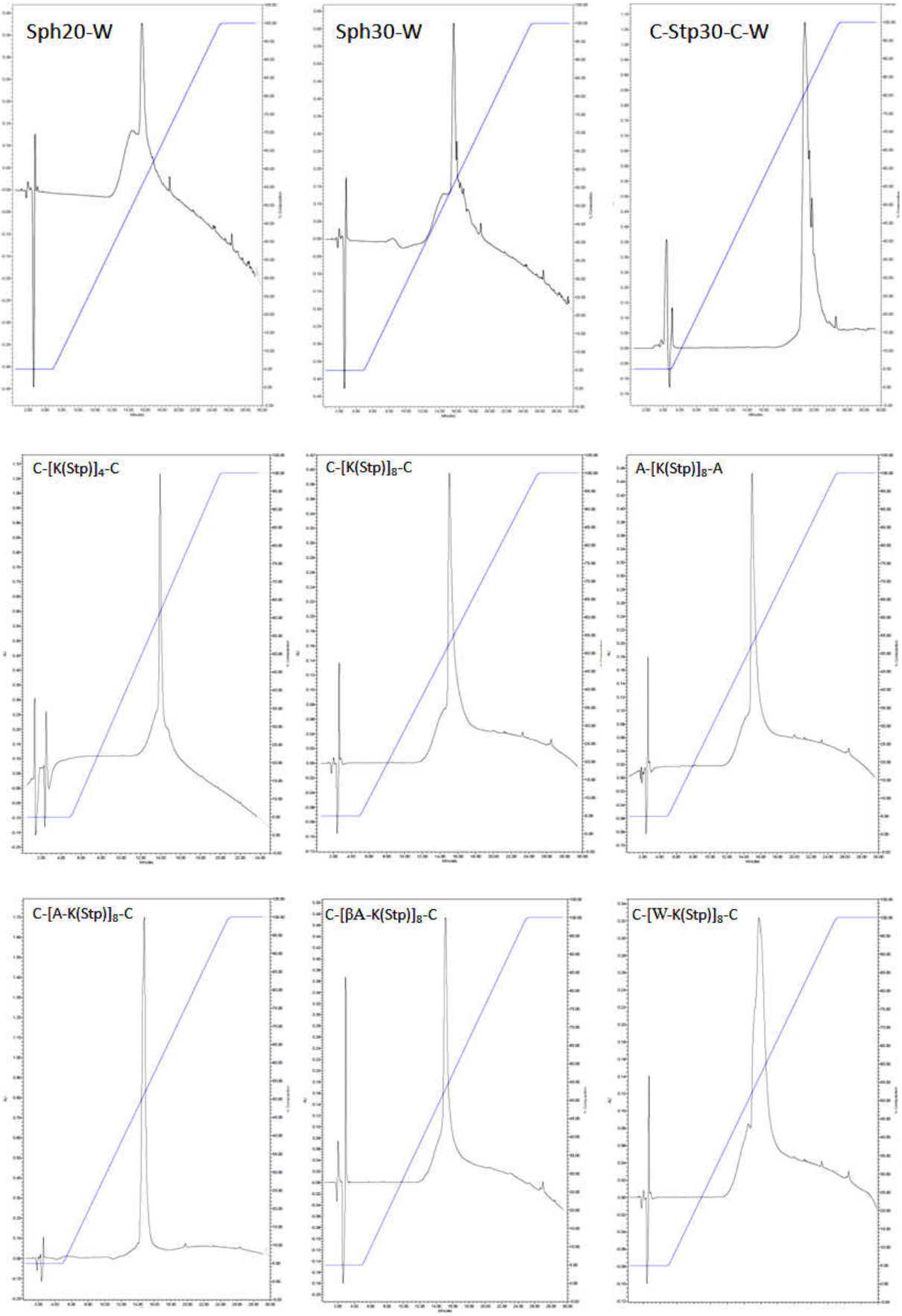
Sph20-W
Sph30-W
C-Stp30-C-W
C-[K(Stp)]4-C
C-[K(Stp)]8-C
A-[K(Stp)]8-A
C-[A-K(Stp)]8-C
C-[βA-K(Stp)]8-C
C-[W-K(Stp)]8-C

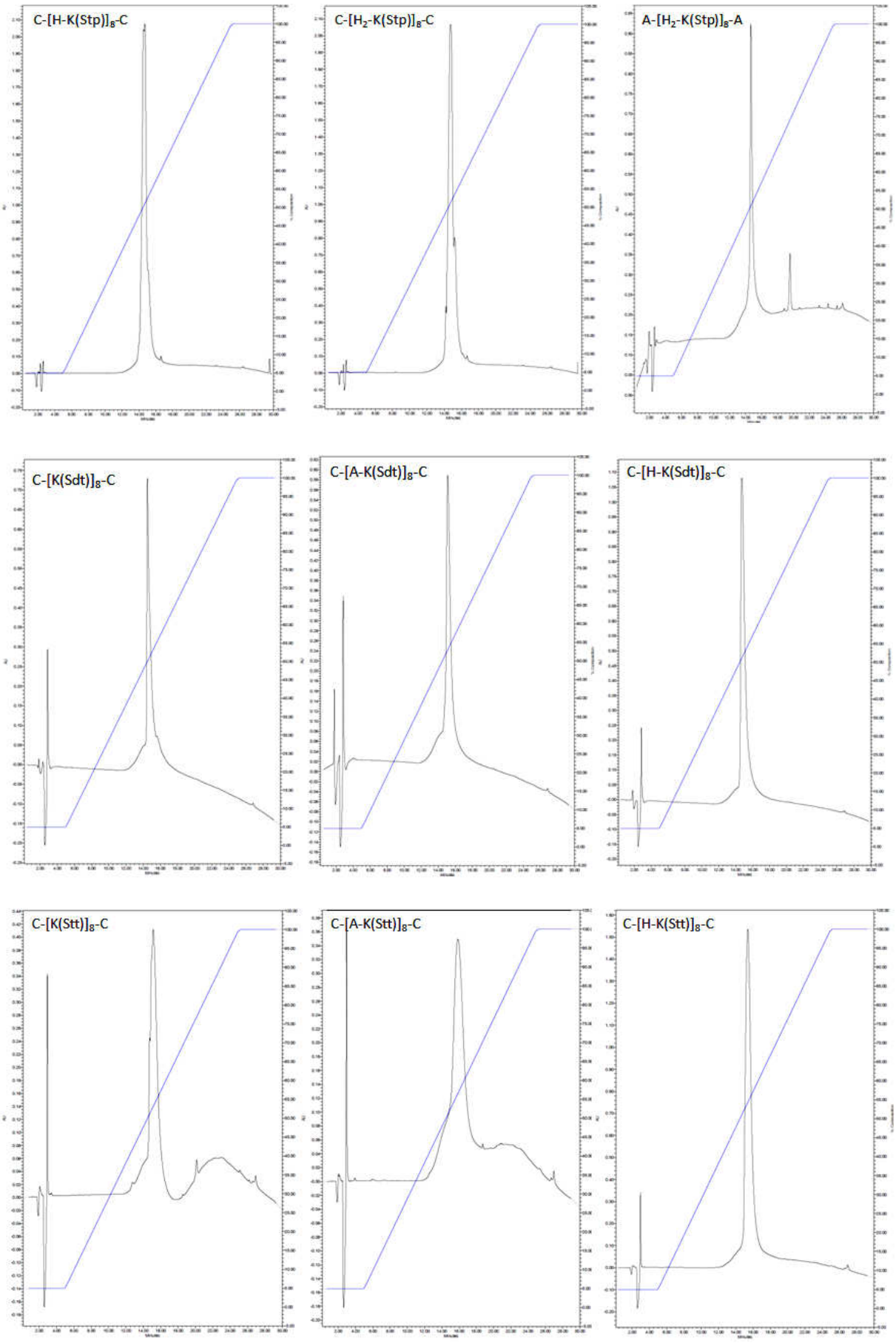
C-[H-K(Stp)]$_8$-C
C-[H$_2$-K(Stp)]$_8$-C
A-[H$_2$-K(Stp)]$_8$-A
C-[K(Sdt)]$_8$-C
C-[A-K(Sdt)]$_8$-C
C-[H-K(Sdt)]$_8$-C
C-[K(Stt)]$_8$-C
C-[A-K(Stt)]$_8$-C
C-[H-K(Stt)]$_8$-C

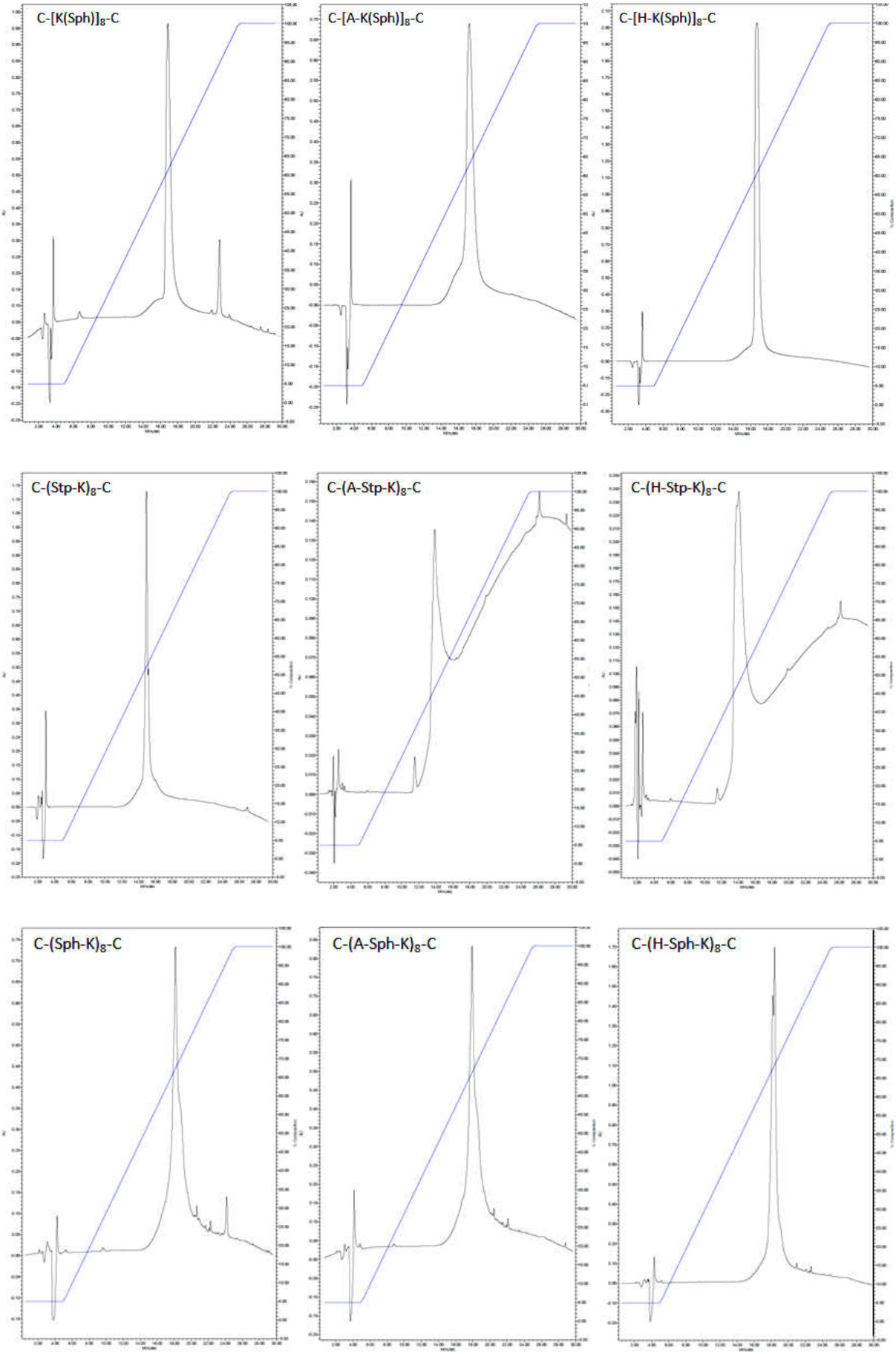
C-[K(Sph)]8-C
C-[A-K(Sph)]8-C
C-[H-K(Sph)]8-C
C-(Stp-K)8-C
C-(A-Stp-K)8-C
C-(H-Stp-K)8-C
C-(Sph-K)8-C
C-(A-Sph-K)8-C
C-(H-Sph-K)8-C

8.4 Publications

8.4.1 Original papers

Scholz, Claudia; Kos, Petra; Leclercq, Laurent; Jin, Xiaoyun; Cottet, Hervé; Wagner, Ernst: *Correlation of length of linear oligo(ethanamino)amides with gene transfer and cytotoxicity;* ChemMedChem 2014 Feb 6. [Epub ahead of print]

Scholz, Claudia; Kos, Petra; Wagner, Ernst: *Comb-like oligoaminoethane carriers: change in topology improves pDNA delivery*; Bioconjugate Chemistry 2013 Dec 20. [Epub ahead of print]

Zhang, Can Yang; Kos, Petra; Müller, Katharina; Schrimpf, Waldemar; Troiber, Christina; Lächelt, Ulrich; Scholz, Claudia; Lamb, Don C.; Wagner, Ernst: *Native Chemical Ligation for Conversion of Sequence-defined Oligomers into Targeted pDNA and siRNA Carriers;* submitted

Kos, Petra; Scholz, Claudia; Salcher, Eveline E.; Herrmann, Annika; Wagner, Ernst: *Gene Transfer with Sequence-Defined Oligo(ethanamino)amides Bioreducibly Attached to a Propylenimine Dendrimer Core*; Pharmaceutical Nanotechnology, 2013, 1, 269-281

8.4.2 Review

Scholz, Claudia; Wagner Ernst: *Therapeutic plasmid DNA versus siRNA delivery: common and different tasks for synthetic carriers,* Journal of Controlled Release. 2012 Jul 20;161(2):554-65

8.4.3 Poster presentations

C. Scholz, E. Salcher, C. Troiber, T. Fröhlich, P. Kos, E. Wagner: *Artificial Fmoc/Boc protected amino acids for the solid-phase-assisted synthesis of defined polyaminoamides for pDNA and siRNA delivery,* 9th International Symposium on Polymer Therapeutics, Valencia, Spain, May 2012

C. Scholz, D. Schaffert, N. Badgujar, I. Martin, E. Salcher, C. Troiber, E. Wagner: *Artificial Fmoc/Boc-protected amino acids for the solid-phase-assisted synthesis of defined polyaminoamides,* CeNS Workshop, Venice, Italy, September 2011

9 ACKNOWLEDGEMENTS

The journey is the goal. Retrospectively, after my four years long journey to get a PhD I have reached my goal by experiencing exciting research in a harmonic social environment. Many people have contributed to this and deserve my gratitude.

First of all, I would like to thank my supervisor Prof. Dr. Ernst Wagner for giving me the opportunity to work in his group. I am especially grateful for his scientific support and guidance over all these years.

In addition, I would like to express my gratitude to our collaboration partners Xiaoyun Jin, Dr. Laurent Leclercq and Prof. Dr. Hervé Cottet for their contribution of valuable methods of analysis.

I want to thank David for introducing me into the lab work. The contact with such an extraordinary scientist was a great motivation. Also Irene helped me getting acquainted with the lab and finding a good friend in Munich. Moreover, I thank Christina for her patience in confirming that my Kaiser test is really positive and for always being helpful. In this context I also have to thank Wolfgang – having him around makes the lab a better place. Thanks also to all other technicians Miriam, Ursula, Anna, Markus (although he did not like my beetroot salad) and Melinda as well as Olga for keeping the lab running. Thank you Martina for maintaining my illusion that Santa Claus exists, as I always found chocolate on my desk on December 6th, and for everything else she does for our group.

Furthermore, I want to thank all former colleagues for their help in the lab and fun times in social events. Thanks to Edith and her singing cow, who were great neighbors in the lab. Exchanging her by Philipp K was a radical change; after getting used to being informed about the current dollar exchange rate, I will surely miss him and the discussions about his innovative ideas for chemical synthesis. Of course, I also want to thank our further newcomers for enriching my last year. Special thanks to Ruth for organizing beautiful hiking tours, Katharina for nice evenings in her comfortable kitchen and Philipp H for funny and relaxing breaks after he succeeded in persuading me to have a coffee.

Thanks also to my former lab-mate Kevin for arranging comfortable “starts into the new day” by taking a seat on my window ledge. As I missed citing Kevin´s work about AzMMMan, I would like to quote from his thesis acknowledgements that “Uli is the most likeable scientist in the world”. In addition, I appreciate Uli as a special friend.

Particular thanks to Petra, not only for testing all my polymers in cell culture, but also for saving my life as my personified brake system on inline skates and for teaching me “useful” Slovenian sayings.

Finally, I would like to thank some persons who are special for my personal life: the Prokop family for making me feel at home in Munich, my best friend Caro for always being there for me, and most of all my family - Elmi for being the best brother in the world and my parents for their love I am experiencing every single day.